Some techniques to search for axions and axion-like particles

GOETHE UNIVERSITÄT FRANKFURT AM MAIN

CRC–TR 211 Strong-interaction matter under extreme conditions

TECHNISCHE UNIVERSITÄT DARMSTADT

DFG

UNIVERSITÄT BIELEFELD

HGS-HIRe for FAIR Helmholtz Graduate School for Hadron and Ion Research

Ahmed Ayad

ayad@physik.uni-bielefeld.de

Faculty of Physics, Bielefeld University
Bielefeld, Germany

July 07, 2022

Introduction and motivation

- QCD Axion solve the strong-CP problem by explaining the smallness of the neutron electric dipole moment.

- ALPs are similar particles proposed by many string theory models to solve other fundamental problems.

- The phenomenology axions of ALPs depends on the energy scale f_a at which the symmetry is spontaneously broken.

- ALPs can explain the observed cold dark matter (CDM) abundance.

Strong CP Problem: $\ell_\theta = \bar{\theta}\frac{g_s^2}{32\pi^2}G_a^{\mu\nu}\tilde{G}_{\alpha\beta}^a$

$\bar{\theta} = \theta + \mathrm{Arg}\det M \quad \Rightarrow \quad |\bar{\theta}| \lesssim 10^{-10}$

$\bar{\theta} \to \bar{\theta} - \frac{a}{f_a}(\simeq 0$ at potential minimum$)$

$$\mathrm{L_{int}} = -\frac{1}{4}g_{\mathrm{a}\gamma}\mathrm{F}_{\mu\nu}\tilde{\mathrm{F}}^{\mu\nu}a - ig_{\mathrm{af}}a\bar{f}\gamma_5 f$$

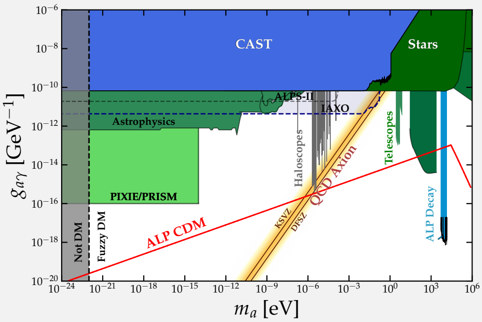

https://cajohare.github.io/AxionLimits/docs/ap.html.

Probing a cosmic axion background (CAB) within the jets of active galactic nuclei (AGN) (Primakoff conversion)

- The mixing model:

$$i\frac{d}{dz}\begin{pmatrix} A_\perp(z) \\ A\|(z) \\ a(z) \end{pmatrix} = -\begin{pmatrix} \Delta_\perp \cos^2\xi + \Delta_\| \sin^2\xi & \cos\xi\sin\xi(\Delta_\| + \Delta_\perp) & \Delta_{a\gamma}\sin\xi \\ \cos\xi\sin\xi(\Delta_\| + \Delta_\perp) & \Delta_\perp \sin^2\xi + \Delta_\| \cos^2\xi & \Delta_{a\gamma}\cos\xi \\ \Delta_{a\gamma}\sin\xi & \Delta_{a\gamma}\cos\xi & \Delta_a \end{pmatrix}\begin{pmatrix} A_\perp(z) \\ A\|(z) \\ a(z) \end{pmatrix}$$

- The conversion probability $\Rightarrow P_{a\to\gamma}(E) = |A_\|(E)|^2 + |A_\perp(E)|^2$.

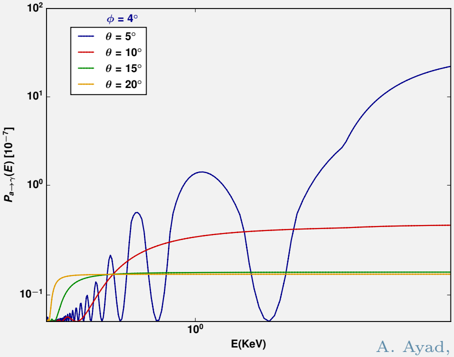

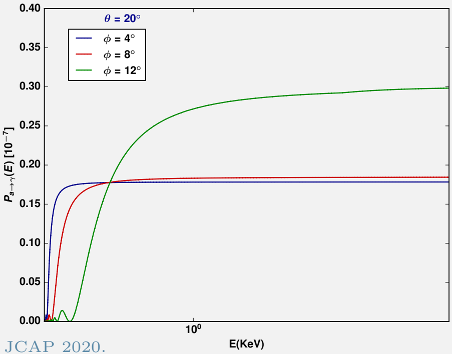

A. Ayad, G. Beck, JCAP 2020.

M87 AGN energy spectra

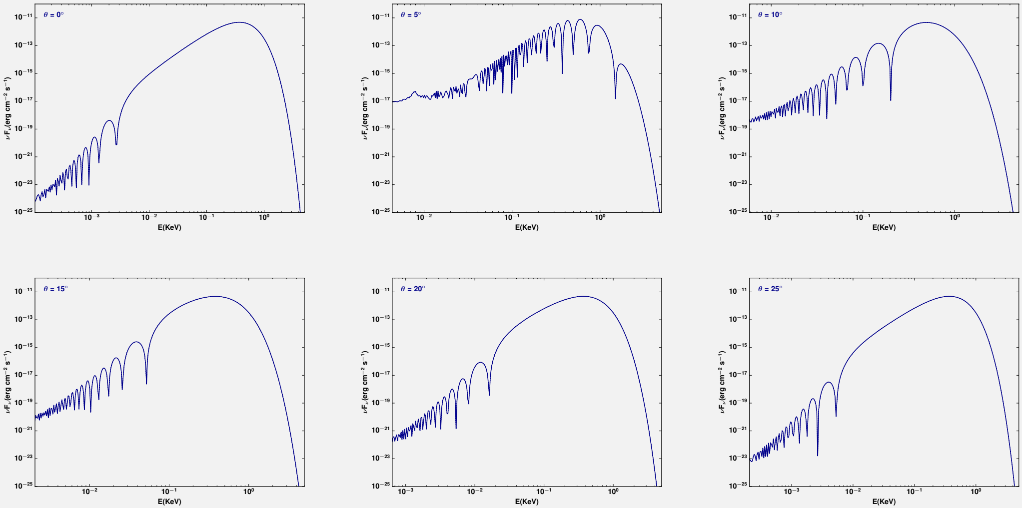

A. Ayad, G. Beck, JCAP 2020.

- The overall X-ray emission for the M87 AGN [Flux (0.3–8) keV $\sim 3.76 \times 10^{-12}$ erg cm^{-2} s^{-1}]. D. Donato, R. Sambruna, M. Gliozzi, ApJ 2004.

ALPs conversion explains Coma cluster soft X-ray excess

θ (°), $\phi = 4°$	$g_{a\gamma}$ (GeV^{-1})	ϕ (°), $\theta = 20°$	$g_{a\gamma}$ (GeV^{-1})
0	$\lesssim 3.91 \times 10^{-13}$	4	$\lesssim 6.56 \times 10^{-14}$
5	$\lesssim 9.17 \times 10^{-15}$	8	$\lesssim 2.32 \times 10^{-14}$
10	$\lesssim 7.50 \times 10^{-15}$	12	$\lesssim 7.99 \times 10^{-15}$
15	$\lesssim 2.08 \times 10^{-14}$		
20	$\lesssim 6.56 \times 10^{-14}$		
25	$\lesssim 1.98 \times 10^{-13}$		

- Recent work explains the Coma cluster soft X-ray excess due to CAB ALPs conversion into photons in the magnetic field of galaxy clusters.

  S. Angus, J. Conlon, M. Marsh, A. Powell, L. Witkowski, JCAP 2014.

- These results cast doubt on the current best fit value on $g_{a\gamma} \sim 2 \times 10^{-13}$ GeV^{-1} obtained in the Coma cluster soft X-ray excess CAB model.

- Instead we suggest a new constraint at the largest allowed value of $g_{a\gamma} \lesssim 6.56 \times 10^{-14}$ GeV^{-1}.

Potential of radio telescopes to detect the stimulated decay of ALPs

- ALPs spontaneously decay with lifetime:

$$\tau_a \equiv \Gamma_{\rm pert}^{-1} = \frac{64\pi}{m_{\rm a}^3 g_{\rm a\gamma}^2} \gg t_0 \,.$$

- ALPs $\Rightarrow$ Bose-Einstein condensate (BEC) $\Rightarrow$ thermalize to clumps.
- Stimulated decay of ALPs is also possible with effective decay rate:

$$\Gamma_{\rm eff} = \Gamma_{\rm pert}(1 + 2f_\gamma) \,.$$

- Equation of Motion for photons is a Mathieu equation

$$\ddot{A}_\pm + \left[k^2 + \omega_p^2 \pm g_{a\gamma} k \omega_0 a_0 \sin(\omega_0 t)\right] A_\pm = 0.$$

- The stimulated decay produces an enhancement of the ALPs decay rate by factors arising from

$$f_\gamma \simeq f_{\gamma,\rm CMB} + f_{\gamma,\rm gal} + f_{\gamma,\rm extra-gal} \,.$$

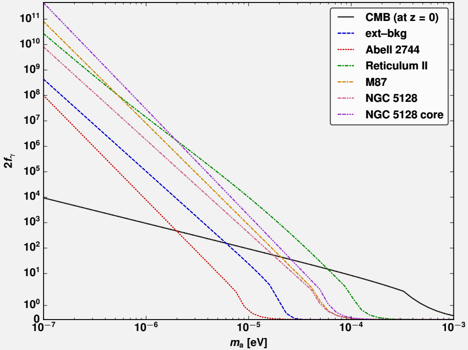

A. Ayad, G. Beck, JCAP 2022.

The potential non-observation constraints

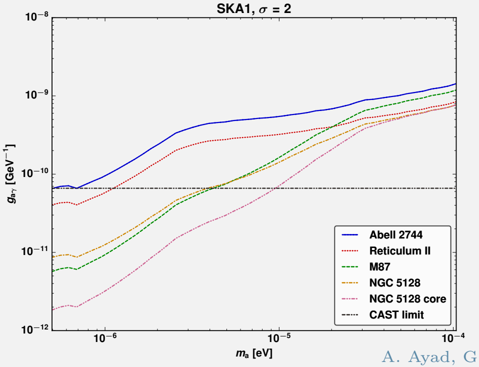

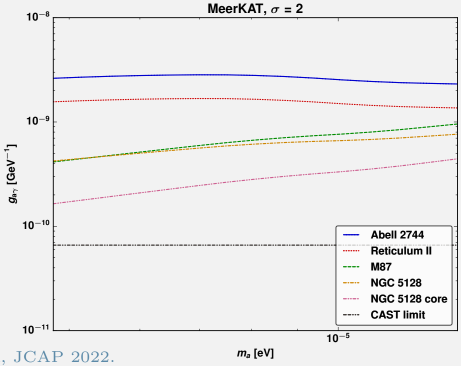

A. Ayad, G. Beck, JCAP 2022.

Confidence interval	SKA1		MeerKAT	
	m_a [eV]	$g_{a\gamma}$ [GeV]$^{-1}$	m_a [eV]	$g_{a\gamma}$ [GeV]$^{-1}$
2σ	1.04×10^{-4}	7.69×10^{-10}	1.36×10^{-5}	4.44×10^{-10}
	4.96×10^{-7}	1.83×10^{-12}	4.80×10^{-6}	1.65×10^{-10}

Table 4. Upper limits of the ALP to photon coupling $g_{a\gamma}$ that can be probed by SKA1 and MeerKAT telescopes with the 2σ confidence intervals for different ALP mass categories and using a 15 arcsecond taper on the visibilities. These limits obtained from the most promising case of the NGC 5128 core.

Concluding remarks

- Axion-like particles are a very well-motivated candidate to account for the cold dark matter content in the universe.
- Result I: suggests new constraints on the ALP-photon coupling lower than the current limits used to explain the Coma cluster soft X-ray excess.
- Result II: shows that radio telescopes such as MeerKAT and SKA can play a strong complementary role to experiments like ALPS-II and IAXO in exploring the ALP parameter space.
- Current efforts to find AMC and measure birefringence effects may help us better understand the nature of ALPs.

Thanks a lot! ☺

Imprint of the seesaw mechanism on feebly interacting dark matter and the baryon asymmetry

Based on
Phys. Rev. Lett. 127, 231801

Arghyajit Datta,

Indian Institute of Technology, Guwahati, India

In collaboration with:
Rishav Roshan and Arunansu Sil

The Abdus Salam International Centre for Theoretical Physics

Dark Matter (DM) :

What we know (from observations like Galactic rotation/Bullet Clusters/CMB etc.):

- Relic density (~**24 % of the Universe)**
- Massive
- Stable object
- Non or **very-weakly** interacting

What we Don't know:

- Nature of DM
- Interaction with SM fields
- Production mechanism in the early Universe

No such candidate within SM

Baryon Asymmetry of the Universe (BAU) :

Why there is solely baryonic matter in the Universe?

$$Y_B = \frac{n_B - n_{\bar{B}}}{s} = (8.70 - 8.73) \times 10^{-11}$$

[PLANCK, 2018]
[BBN, 2015]

Possible explanation:

- C and CP violation
- Baryon number violation
- Out-of-equilibrium decay

[Sakharov, 1967]

Not Possible within SM

What can be the simplest/minimal possibility to bring these unknowns together?

Type-I Seesaw

[Minkowsky, 1977]

[Yanagida, 1979]

[Gell-Mann,Ramond,Slansky,1979]

[Mohapatra,Senjanovic,1980]

Type-I seesaw and Neutrino mass :

Extension: SM + 3 Right-Handed Neutrinos

$$\mathcal{L}_{\mathbf{BSM}} = \mathbf{Y}^{\nu}_{\alpha \mathbf{i}} \bar{\ell}_{L_\alpha} \tilde{H} N_i + \frac{M_N}{2} \bar{N_i}^c N_i + h.c$$

After S.S.B.

$$\begin{pmatrix} \bar{\nu}_L & \overline{(N_R)^c} \end{pmatrix} \underbrace{\begin{pmatrix} 0_{3\times3} & m^D_{3\times3} \\ m^{D^T}_{3\times3} & M_{N_{3\times3}} \end{pmatrix}}_{m_{seesaw}} \begin{pmatrix} (\nu_L)^c \\ N_R \end{pmatrix} \xrightarrow[\text{Active-sterile mixing}]{\mathbb{L}^\dagger m_{seesaw} \mathbb{L}^* = m^{block}_{diag}} \begin{pmatrix} m_{\nu_{3\times3}} & 0_{3\times3} \\ 0_{3\times3} & M_{N_{3\times3}} \end{pmatrix}$$

$$m_\nu = -m_D M_N^{-1} m_D^T$$

$$\nu_L = U\nu + \underbrace{V}_{\mathbf{V} = \mathbf{m_D M_N^{-1}}} N$$

$$U^\dagger m_\nu U^* = D_m$$

$$\begin{pmatrix} D_{m_{3\times3}} & 0_{3\times3} \\ 0_{3\times3} & D_{M_{3\times3}} \end{pmatrix}$$

$$\mathbf{D_m} = \mathrm{diag}(\mathrm{m_1, m_2, m_3}) \qquad D_M = \mathrm{diag}(\mathrm{M_1, M_2, M_3})$$

Type-I seesaw and Leptogenesis : [Fukugita, Yanagida 1986]

$$\mathcal{L}_{\mathrm{BSM}} = \mathbf{Y}^{\nu}_{\alpha \mathbf{i}} \bar{\ell}_{L_\alpha} \tilde{H} N_i + \frac{M_R}{2} \bar{N_i}^c N_i + h.c$$

CP Violation

Lepton number Violation

Out-of equilibirum decay of RHN $\longrightarrow$ Compare decay rate and Hubble

$$\mathbf{\Delta L \neq 0} \xrightarrow{\text{Sphaleron Process}} \mathbf{\Delta B \neq 0}$$

Can it also explain the existence of DM in the Universe?

DM in type-I seesaw:

Can one of the RHN play a role of the DM ??

- **Issues:** **Stability:** RHN should not decay

One of the RHN is strictly Stable

$$Y^\nu = \begin{pmatrix} 0 & y_{e2} & y_{e3} \\ 0 & y_{\mu 2} & y_{\mu 3} \\ 0 & y_{\tau 2} & y_{\tau 3} \end{pmatrix}$$

Existence of such DM is questionable!!

DM cannot be produced via any interaction

Our Proposal:

If lightest RHN is considered as a FIMP, it can play a role of a CDM candidate.

How to explain Feebly interacting Massive Particle with coupling $\sim 10^{-10}$ naturally ?

$$\downarrow$$

Can it be connected to smallness of neutrino masses ?

$$Y^{\nu} = \begin{pmatrix} 0 & y_{e2} & y_{e3} \\ 0 & y_{\mu 2} & y_{\mu 3} \\ 0 & y_{\tau 2} & y_{\tau 3} \end{pmatrix} \longrightarrow \begin{pmatrix} \epsilon_1 & y_{e2} & y_{e3} \\ \epsilon_2 & y_{\mu 2} & y_{\mu 3} \\ \epsilon_3 & y_{\tau 2} & y_{\tau 3} \end{pmatrix} \qquad \epsilon_i << 1$$

Role of active-sterile mixing:

Entries of Yukawa or Dirac mass matrix (using CI parametrisation): [Casas, Ibarra, 2001]

$$\mathbf{m_D = -i\, U D_{\sqrt{m}} R^T D_{\sqrt{M}}} \longrightarrow \boxed{\epsilon_i \propto \sqrt{m_1 M_1}}$$

$$\mathrm{D}_{\sqrt{\mathrm{m}}} = \mathrm{diag}(\sqrt{\mathrm{m}_1}, \sqrt{\mathrm{m}_2}, \sqrt{\mathrm{m}_3})$$

$$\mathrm{D}_{\sqrt{\mathrm{M}}} = \mathrm{diag}(\sqrt{\mathrm{M}_1}, \sqrt{\mathrm{M}_2}, \sqrt{\mathrm{M}_3})$$

$$\begin{pmatrix} 1 & 0 & 0 \\ 0 & \cos\theta_R & \sin\theta_R \\ 0 & -\sin\theta_R & \cos\theta_R \end{pmatrix}$$

Complex Angle

Active-sterile mixing relevent to Lightest RHN:

$$V_{i1} = m_{D_{i1}}/M_1 = \epsilon_i \frac{v}{\sqrt{2}M_1} \propto \sqrt{\frac{m_1}{M_1}}$$

Effects of active-sterile mixing: production of DM

After S.S.B: → **Neutrinos get mass**

$$V_{i1} = m_{D_{i1}}/M_1 \propto \sqrt{\frac{m_1}{M_1}}$$

In mass diagonal basis

$$\nu_L = U\nu + VN$$

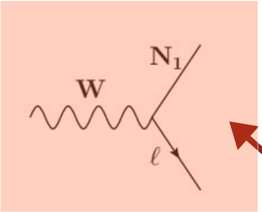

Gauge Interaction

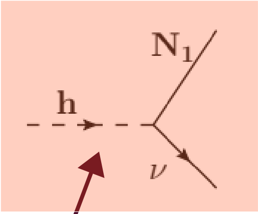

Yukawa Interaction

$$\mathcal{L}_{\mathcal{G}} \subset \frac{g}{\sqrt{2}} W_\mu^+ \sum_{i,j=1}^{3} \left[\bar{N}_i^c (V^\dagger)_{ij} \gamma^\mu P_L \ell_j\right]$$

$$+ \frac{g}{2C_{\theta_w}} Z_\mu \times \sum_{i,j=1}^{3} \left[\bar{\nu}_i (U^\dagger V)_{ij} \gamma^\mu P_L N_j^c + \bar{N}_i^c (V^\dagger V)_{ij} \gamma^\mu P_L N_j^c\right],$$

$$\mathcal{L}_{\mathcal{Y}} \subset \frac{\sqrt{2}}{v} h \sum_{i,j=1}^{3} \left[\bar{\nu}_i (U^\dagger V)_{ij} M_j N_j\right.$$

$$\left. + \bar{N}_i^c (V^\dagger V)_{ij} M_j N_j\right],$$

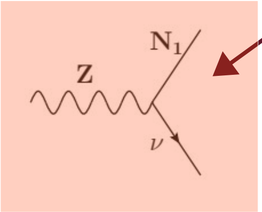

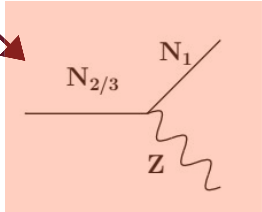

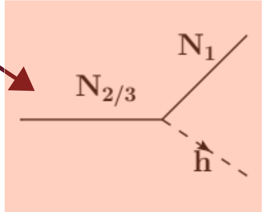

(Assuming $M_1 < M_W$)

Evolution of DM:

$$\frac{dY_{N_1}}{dz} = \frac{2M_{pl}z}{1.66M_2^2}\frac{g_\rho^{1/2}}{g_s}\Big[\sum_{i=2,3}\Big(Y_{N_i}\sum_{x=Z,W}\Big\langle\Gamma(N_i \to N_1 x)\Big\rangle\Big) + \sum_{x=W,Z,h} Y_x^{eq}\times \Big\langle\Gamma(x \to N_1 \ell)\Big\rangle\Big],$$

$$\frac{dY_{N_i}}{dz} = -\frac{2M_{pl}z}{1.66M_2^2}\frac{g_\rho^{1/2}}{g_s}\Big[(Y_{N_i} - Y_{N_i}^{eq})\Big\langle\Gamma^D\Big\rangle + Y_{N_i}\sum_{x=h,Z}\Big\langle\Gamma(N_i \to N_1 x)\Big\rangle\Big], \quad i = 2,3$$

Interaction	Decay Width
$W \to N_1 \ell_i$	$\frac{M_W^3}{48\pi v^2 M_1^2}(m_D)_{i1}(m_D)^*_{i1}$
$Z \to N_1 \nu_i$	$\frac{M_Z^3}{96\pi v^2 M_1^2}(U^\dagger m_D)_{i1}(U^\dagger m_D)^*_{i1}$
$h \to N_1 \nu_i$	$\frac{m_h}{32\pi v^2}(U^\dagger m_D)_{i1}(U^\dagger m_D)^*_{i1}$
$N_i \to N_1 h$	$\frac{M_i}{64\pi v^2 M_1^2}(m_D^\dagger m_D)_{1i}(m_D^\dagger m_D)^*_{1i}$
$N_i \to N_1 Z$	$\frac{Mi}{128\pi v^2 M_1^2}(m_D^\dagger m_D)_{1i}(m_D^\dagger m_D)^*_{1i}$

$$\Omega_{N_1} h^2 = 2.755 \times 10^5 \left(\frac{M_1}{\text{MeV}}\right) \boxed{Y_{N_1}(z_\infty)}$$

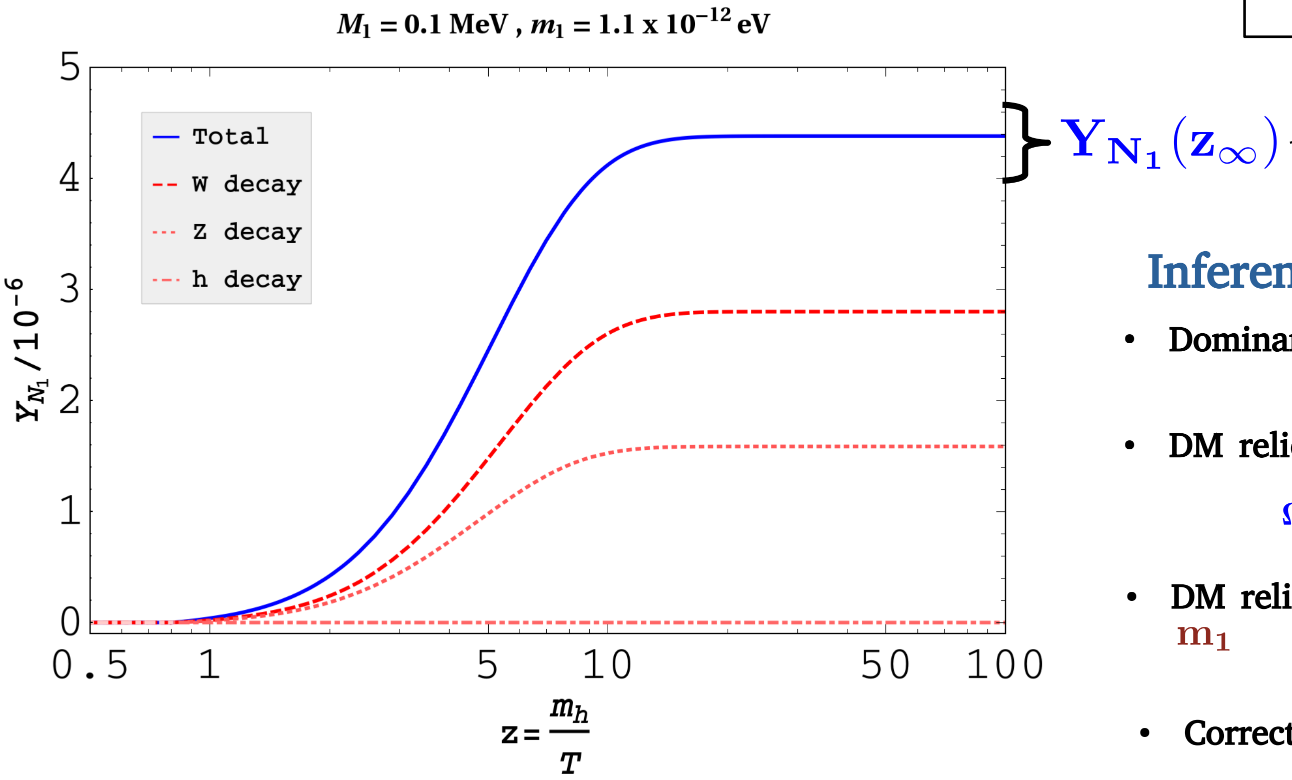

Inferences:

- Dominant contribution to Relic density ← $W^\pm$ decay, Z decay
- DM relic is independent of its mass

$$\Omega_{N_1} h^2 \propto M_1 Y_{N_1}(Z_\infty) \sim M_1 \Gamma_{W/Z} \sim M_1 \frac{m_1}{M_1}$$

- DM relic only depends on lightest active neutrino mass m_1
- Correct relic observed for $m_1 \sim 10^{-12}$ eV

Constraints from the decay of the DM:

Active-sterile mixing $\longrightarrow$ **Decay of DM**

- **Via offshell W/Z:**

$$\mathrm{N}_1 \to l_1^- l_2^+ \nu_{l_2},\ N_1 \to l^- q_1 \bar{q}_2,\ N_1 \to l^- l^+ \nu_l,\ N_1 \to \nu_l \bar{l}' l',\ N_1 \to \nu_l q \bar{q},\ N_1 \to \nu_l \nu_{l'} \bar{\nu}_{l'},\ N_1 \to \nu_l \nu_l \bar{\nu}_l$$

- **Via offshell h:**

$$N_1 \to \nu_\ell \bar{\ell} \ell$$

- **Radiative decay:**

$$\theta_1^2 = \sum_{i=1,2,3} \frac{|(m_D)_{i1}|^2}{M_1^2} \equiv \sum_{i=1,2,3} |V_{i1}|^2$$

$\mathbf{N_1} \to \gamma\nu$ $\longrightarrow$

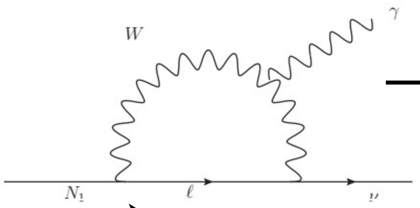

$\longrightarrow$ $$\Gamma_{N_1 \to \gamma\nu} = \frac{9\alpha G_F^2}{1024\pi^4} \sin^2 2\theta_1 M_1^5$$

[Pal, Wolfenstein, 1982]

V_{i1}

Most stringent bound comes from this

Constraints :

Non-observance of specific X-ray signal: Set a limit on θ_1^2 :

$$\theta_1^2 \leq 2.8 \times 10^{-18} \left(\frac{\text{MeV}}{M_1}\right)^5$$

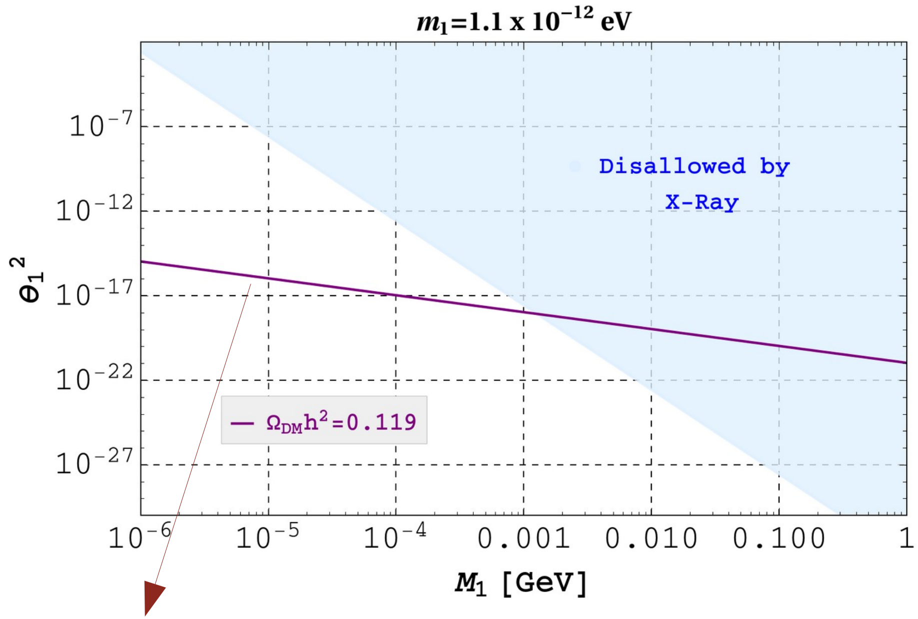

$\theta_1^2 = m_1/M_1$ dependence with m_1 fixed from relic requirement

Take away:

- N_1 as a successful FIMP type dark matter below **1 MeV**.
- The lower limit on M_1 is considered as **1 keV** to be in consistent with **Tremaine–Gunn bound** on sterile neutrino mass.
- **1 keV - 1 MeV** mass of N_1 as **FIMP dark matter** is allowed.

Matter-Antimatter Asymmetry:

Aim:

Utilise remaining two RHNs to generate BAU
Reduce the hierarchy among RHNs as much as possible.

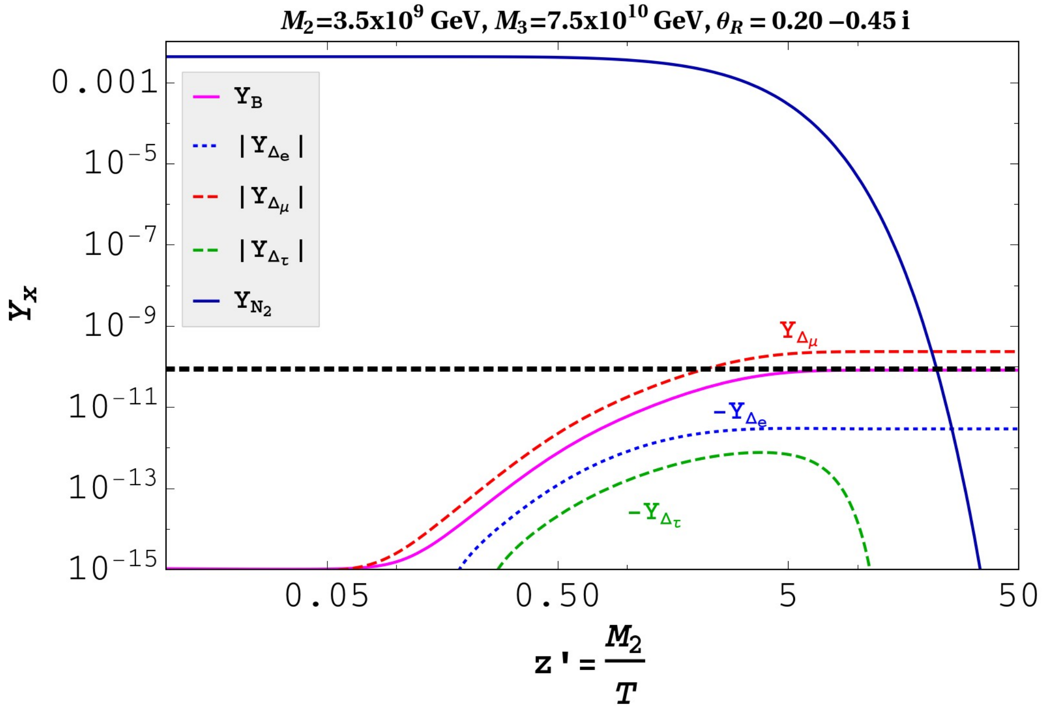

$$Y^\nu = \begin{pmatrix} \epsilon_1 & y_{e2} & y_{e3} \\ \epsilon_2 & y_{\mu 2} & y_{\mu 3} \\ \epsilon_3 & y_{\tau 2} & y_{\tau 3} \end{pmatrix}$$

Complex Angle $\theta_{\mathbf{R}}$

Involved in CI

$$\epsilon_{2\alpha}^{cp} = \frac{\Gamma(N_2 \to \ell_\alpha H) - \Gamma(N_2 \to \bar{\ell}_\alpha \bar{H})}{\sum_\alpha [\Gamma(N_2 \to \ell_\alpha H) + \Gamma(N_2 \to \bar{\ell}_\alpha \bar{H})]}$$

Conclusion:

Type-I seesaw itself (only with SM + 3 RHNs) provides the MOST MINIMAL PLATFORM to explain neutrino mass, DM (lightest RHN), and baryon asymmetry.

- The **feeble interaction of the DM with** the bath is connected to the **lightness of the active neutrino mass** .

m_1

- Correct relic density uniquely determines $m_1 = \mathcal{O}(10^{-12})$ **eV** (remains falsifiable at KATRIN, PROJECT-8 experiments).

- **Relic density** turns out to be **independent to DM mass**.

- **DM is non-thermally produced** predominantly from the decay of the **SM gauge bosons**, thanks to the active-sterile neutrino mixing.

- The allowed range of **DM mass: 1 keV to 1 MeV**.

- **BAU** can be explained via **flavor leptogenesis** with $M_{2,3} \sim 10^{9-10}$ **GeV**.

Thank You !

Whats new? :

SM + 3 RHN

Attemps in past

νMSM

- Lightest RHN is **DM**
- DM produced via **Dodelson-Widrow** Mechanism
- BAU can be explained by coherent oscillation of heavy RHNs **(ARS mechanism)**

Shortfall

- Need **comparatively larger active-sterile mixing** to produce **required relic.**
- Such **high mixing** is completely **disallowed** by **X-ray exp.**
- A variant, **Shi-Fuller mechanism**, can be **operative**; however requires **fine tuning**.
- Other attempts require **additional fields and/or enhanced symmetry…**

Our Scenario

- Lightest RHN is **DM**
- DM **non-thermally produced** predominantly from decay of **SM gauge Bosons** and **higgs.**
- BAU can be explained by **Standard Thermal Leptogenesis** from **CP violating decay** of other **two heavy RHNs.**

Interesting Features

- Required **active-sterile mixing** to produce DM relic is **respecting** the **X-ray bound.**
- **Relic density** turns out to be independent to **DM mass.**
- The **smallness of the DM coupling** to the SM fields is connected to the **lightness of the lightest active neutrino mass.**

WIMP vs FIMP :

WIMP (abundance via freeze-out)

$$\frac{Hx}{Y_{DM}^{Eq}}\frac{dY_{DM}}{dx} = -\Gamma\left[\left(\frac{Y_{DM}}{Y_{DM}^{Eq}}\right)^2 - 1\right]$$

- **ann. Rate:** $\Gamma(= n_{DM}^{Eq}\langle\sigma v\rangle) >> H$
- **DM in thermal equilibrium**

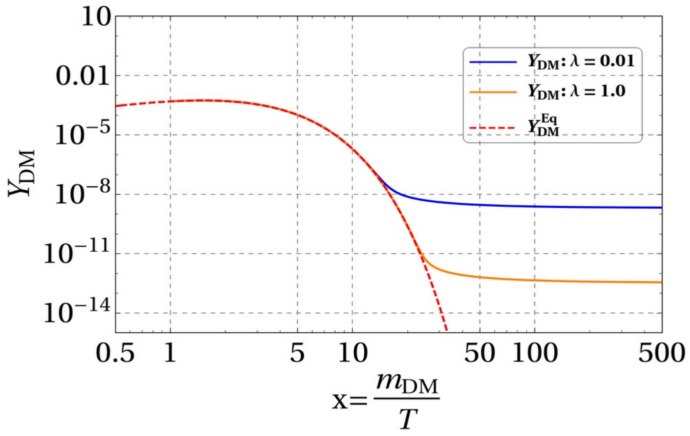

- **Direct detection constraints are applicable**

FIMP (abundance via freeze-in)

$$Hx\frac{dY_{DM}}{dx} = Y_p^{Eq}\frac{K_1}{K_2}\Gamma_{P\to DM,DM}$$

- **DM interact feebly with the bath :** $\Gamma_{P\to DM,DM} << H$
- **DM never reach thermal equilibrium**

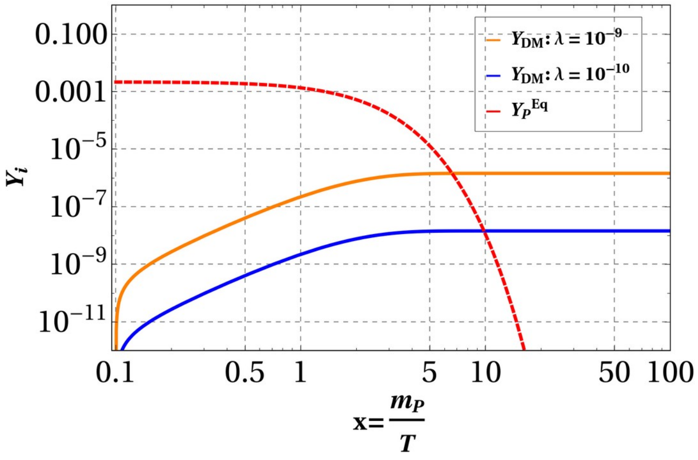

- **Direct detection is practically impossible (coupling $\sim 10^{-10}$)**

Neutrinos :

What we know:
(from Neutrino oscillation)

- 3 mixing angles
- 2 mass-square difference
- CP-violating phase (?)

Don't

What we know:

- Origin of neutrino mass
- Nature [Dirac/Majorana]
- Absolute neutrino mass

SM Fails to accomodate the tiny neutrino mass

Hunting for ultra-light axion dark matter in the Dark Ages

ICTP Summer School on Cosmology 2022
7th July 2022

Eleonora Vanzan

Università degli Studi di Padova

INFN Padova

Why ULAs?

- Mass range: $m_a \sim 10^{-19} - 10^{-21}$ eV

Why ULAs?

- Mass range: $m_a \sim 10^{-19} - 10^{-21}$ eV

- Puzzles in the cold dark matter model: lack of structures on small scales with respect to predictions

Why ULAs?

- Mass range: $m_a \sim 10^{-19} - 10^{-21}$ eV

- Puzzles in the cold dark matter model: lack of structures on small scales with respect to predictions

$\Longrightarrow$ If dark matter is comprised of very light bosons or axions, large-scale predictions are the same as in ΛCDM, but small-scale structure is suppressed by the particle's large de Broglie wavelength (fuzzy dark matter)

ULAs effects on the matter power-spectrum

$$\frac{\partial \delta_c}{\partial t} = -\theta_c \tag{1a}$$

$$\frac{\partial \theta_c}{\partial t} = -\frac{3H^2}{2}\left(\Omega_c \delta_c + \Omega_b \delta_b\right) - 2H\theta_c + \frac{k^4 \delta_c}{4 m_a^2 a^4} \tag{1b}$$

$$\frac{\partial \delta_b}{\partial t} = -\theta_b \tag{1c}$$

$$\frac{\partial \theta_b}{\partial t} = -\frac{3H^2}{2}\left(\Omega_c \delta_c + \Omega_b \delta_b\right) - 2H\theta_b + \frac{c_s^2 k^2}{a^2}\delta_b \tag{1d}$$

ULAs effects on the matter power-spectrum

$$\frac{\partial \delta_c}{\partial t} = -\theta_c \tag{1a}$$

$$\frac{\partial \theta_c}{\partial t} = -\frac{3H^2}{2}\left(\Omega_c\delta_c + \Omega_b\delta_b\right) - 2H\theta_c + \frac{k^4\delta_c}{4m_a^2a^4} \tag{1b}$$

$$\frac{\partial \delta_b}{\partial t} = -\theta_b \tag{1c}$$

$$\frac{\partial \theta_b}{\partial t} = -\frac{3H^2}{2}\left(\Omega_c\delta_c + \Omega_b\delta_b\right) - 2H\theta_b + \frac{c_s^2k^2}{a^2}\delta_b \tag{1d}$$

axion effective sound speed $c_a^2 \approx \frac{k^2}{4m_a^2a^2}$

suppresses power on scales $k_{J,a} \sim a\sqrt{Hm_a}$ with respect to the cdm case

ULAs effects on the matter power-spectrum

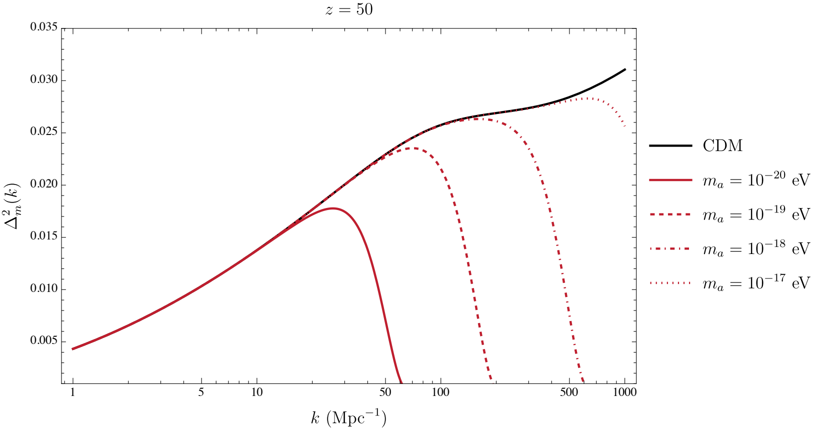

Idea

- Why the Dark Ages $z \sim 30 - 200$?

Idea

- Why the Dark Ages $z \sim 30 - 200$?

- 21cm line intensity mapping will be a powerful probe

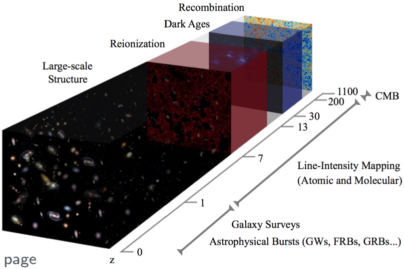

Figure from Ely Kovetz's page

Idea

- Why the Dark Ages $z \sim 30 - 200$?

- 21cm line intensity mapping will be a powerful probe

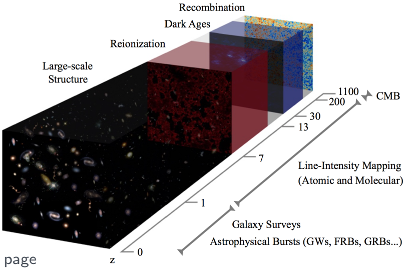

Figure from Ely Kovetz's page

- Look for the effects of ULAs on the angular power-sepctrum, the C_ℓs

21cm C_ℓ: first order

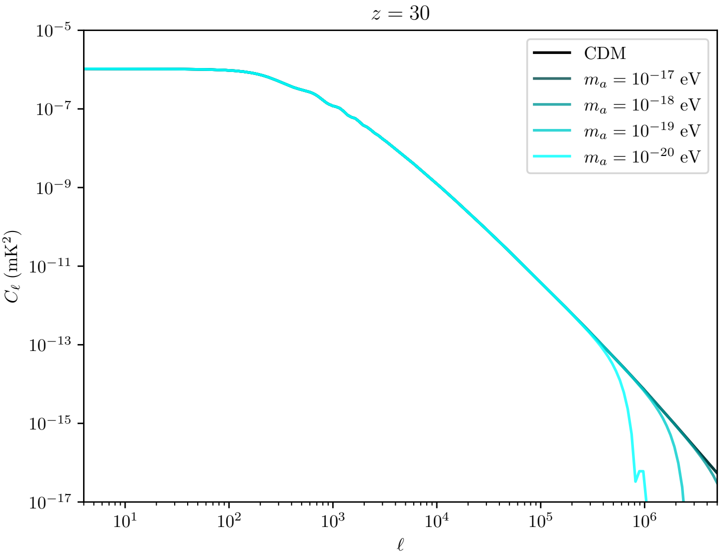

21cm C_ℓ: first order

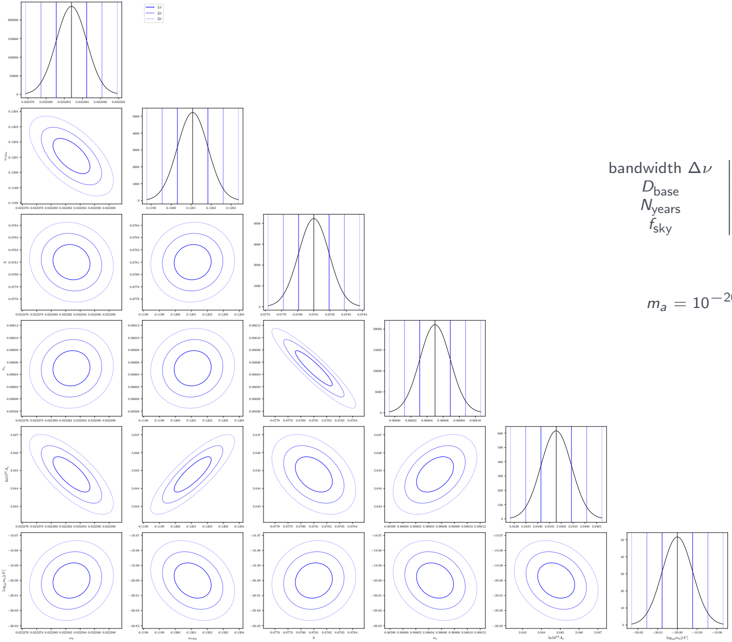

bandwidth $\Delta\nu$	1 MHz
D_{base}	3474 km
N_{years}	10
f_{sky}	0.75

$m_a = 10^{-20}$ eV

21cm C_ℓ: second order effects

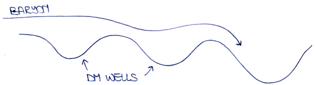

Relative velocity $v_{\rm bc}$ between baryons and cdm at recombination $\longrightarrow$ important on scales $k_{v_{\rm bc}} \equiv \left.\frac{aH}{\sqrt{\langle v_{\rm bc}^2 \rangle}}\right|_{\rm decoupling} \sim 30 - 40\ {\rm Mpc}^{-1}$

21cm C_ℓ: second order effects

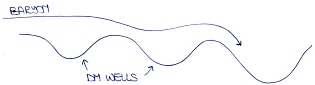

Relative velocity $v_{\rm bc}$ between baryons and cdm at recombination $\longrightarrow$ important on scales $k_{v_{\rm bc}} \equiv \left.\frac{aH}{\sqrt{\langle v_{\rm bc}^2\rangle}}\right|_{\rm decoupling} \sim 30 - 40\ \mathrm{Mpc}^{-1}$

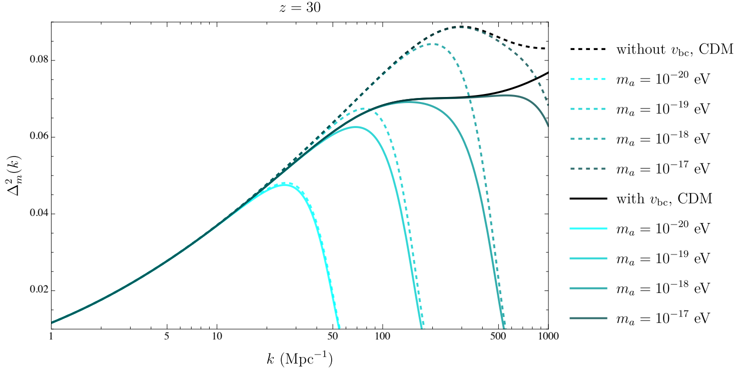

21cm C_ℓ: second order effects

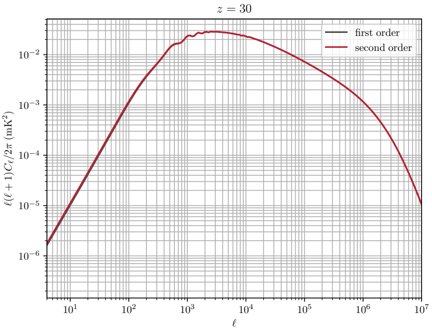

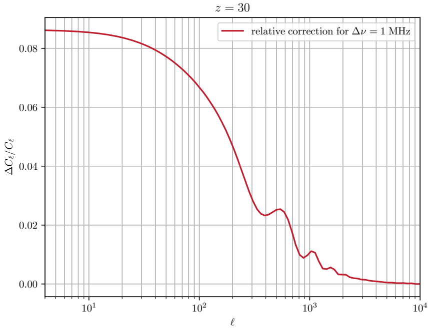

21cm C_ℓ: second order effects

21cm C_ℓ: second order effects

Thank you for your attention.

Literature

- for ULAs: Marsh 2015 **1504.00308**
- for baryon-dark matter relative velocity at recombination: Tseliakhovich & Hirata 2010 **1005.2416**
- for second order relative velocity effects on 21cm: Ali-Haïmoud, Meerburg, Yuan 2014 **1312.4948**

The spin bias of dark-matter halos

Beatriz Tucci

Max Planck Institute for Astrophysics

In collaboration with Raul Abramo,
Antonio Montero-Dorta and Fabian Schmidt

beatriz.tucci@gmail.com
wwwmpa.mpa-garching.mpg.de/~tucci

MAX-PLANCK-GESELLSCHAFT

Fundação de Amparo à Pesquisa do Estado de São Paulo

Outline

Secondary Bias
Low-Mass Spin Bias
High-Mass Spin Bias
Spin Bias in observations
Conclusions

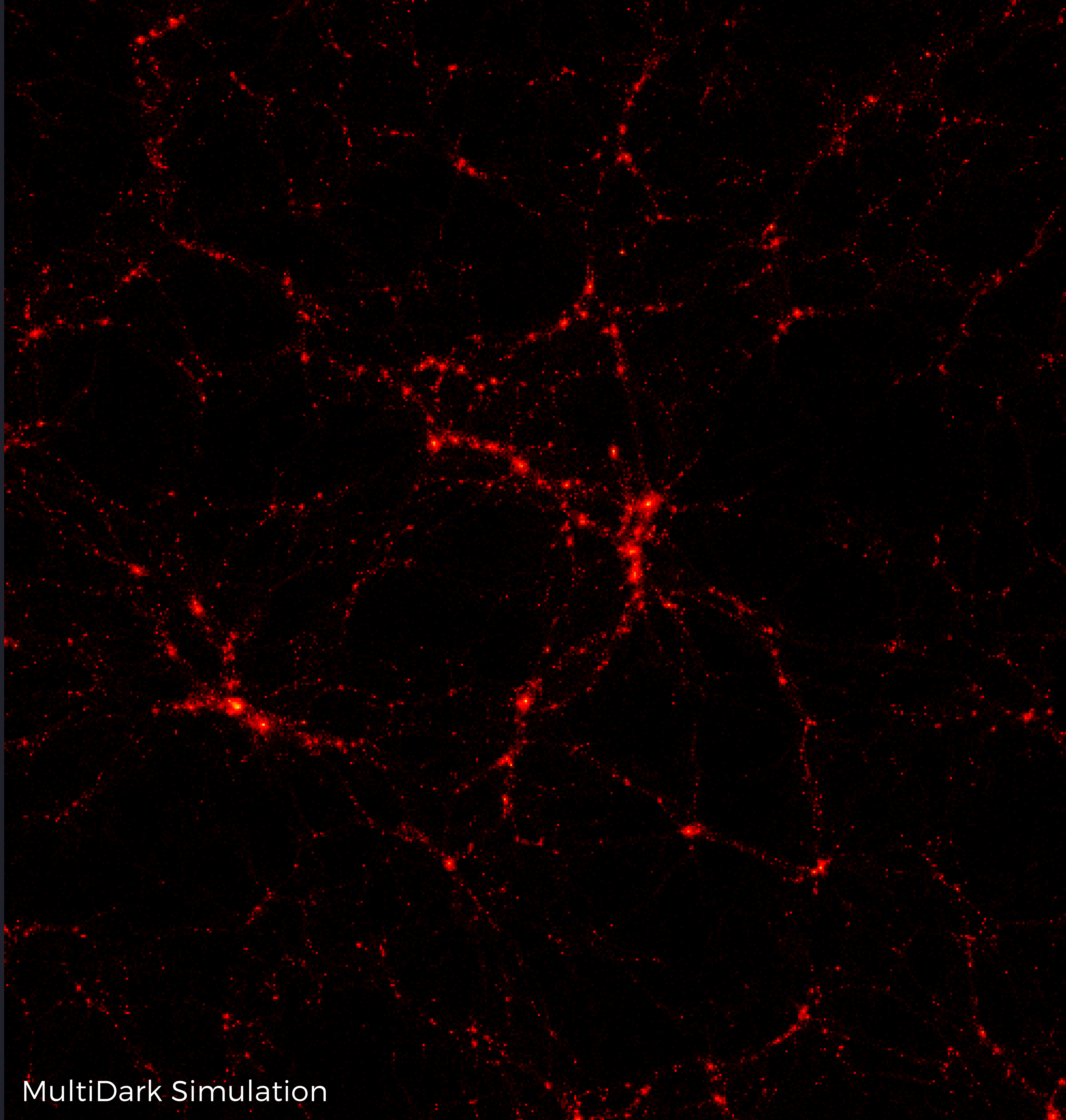

MultiDark Simulation

Large Scale Structure

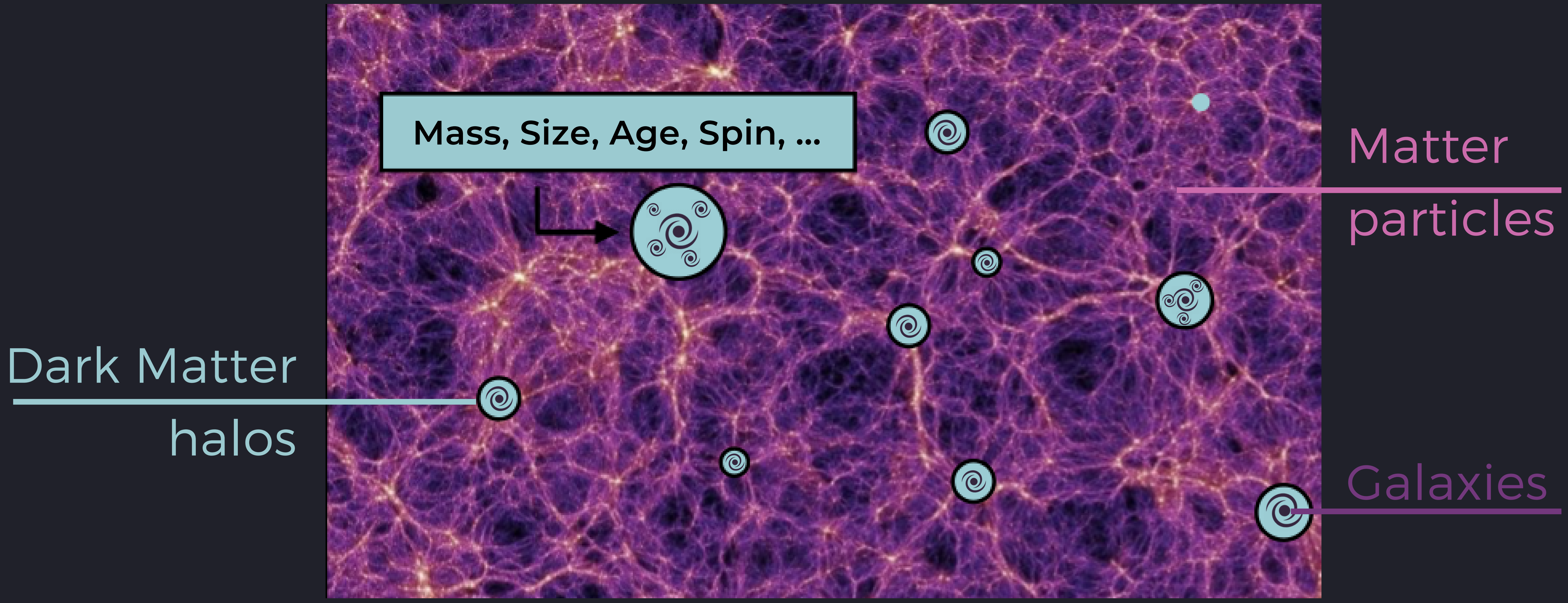

Millennium Simulation

Bias

$$\delta_g(\mathbf{x}) \supset b_1\, \delta_m(\mathbf{x})$$

Cooray & Sheth (2002)

What we observe

galaxies
quasars
clusters

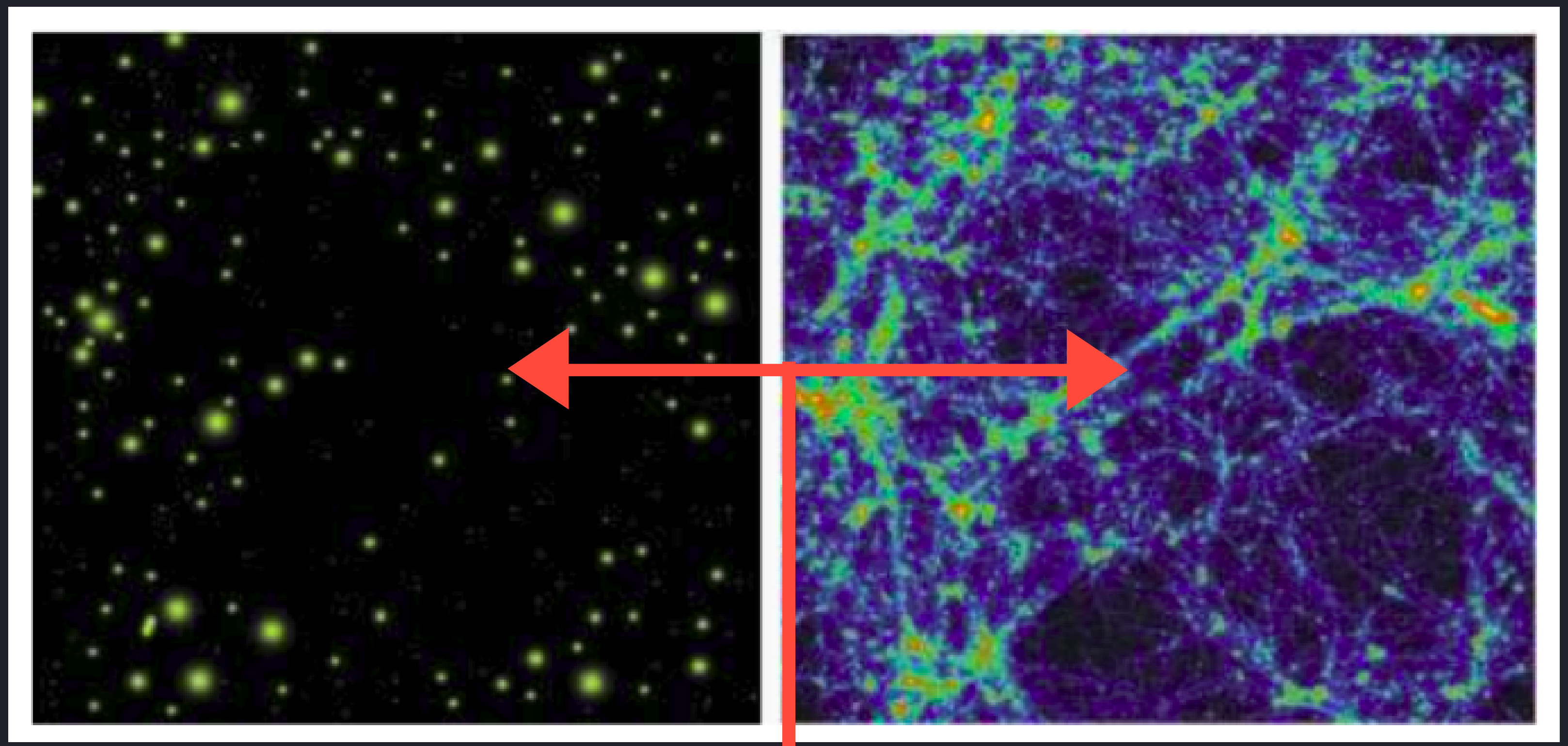

matter distribution

$$\delta_g(\mathbf{x}) \equiv \frac{n_g(\mathbf{x})}{\bar{n}_g} - 1 \qquad \delta_m(\mathbf{x}) \equiv \frac{\rho_m(\mathbf{x})}{\bar{\rho}_m} - 1$$

new physics

Secondary Halo Bias

Halo mass is usually considered the primary bias property.

At fixed mass, halo clustering depends on several secondary halo properties:

- age
- concentration
- spin
- shape
- substructure...

Sheth & Tormen (2004)
Gao et al. (2005)
Wechsler et al. (2006)
Gao & White (2007)
Sato-Polito et al. (2019)

Sato-Polito et al. (2019)

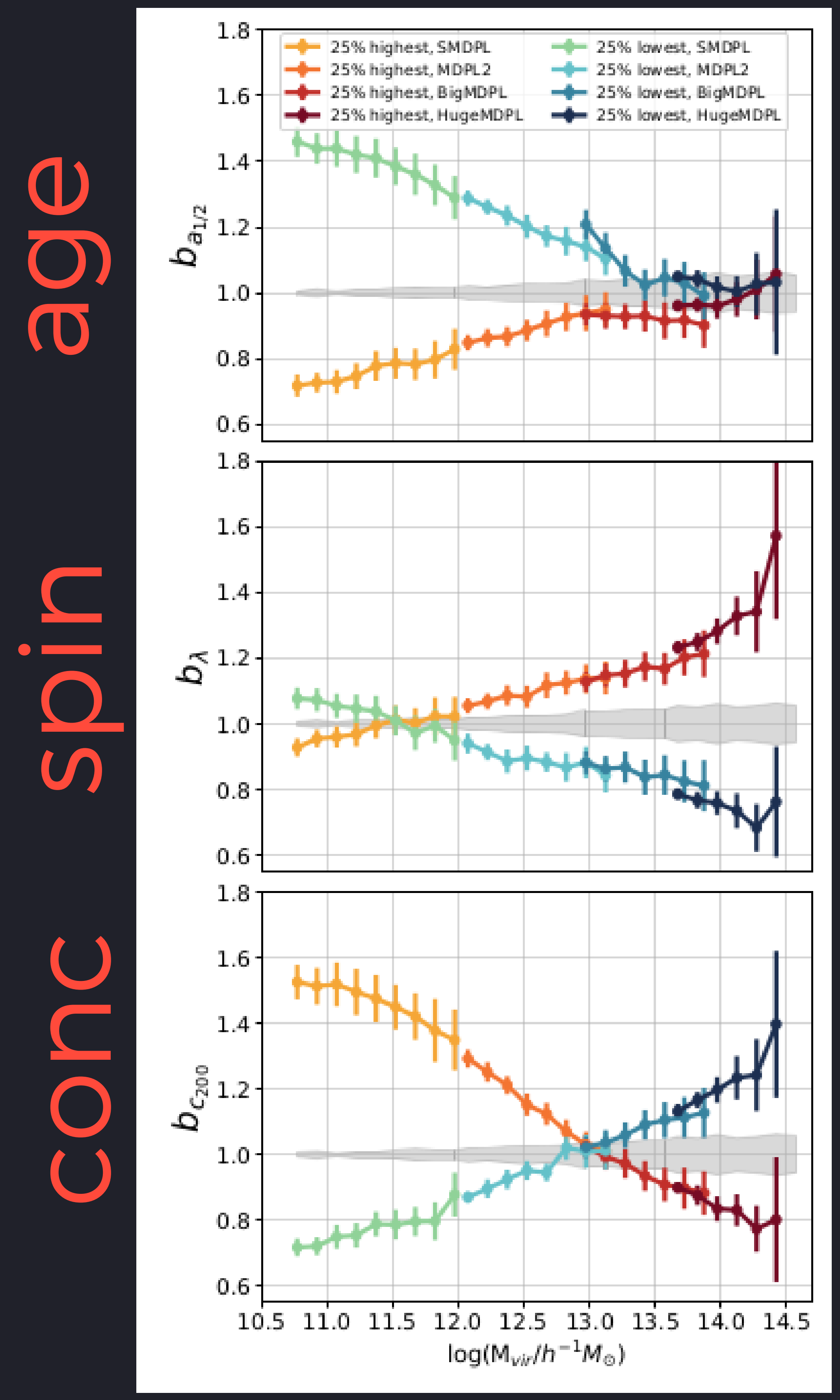

halo mass

Secondary Halo Bias

To this day, we have neither an agreement in the scientific community about **observational evidence** of secondary bias, nor a complete **analytical framework** to explain all the trends seen in simulations

Sato-Polito et al. (2019)

age

spin

conc

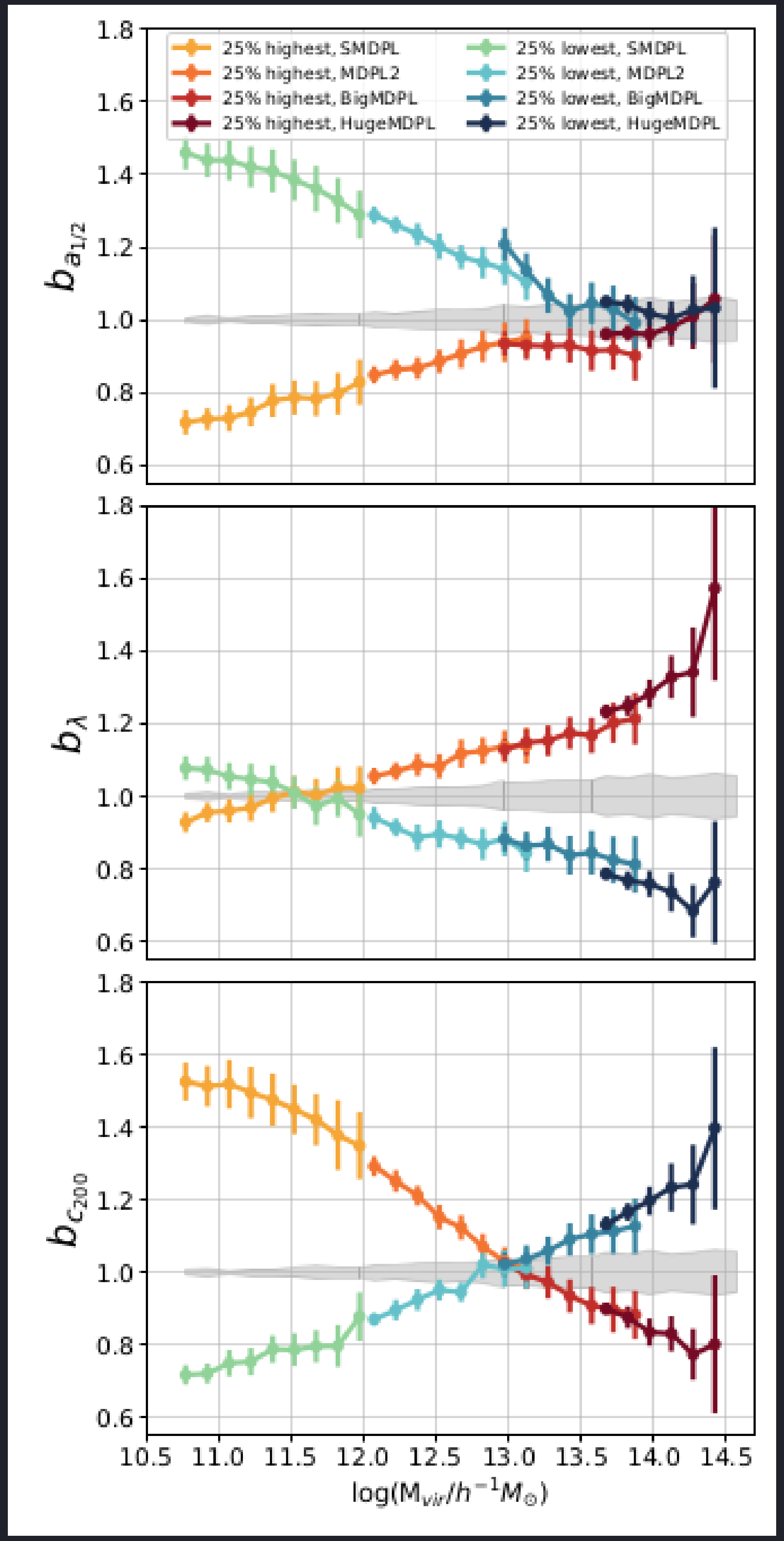

halo mass

Assembly Bias

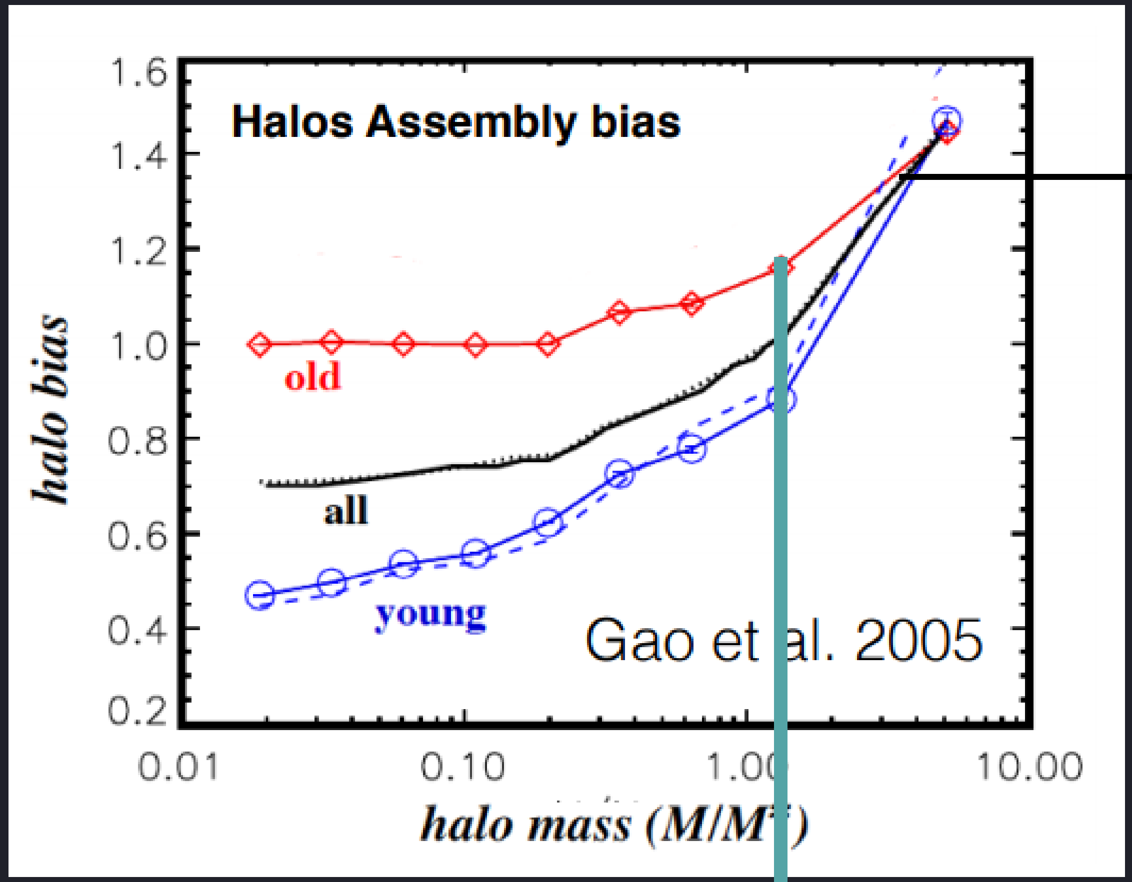

High-mass halos have higher bias

at fixed mass, halos that assembled earlier (older) are more tightly clustered than halos that assembled later (younger)

$\log(M_{\rm vir}/M_{\odot}h^{-1}) = 10.8$

5% more concentrated 5% less concentrated

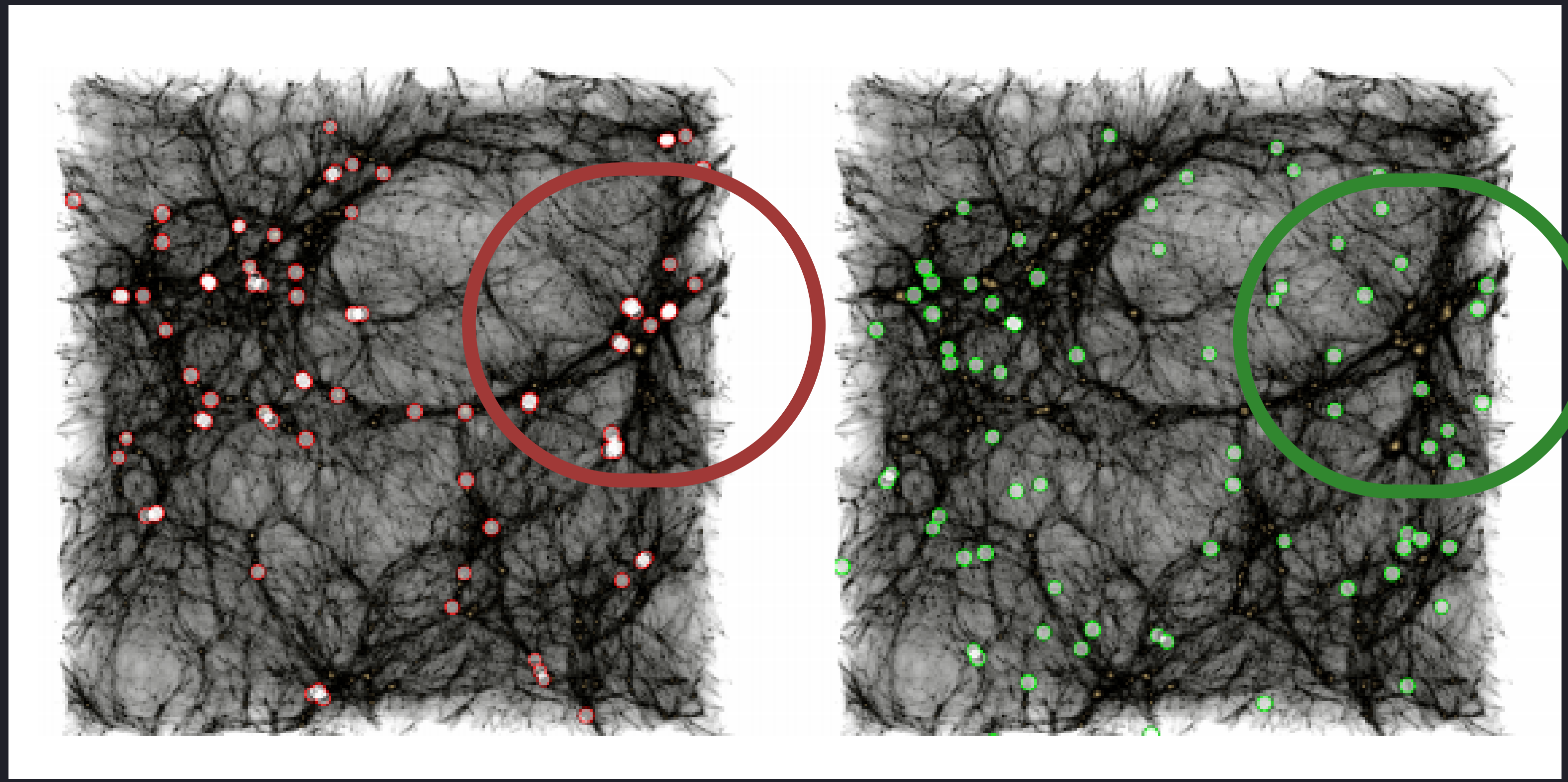

Li, Mo & Gao (2008);
Wechsler & Tinker (2018)

Spin Bias

$b(\lambda|\mathrm{M_{vir}})$

The secondary dependence of halo clustering on spin at fixed halo mass

Gao & White (2007)
Bett et al. (2007)
Sato-Polito et al. (2019)
Johnsonn et al. (2020)
Tucci et al. (2021)
Lazeyras et al. (2021)

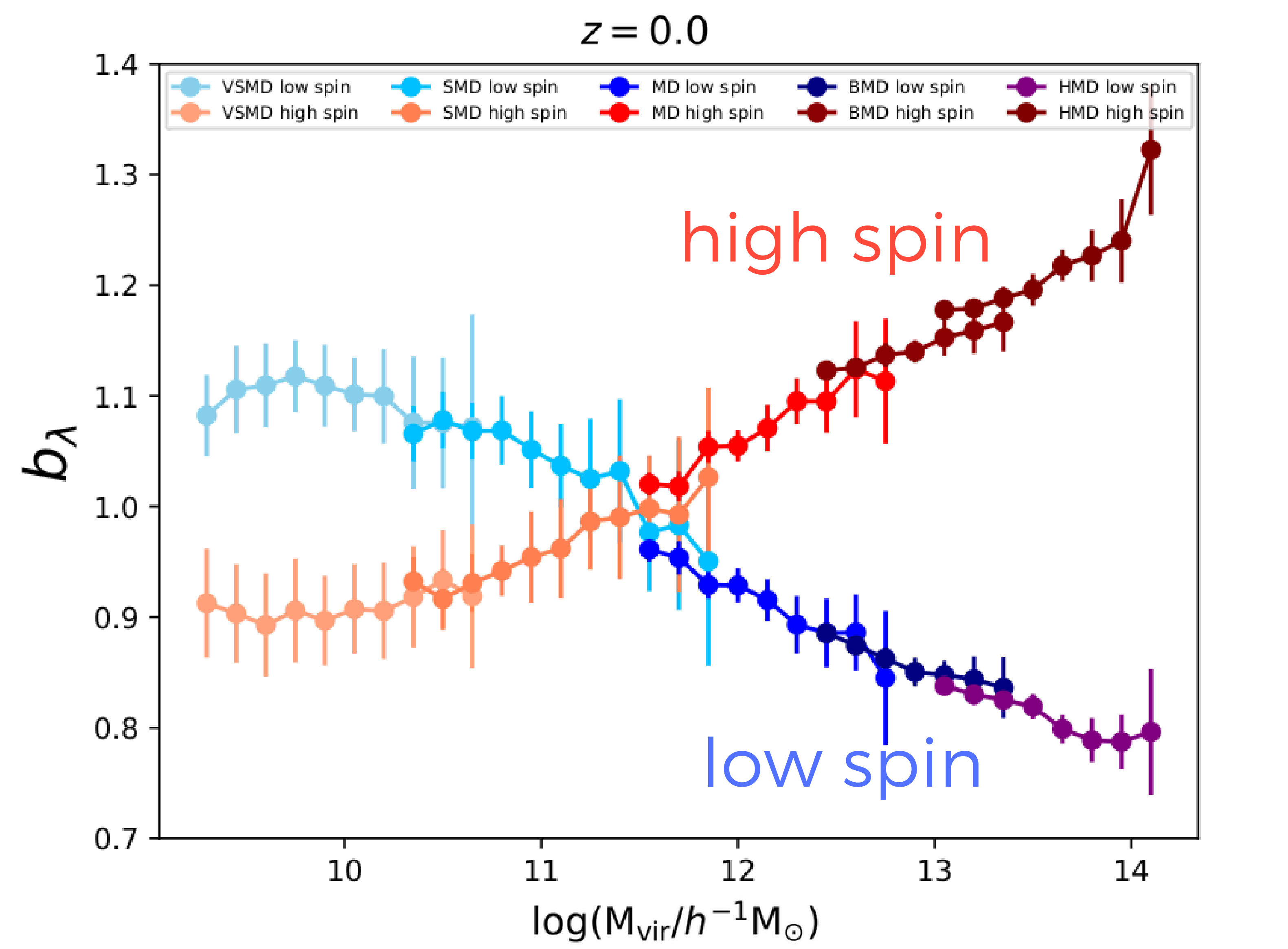

halo mass

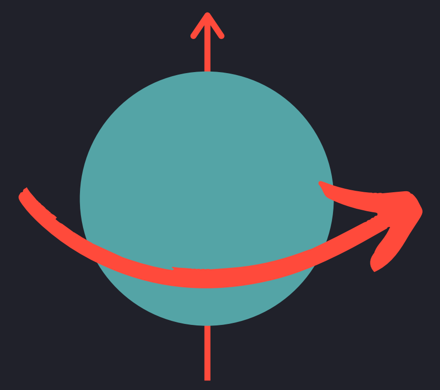

$$\lambda = \frac{|J|}{\sqrt{2}\, M_{\mathrm{vir}}\, V_{\mathrm{vir}}\, R_{\mathrm{vir}}}$$

The Spin Bias of Dark Matter Halos

Low-mass spin bias

Sato-Polito et al. (2019)
Johnsonn et al. (2020)
Tucci et al. (2021)

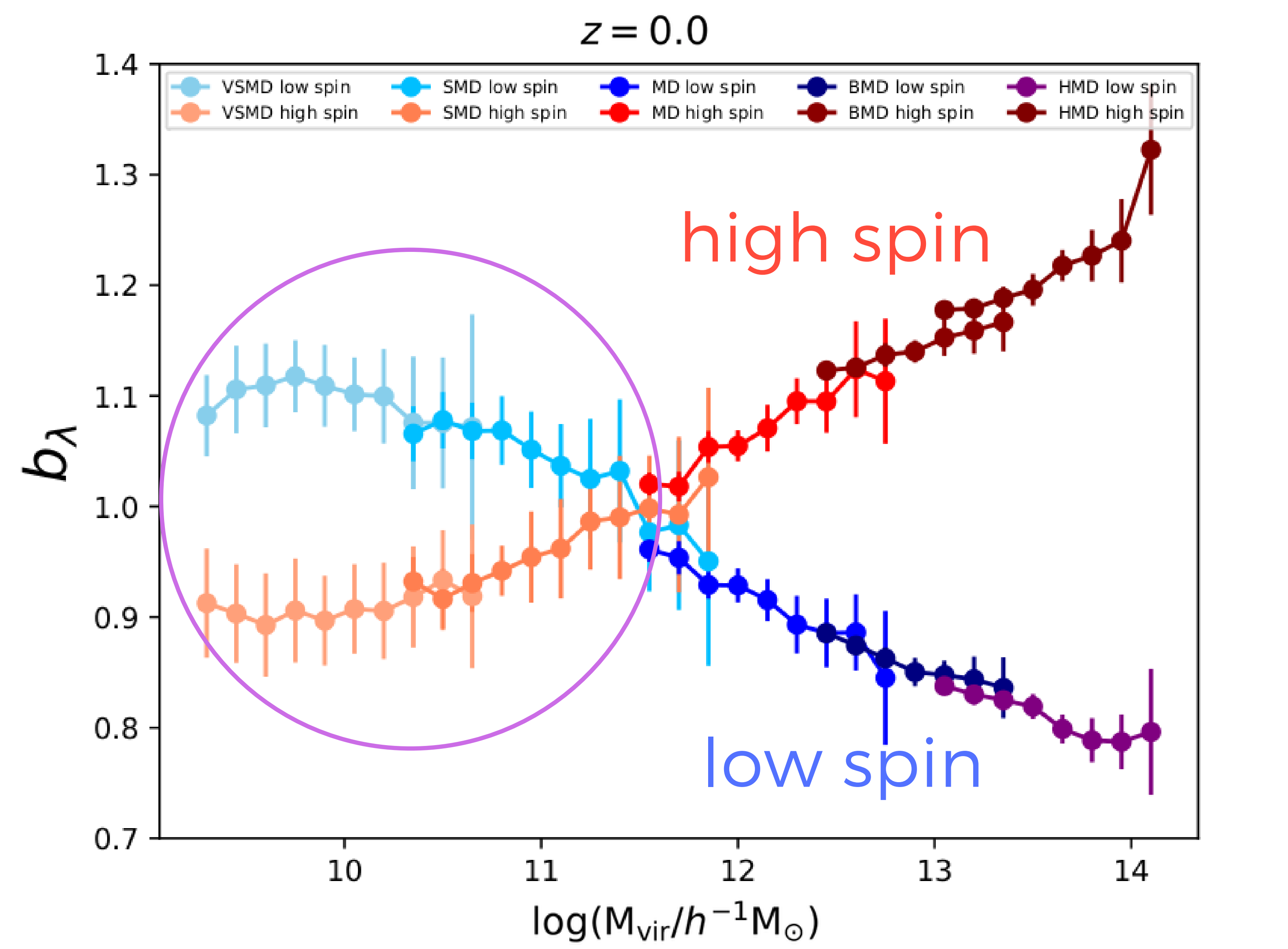

halo mass

Splahsback Halos

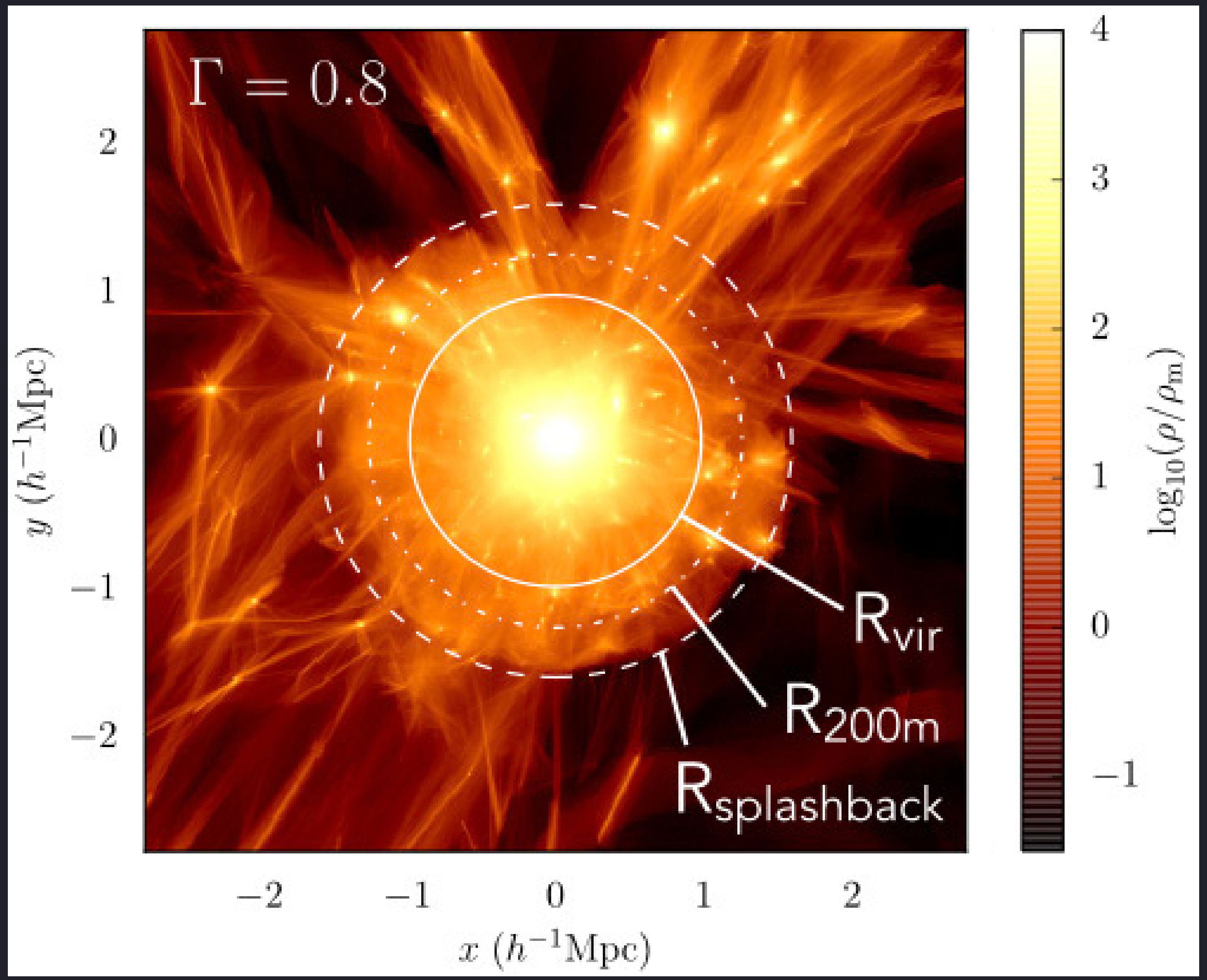

http://www.benediktdiemer.com/research/splashback/

They are small halos that live in the vicinity of massive halos up to the so-called splashback radius (e.g., Wang et al. 2009, Adhikari et al. 2014)

Splashback halos are distinct halos that were subhalos at some previous time, i.e., passed through the virial radius of a larger halo

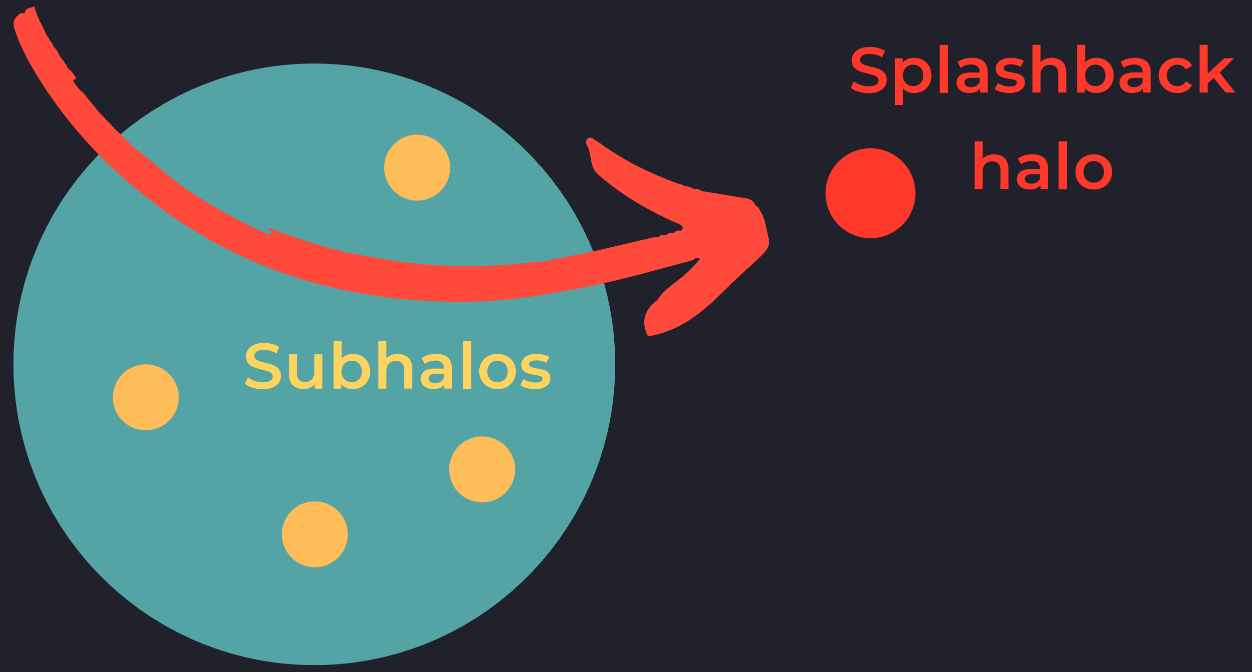

Known to be one of the main causes of low-mass assembly bias (i.e., secondary dependence on halo assembly history) at the low-mass end (e.g., Dalal 2008, Sunayama et al. 2016, Mansfield & Kravtsov 2020)

Low-Mass Spin Bias

Tucci et al. (2021)
MNRAS, 500 3, 2777–2785
arXiv:2007.10366

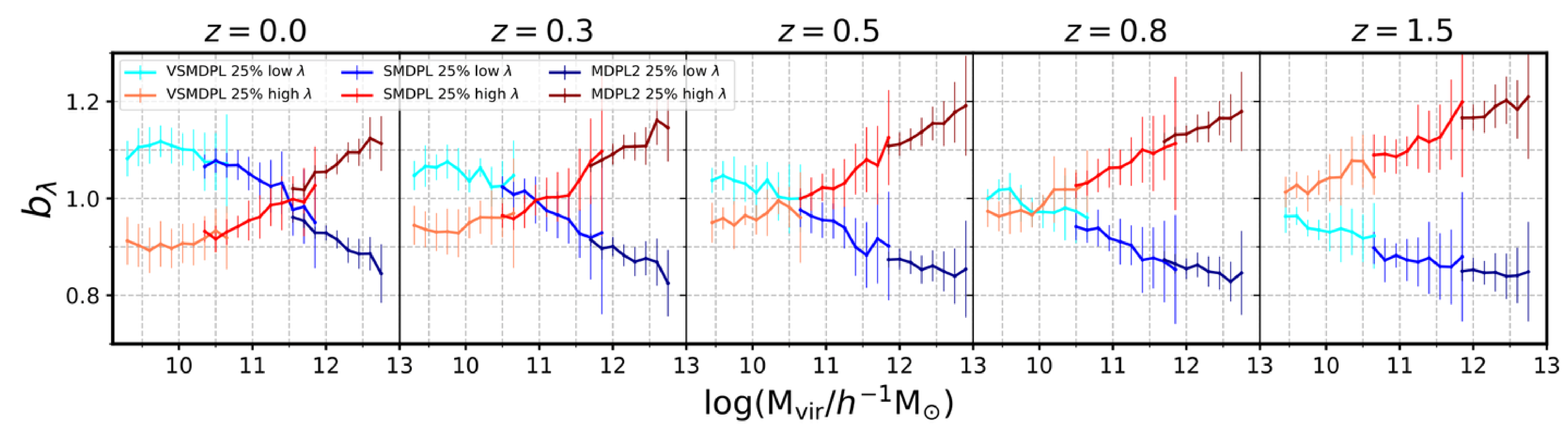

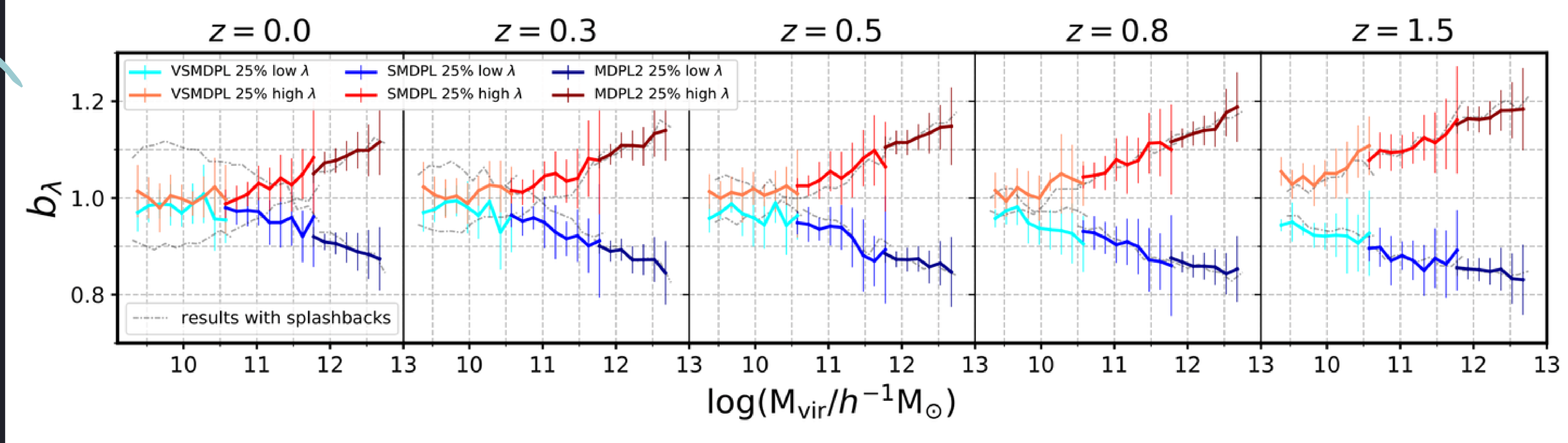

low-mass spin bias
inversion disappears
after removing
splashback halos

Tidal Stripping

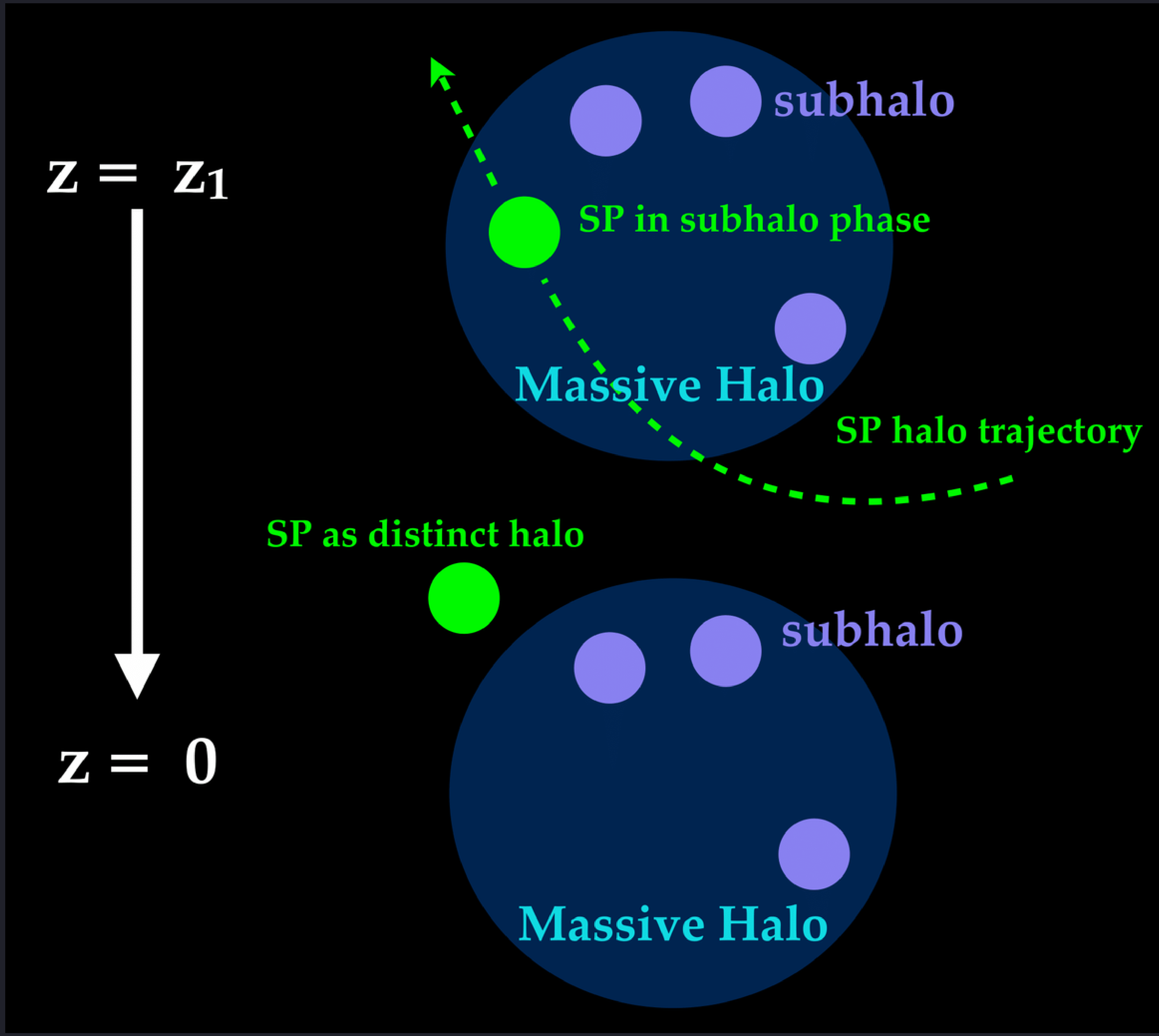

Tidal stripping in dense environments (high b), makes SP halos lose mass and angular momentum (spin), specially during the "subhalo" phase

Kravtsov et al. (2004)
Green & van den Bosch (2019)
Lee et al. (2018)

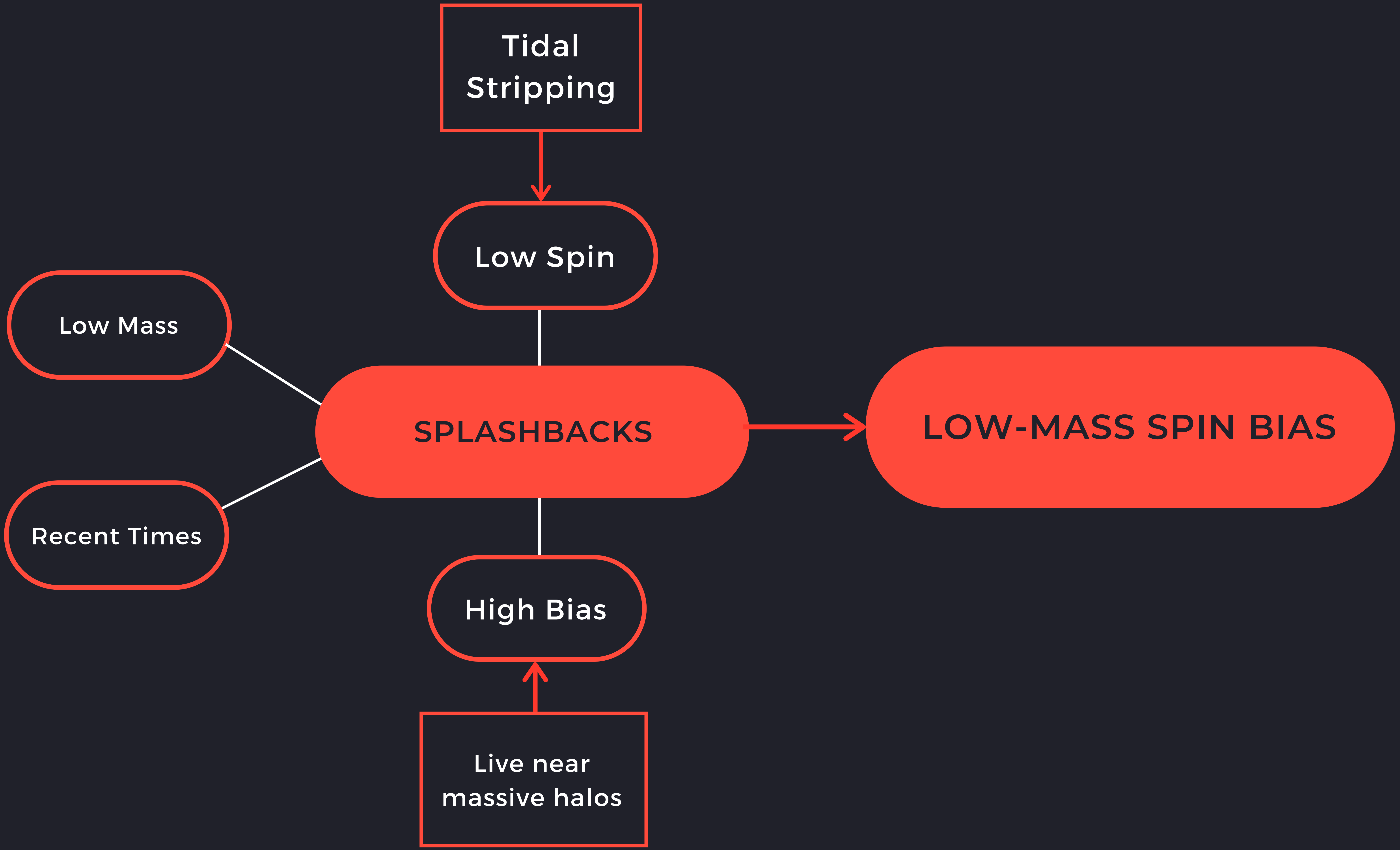
Tidal Stripping
Low Spin
Low Mass
SPLASHBACKS
LOW-MASS SPIN BIAS
Recent Times
High Bias
Live near massive halos

The Spin Bias of Dark Matter Halos

Low-mass spin bias

Tucci et al. (2021)

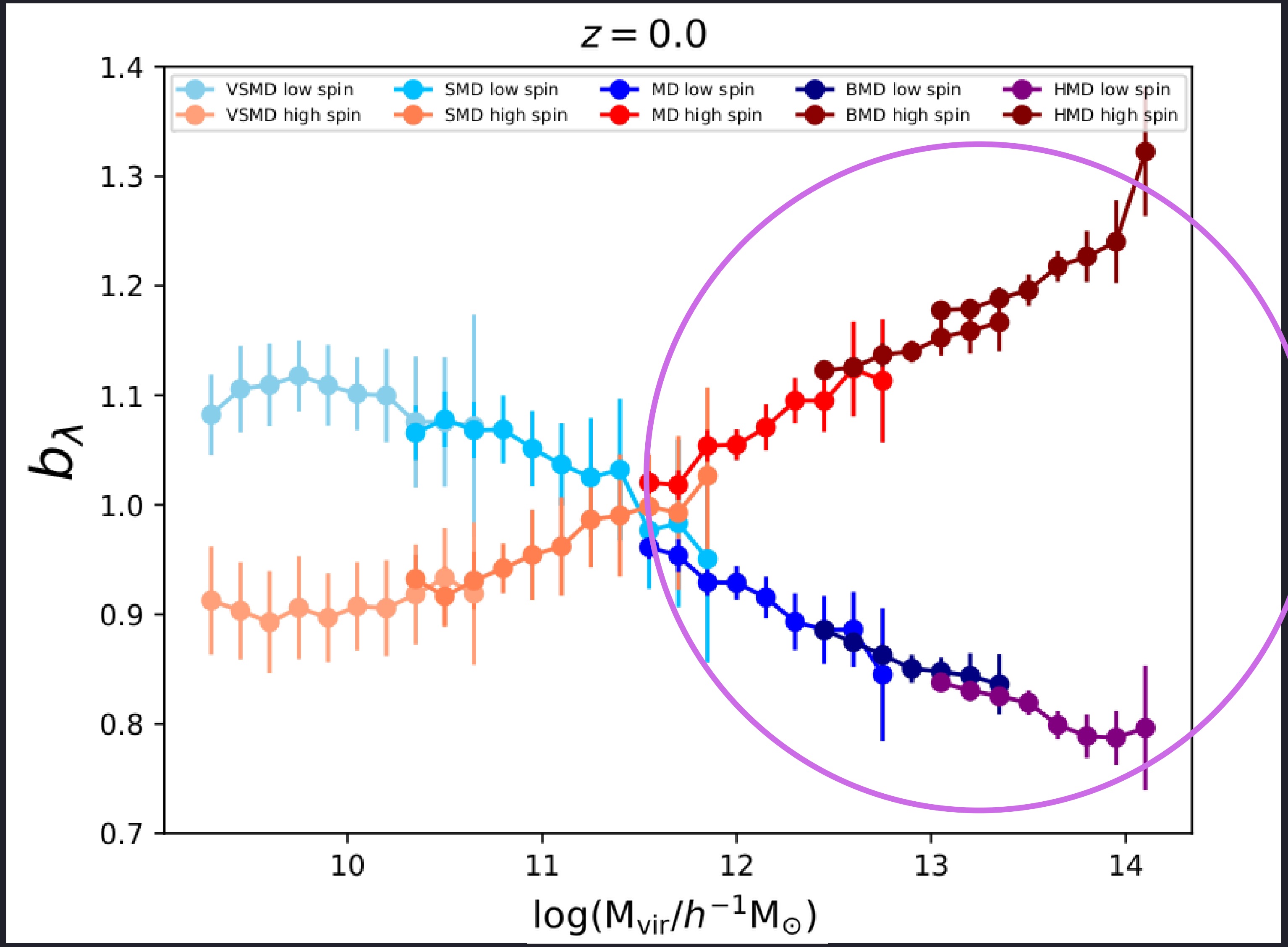

halo mass

High-mass spin bias

Spin bias from peak curvature

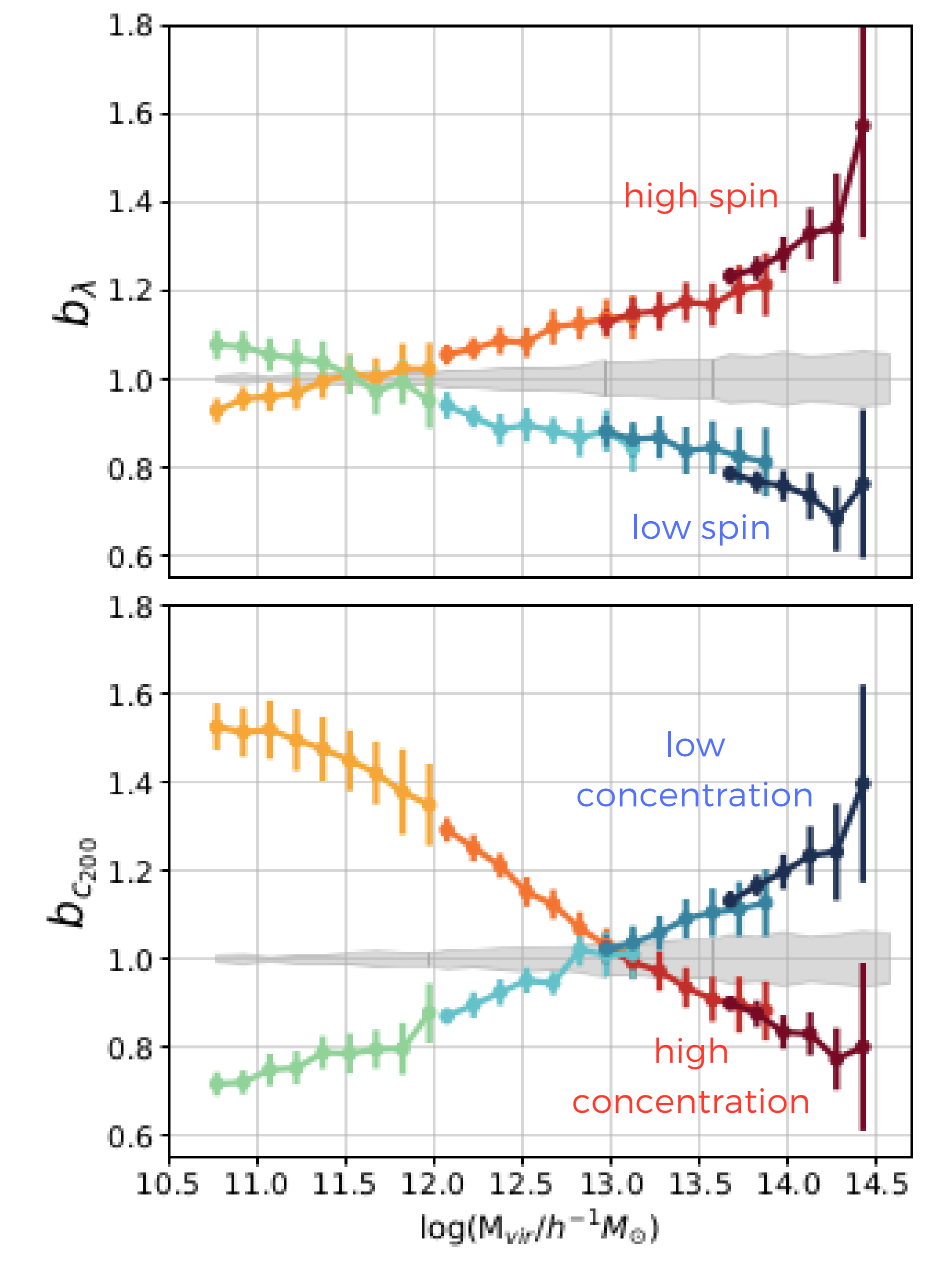

Sato-Polito et al. (2019)

Bardeen et al. (1986) Halos with a shallower peak curvature have a higher bias at fixed peak height

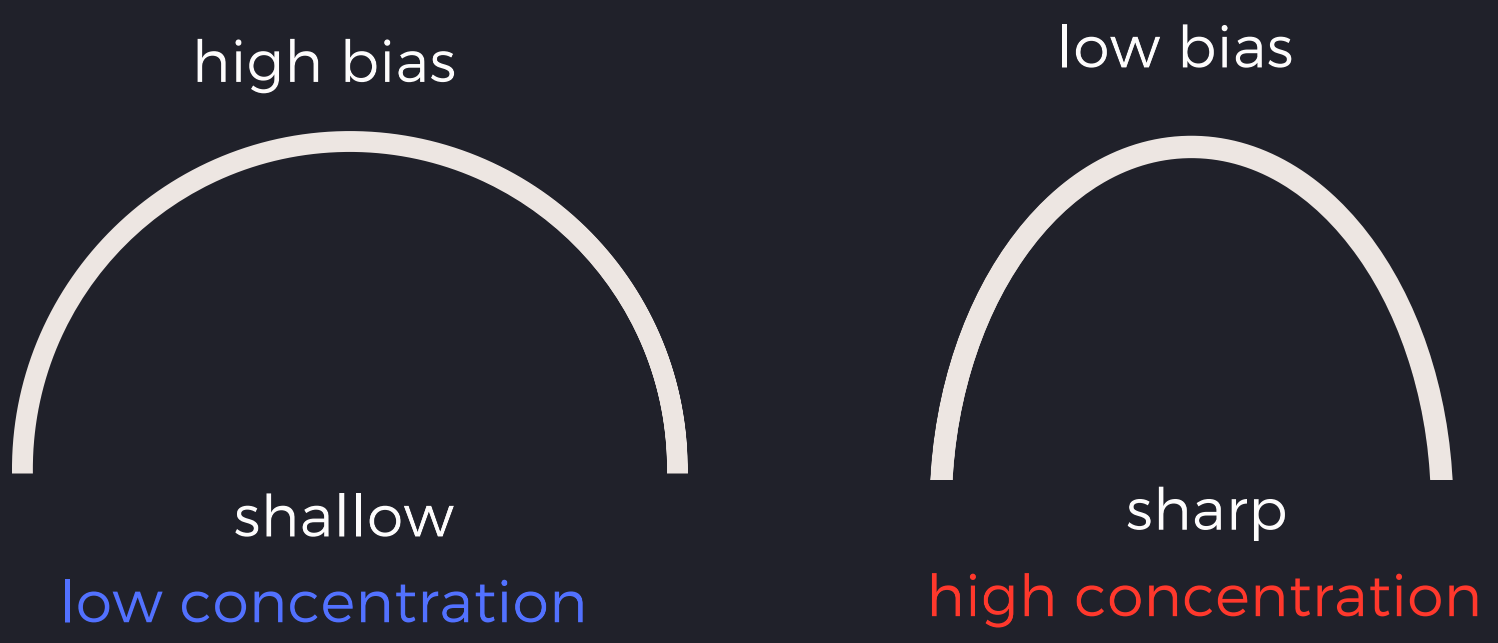

Dalal et al. (2008) High-mass assembly bias reflects the fact that low concentration halos formed from shallower peaks

Spin bias from peak curvature

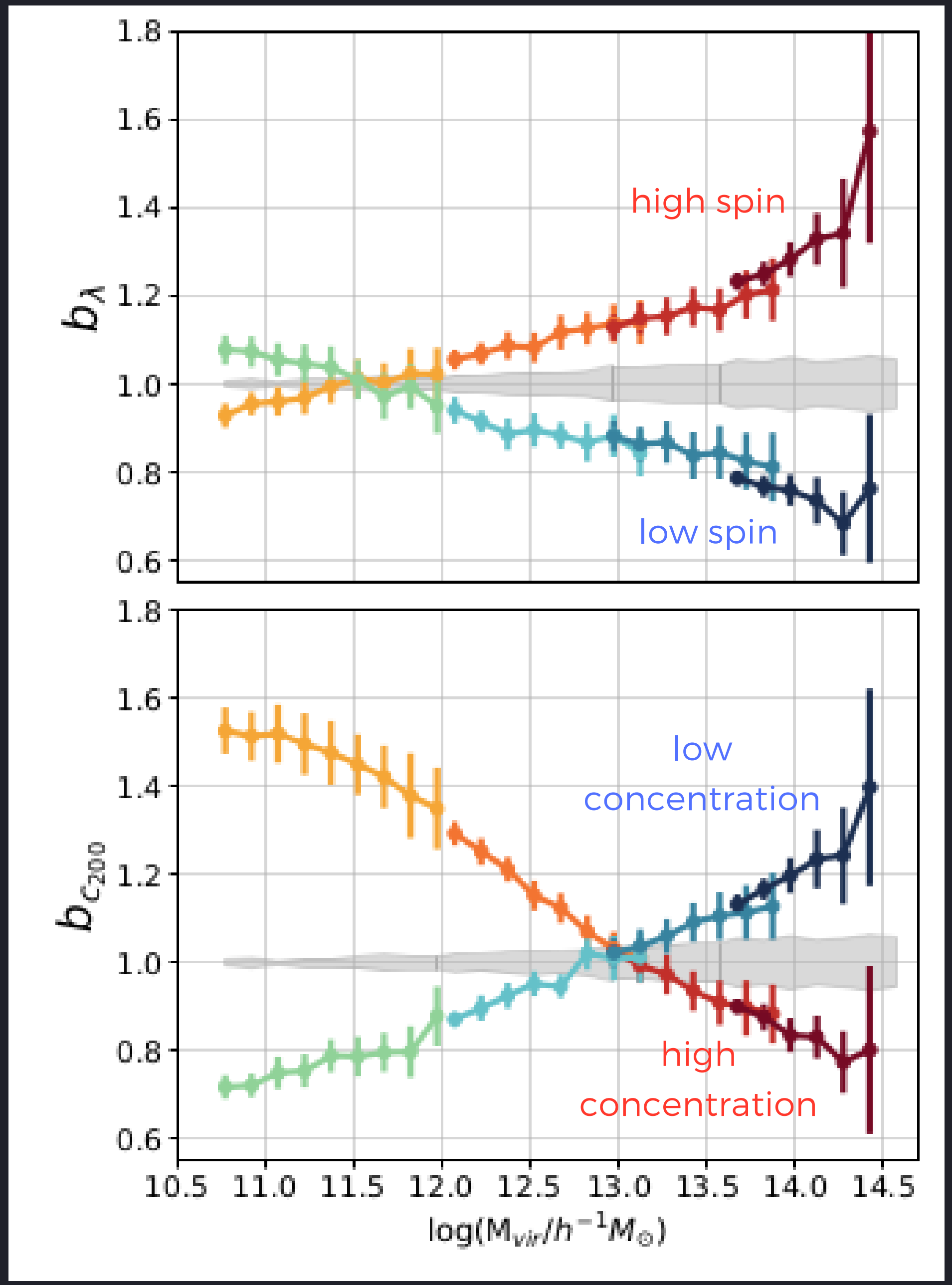

Sato-Polito et al. (2019)

Bardeen et al. (1986) Halos with a shallower peak curvature have a higher bias at fixed peak height

high bias

shallow

low concentration

↕

high spin!

low bias

sharp

high concentration

↕

low spin!

Catelan & Theuns (1986)

$$L \propto \frac{1}{x}$$

curvature
(sharpness of the peak)

Spin bias from ESP

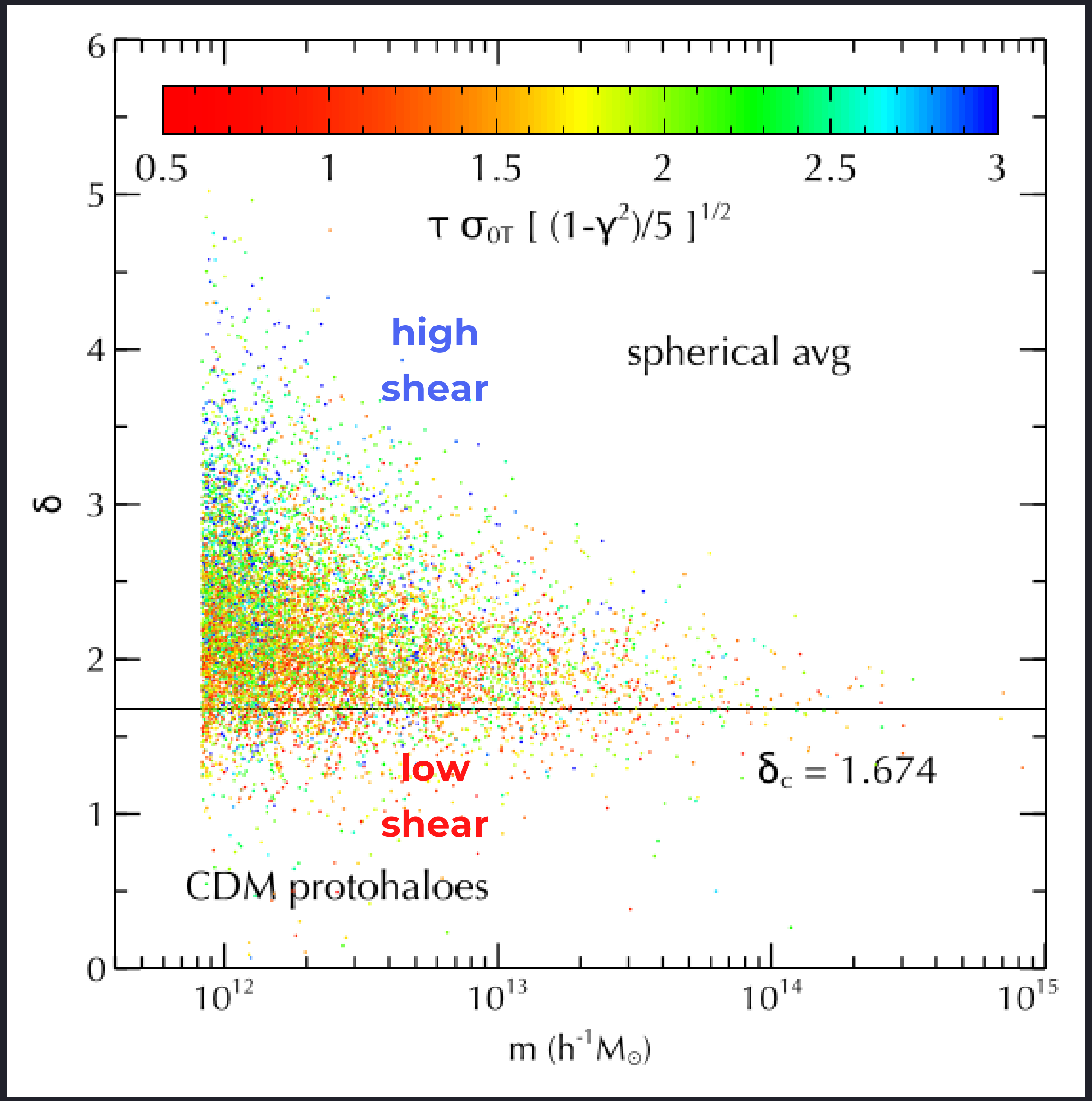

Castorina et al. (2016)

Halo formation depends on initial shear

Sheth, Mo & Tormen (2001)
Sheth & Tormen (2002)

ESPτ

$$B = \delta_c + \beta\, \sigma_{0T}\, \tau \sqrt{(1-\gamma^2)/5}$$

misalignment between shape and shear

angular momentum!

$$L_\alpha(t) = a^2(t)\dot{D}(t)\, \varepsilon_{\alpha\beta\gamma}\, \mathcal{D}_{\beta\sigma}\, \mathcal{I}_{\sigma\gamma}$$

Tidal Torque Theory (TTT)

Doroshkevich (1970)
White (1984)
Heavens & Peacock (1988)
Catelan & Theuns (1986)

Preliminar results

Following methodology of Hahn & Paranjape (2014)

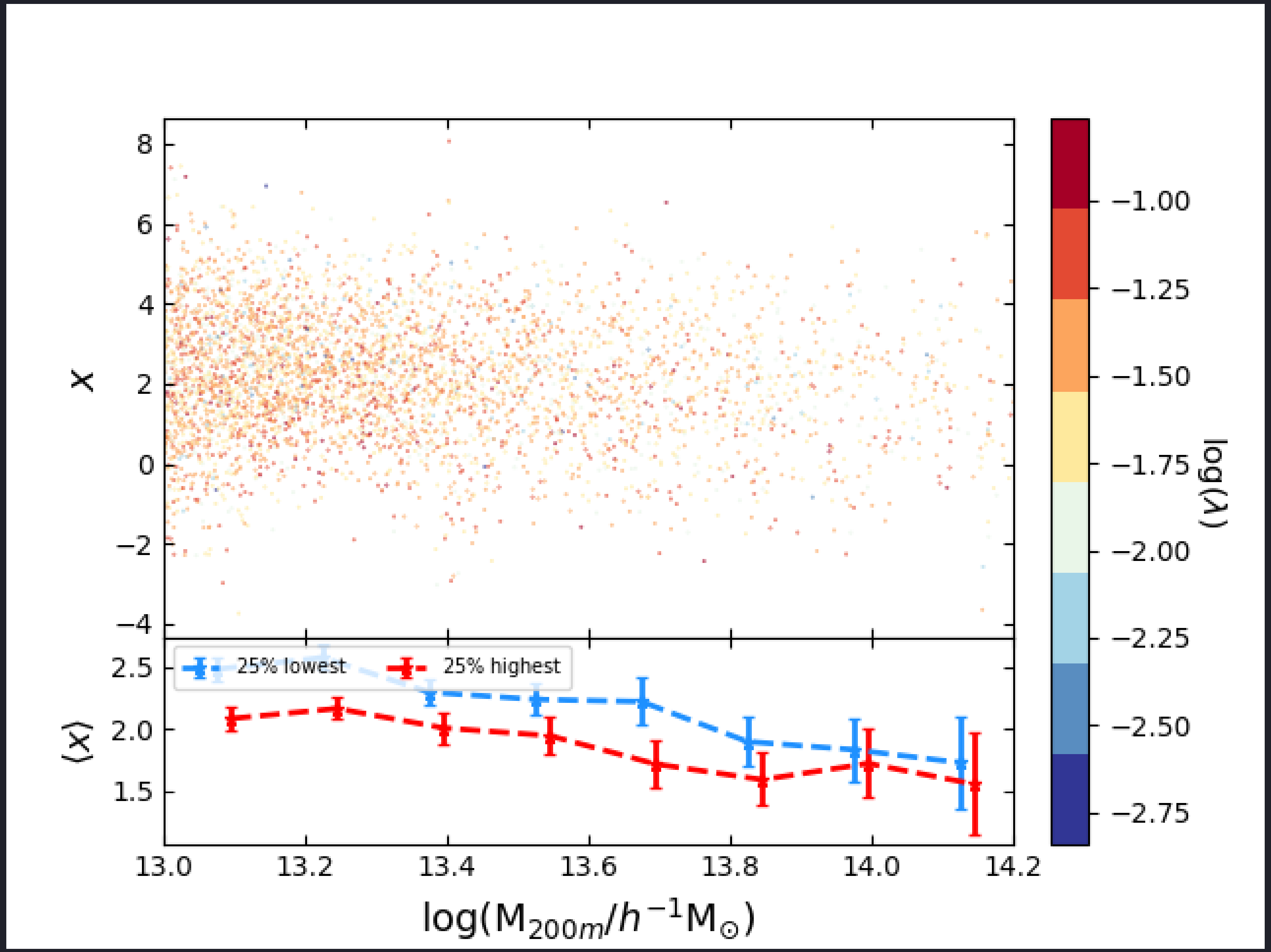

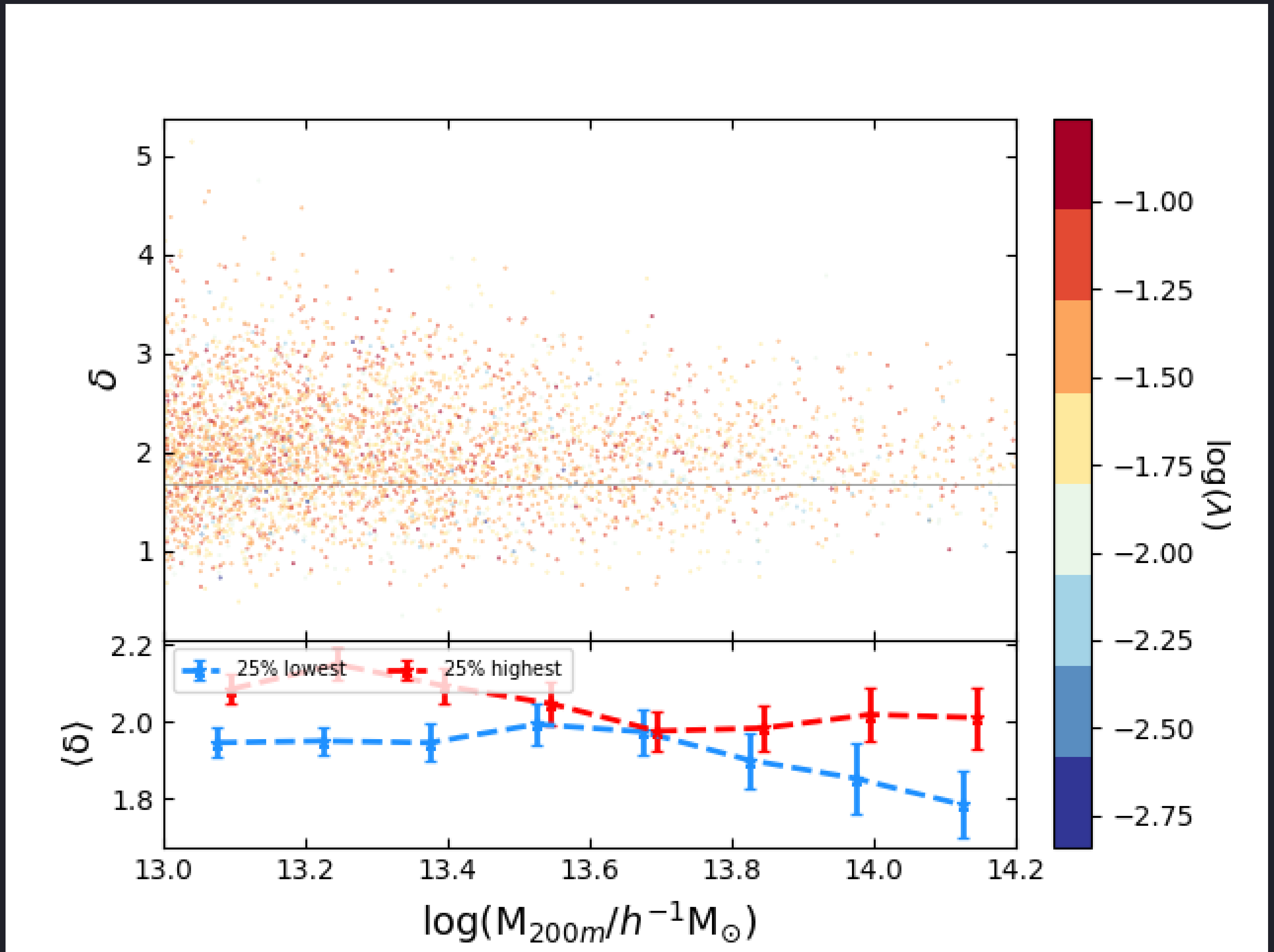

How can we detect halo spin bias and observations?

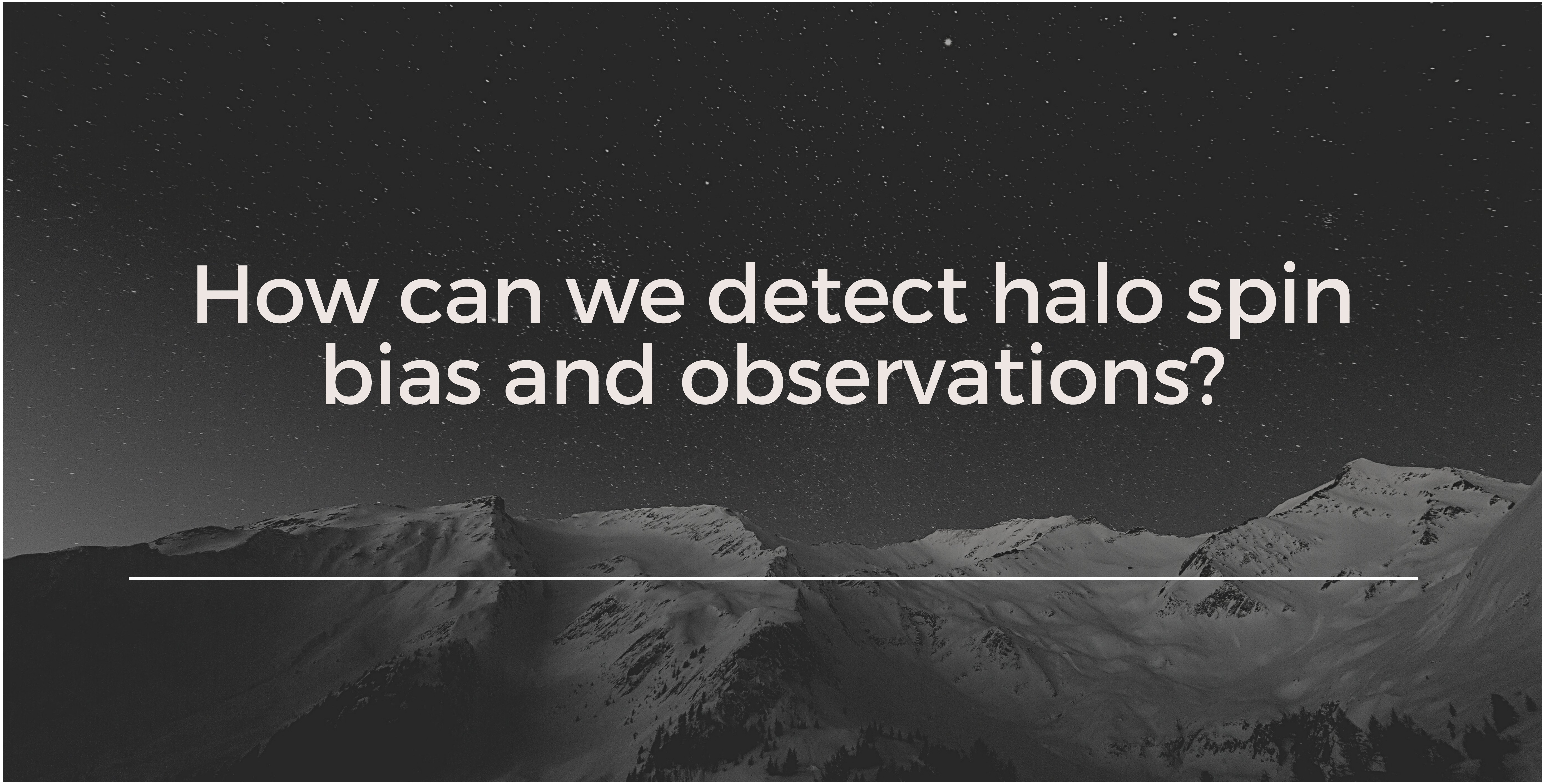

Connection with observations

IllustrisTNG: integrated signal of the kinetic Sunyaev-Zel'dovich effect (kSZ) traces halo angular momentum, while of the thermal Sunyaev-Zel'dovich effect (tSZ) traces halo mass

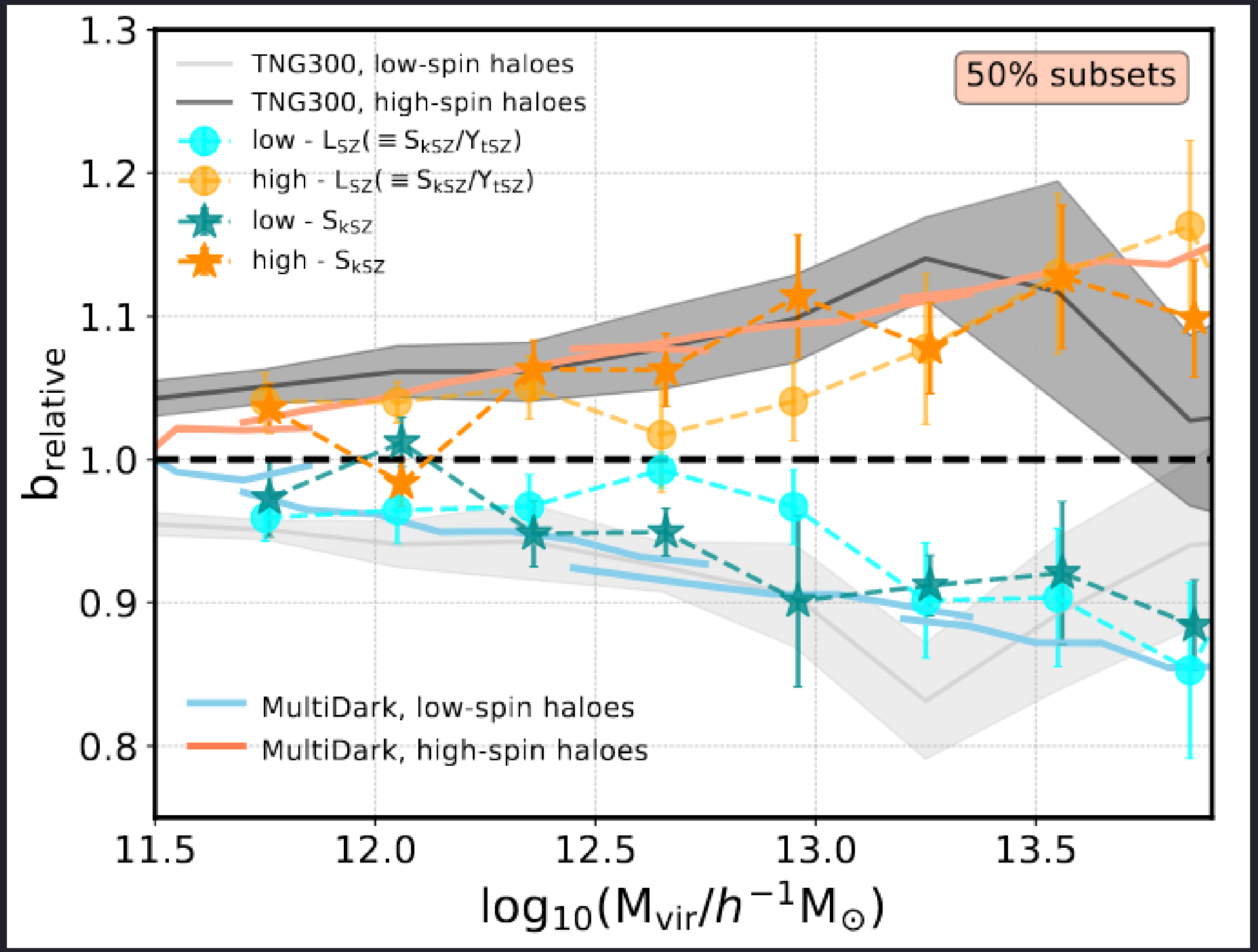

Montero-Dorta, Artale, Abramo, Tucci (2021)
arXiv:2008.08607

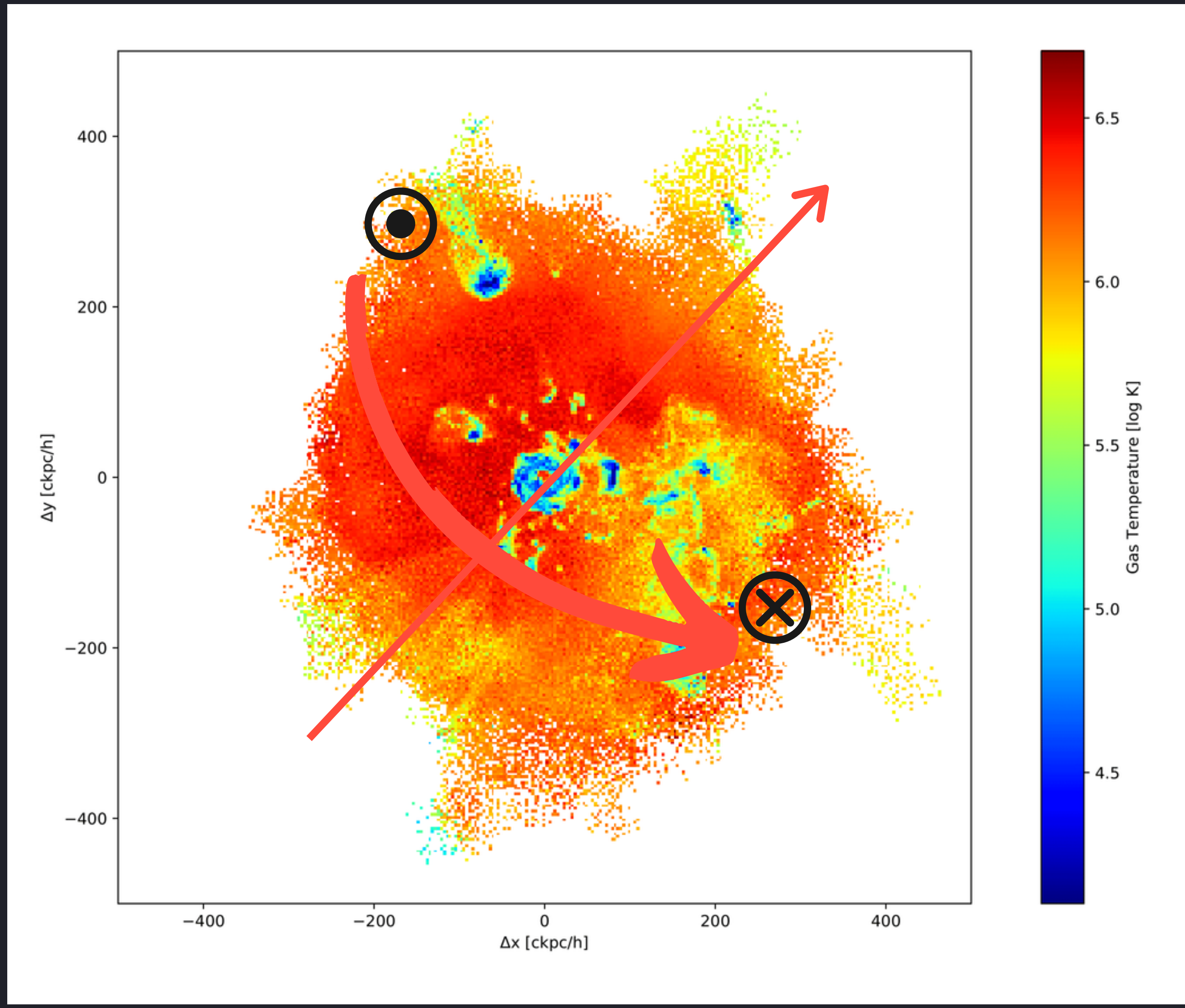

TNG100

$$\log(M_{200}/h^{-1}M_{\odot}) = 12.83$$

Conclusions

- Low-mass spin bias is caused by the population of splashback halos
- We are investigating how we can predict high-mass spin bias from peak formalism and ESP
- The kSZ effect provides an interesting route for probing high-mass halo spin bias in observations

Conclusions

- Low-mass spin bias is caused by the population of splashback halos
- We are investigating how we can predict high-mass spin bias from peak formalism and ESP
- The kSZ effect provides an interesting route for probing high-mass halo spin bias in observations

Beatriz Tucci
Max Planck Institute for Astrophysics
beatriz.tucci@gmail.com

Thank you!
Questions?

SUMMER SCHOOL ON COSMOLOGY 2022

IMPACT OF GALAXY FORMATION ON THE DARK MATTER HALOES IN THE COSMIC WEB

PremVijay Velmani[1]

ARXIV:2206.07733

The Inter-University Centre for Astronomy and Astrophysics, India
Supervisor: Prof. Aseem Paranjape

IUCAA

[1]premv@iucaa.in

INTRODUCTION

- In ΛCDM cosmology, typical galaxy is enclosed by a much larger non-luminous halo, made of the so-called dark matter, that interacts predominantly by gravity.
- Dark matter constitutes more than 80% of all matter in the Universe.
- Formation of dark matter haloes have been modeled as pure gravitational collapse of overdensities in the primordial density field.
- Halo properties have been extensively studied using gravity-only N-body simulations.

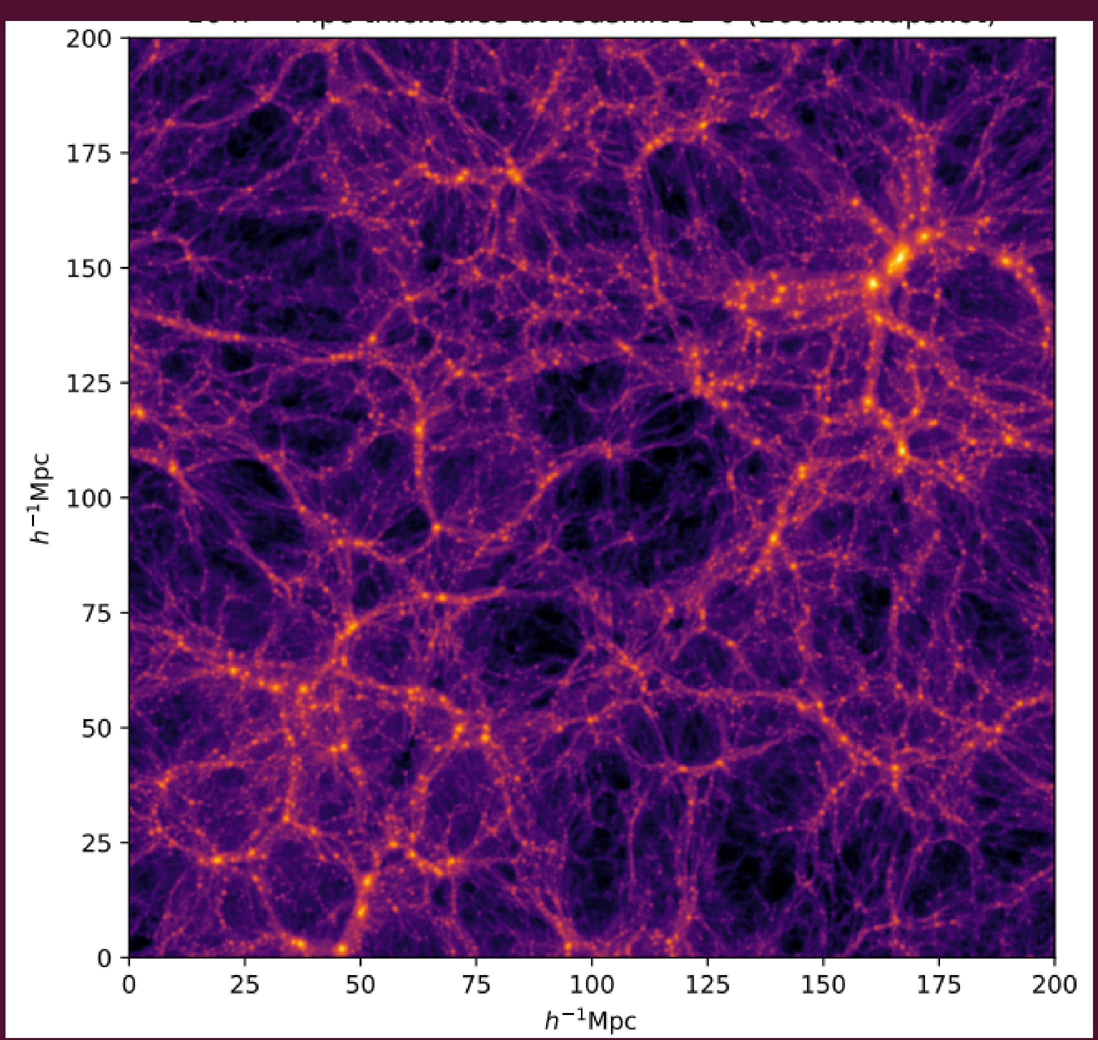

QUESTION

How the formation of galaxy within a halo in turn affects the host halo?

Gravitational collapse of an over-dense region

Halo forms in the cosmic web

Assembly of baryons forms galaxy within the halo

Back-reaction on the halo?

METHODS

Hydrodynamical Simulations

- Galaxy forms as a result of various baryonic processes like cooling, star formation, etc.
- Full hydrodynamical simulation of galaxy formation can incorporate subgrid prescription for all the unresolved baryonic physics.
- The response in the dark matter haloes can be studied by matching the haloes in these simulations with their corresponding gravity-only run.

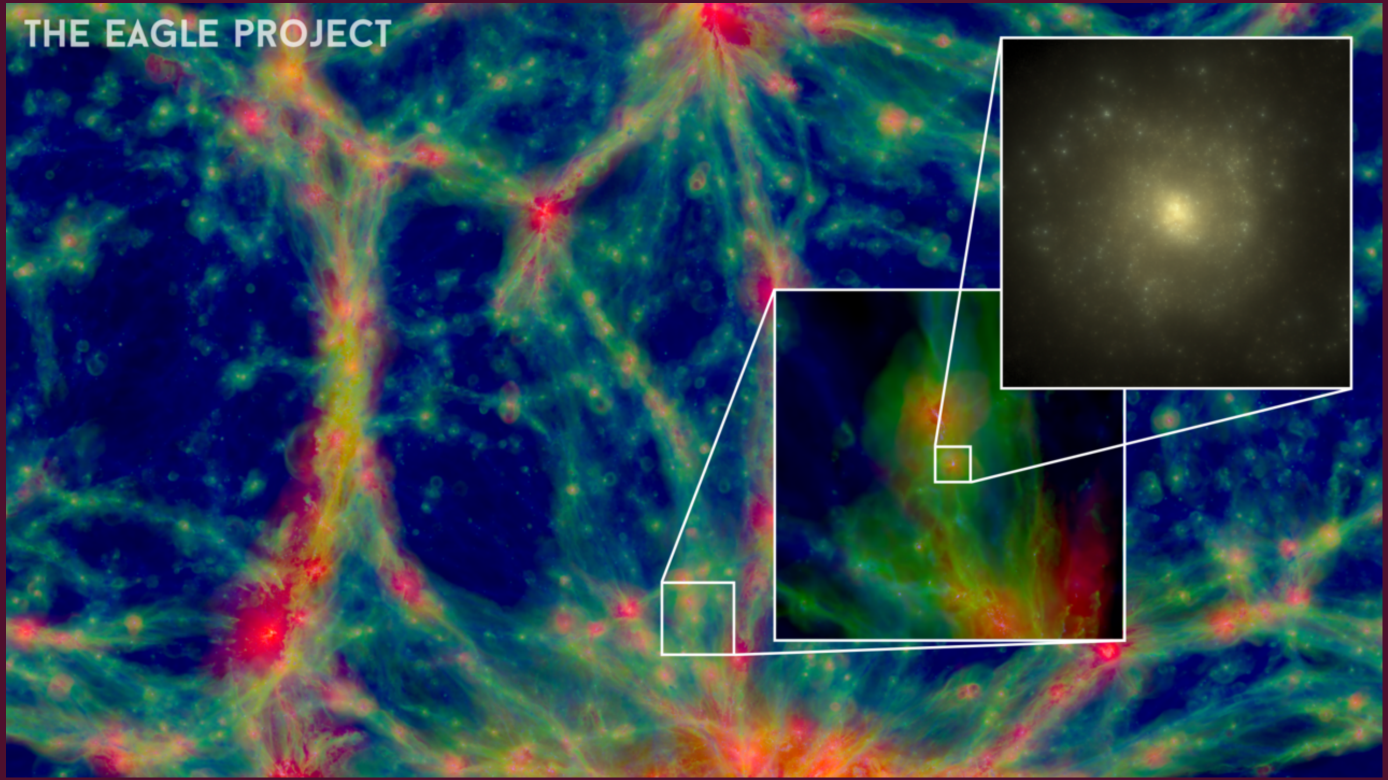

METHODS

Hydrodynamical Simulations

- Visual comparison of randomly chosen haloes between hydrodynamical and gravity-only runs.

- Noticibly spherical, compact and offset spatially.

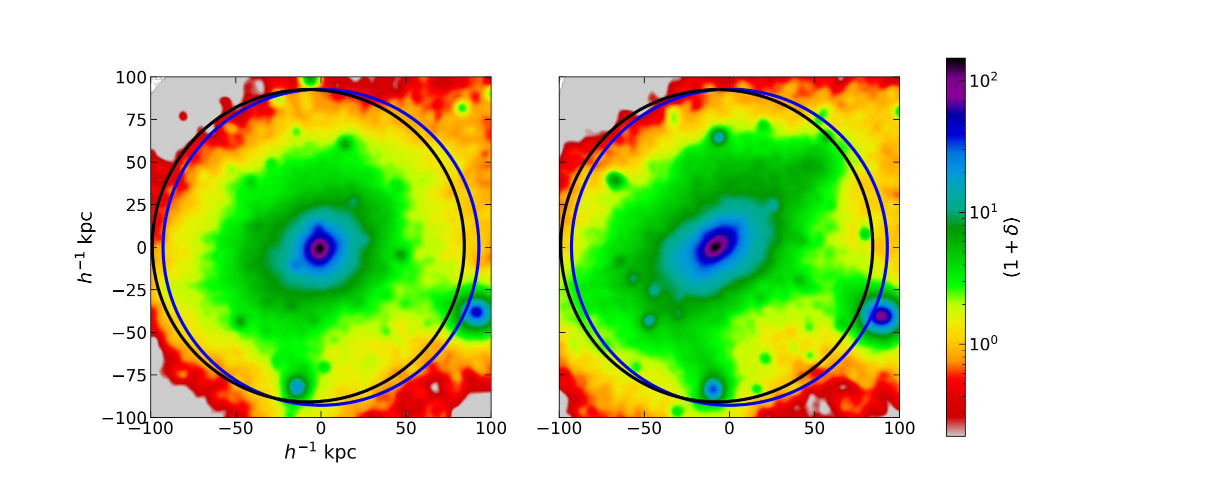

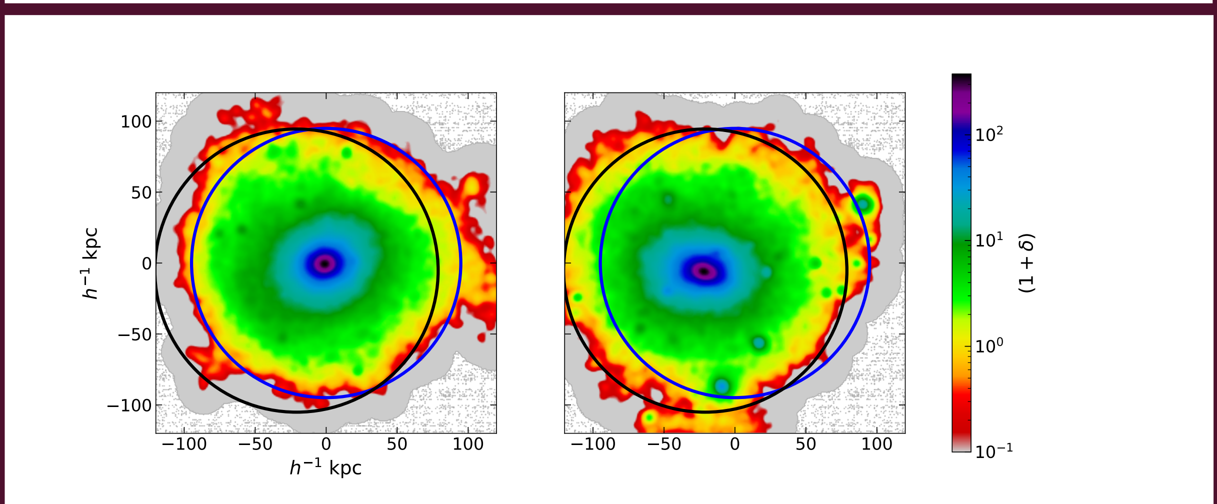

METHODS and MODEL

(Quasi-) Adiabatic relaxation

- Ideal assumption: spherical symmetry, perfect angular momentum conservation, circular particle orbits and no shell crossing.
- The change in the radius of a given shell is related to the change in total mass enclosed by that shell.

$$r_i\, M_i(r_i) = r_f\, M_f(r_f) \implies \frac{r_f}{r_i} = \frac{M_i(r_i)}{M_f(r_f)}$$

$$M_f^d(r_f) = M_i^d(r_i)$$

- Quasi-adiabatic relaxation:

$$\frac{r_f}{r_i} = 1 + \chi\left(\frac{M_i(r_i)}{M_f(r_f)}\right)$$

RESULTS

Relaxation across halos in cosmological simulations

- Relaxation ratio and mass ratio for a dark matter shell as a function of its radius.
- Stacking relaxation relation across halos in two different ways.
- Wide variation across haloes and different behaviour at different halo mass scales.

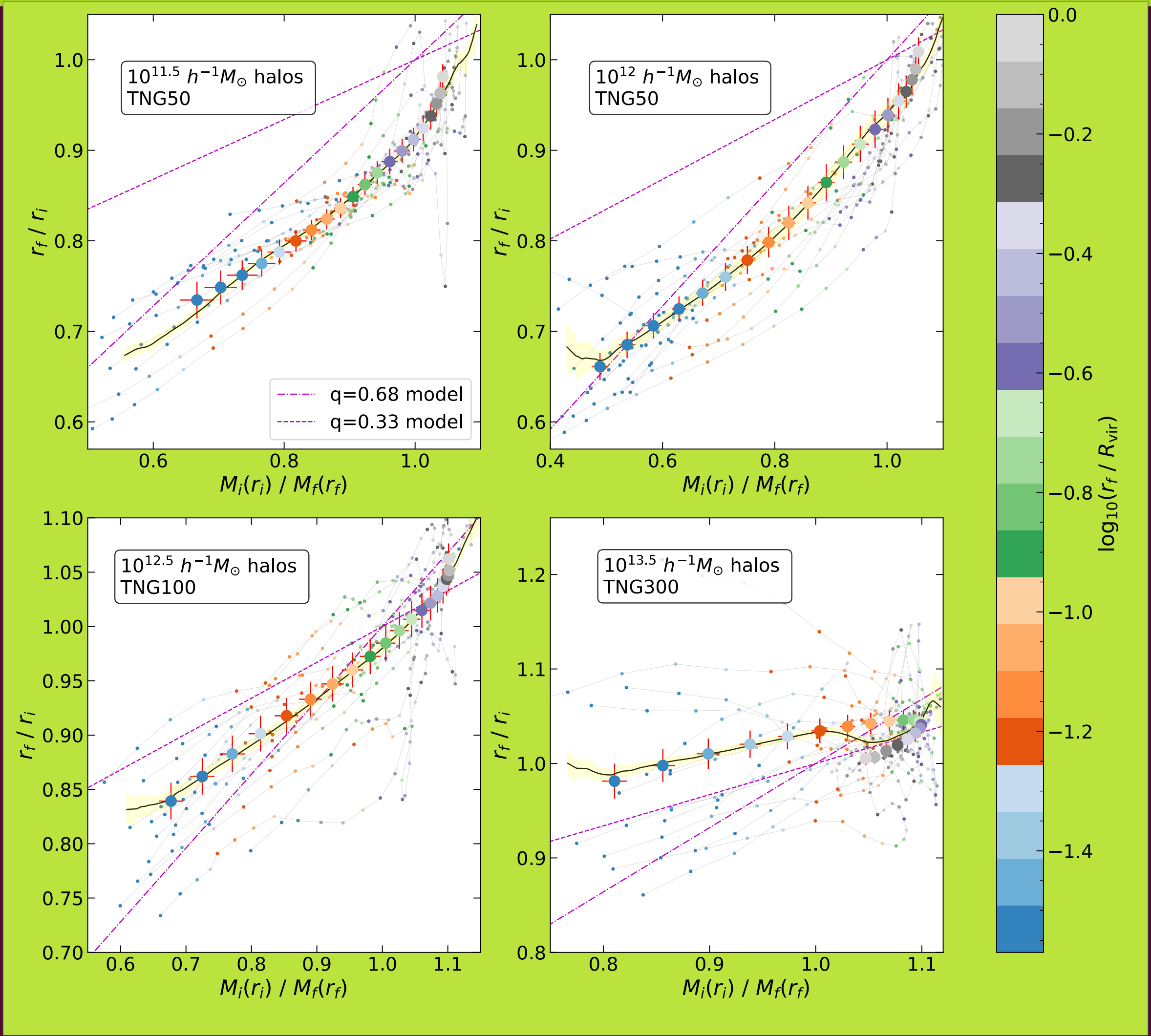

RESULTS

Trend in relaxation with halo mass

- We make use of different cosmological boxes available in IllustrisTNG and EAGLE suite of simulation.
- Relaxation shows strong dependence with mass.

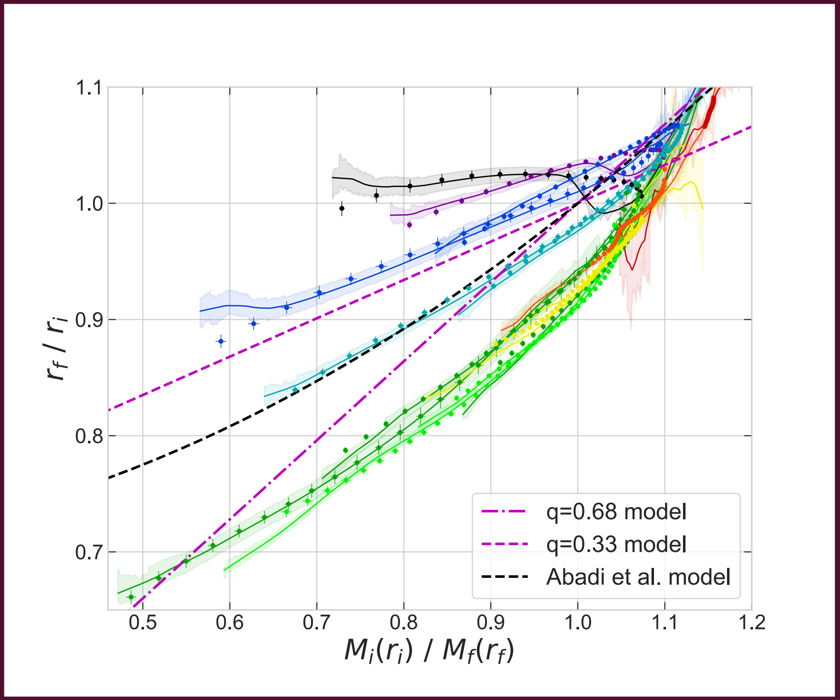

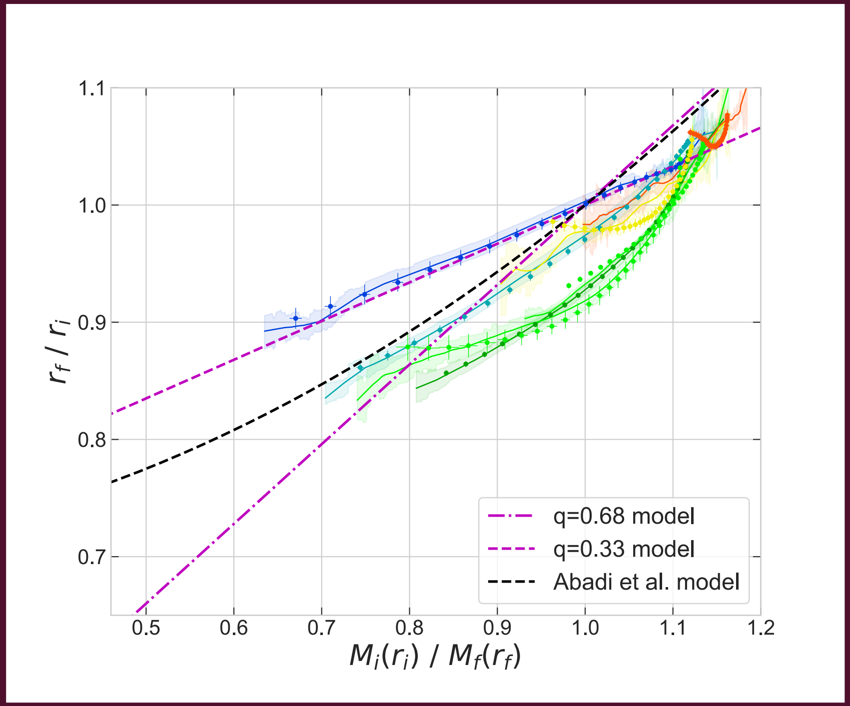

Figure: The stacked relation between relaxation ratio and mass ratio as a function of halo mass in IllustrisTNG (left panel) and EAGLE (right panel) simulations.

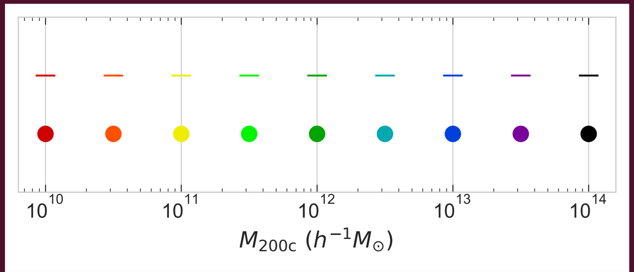

RESULTS

Radially dependent relaxation

- Both relaxation ratio and mass ratio vary significantly across halos even at fixed r_f.
- Stacked relaxation relation at every radii show a simple behaviour.

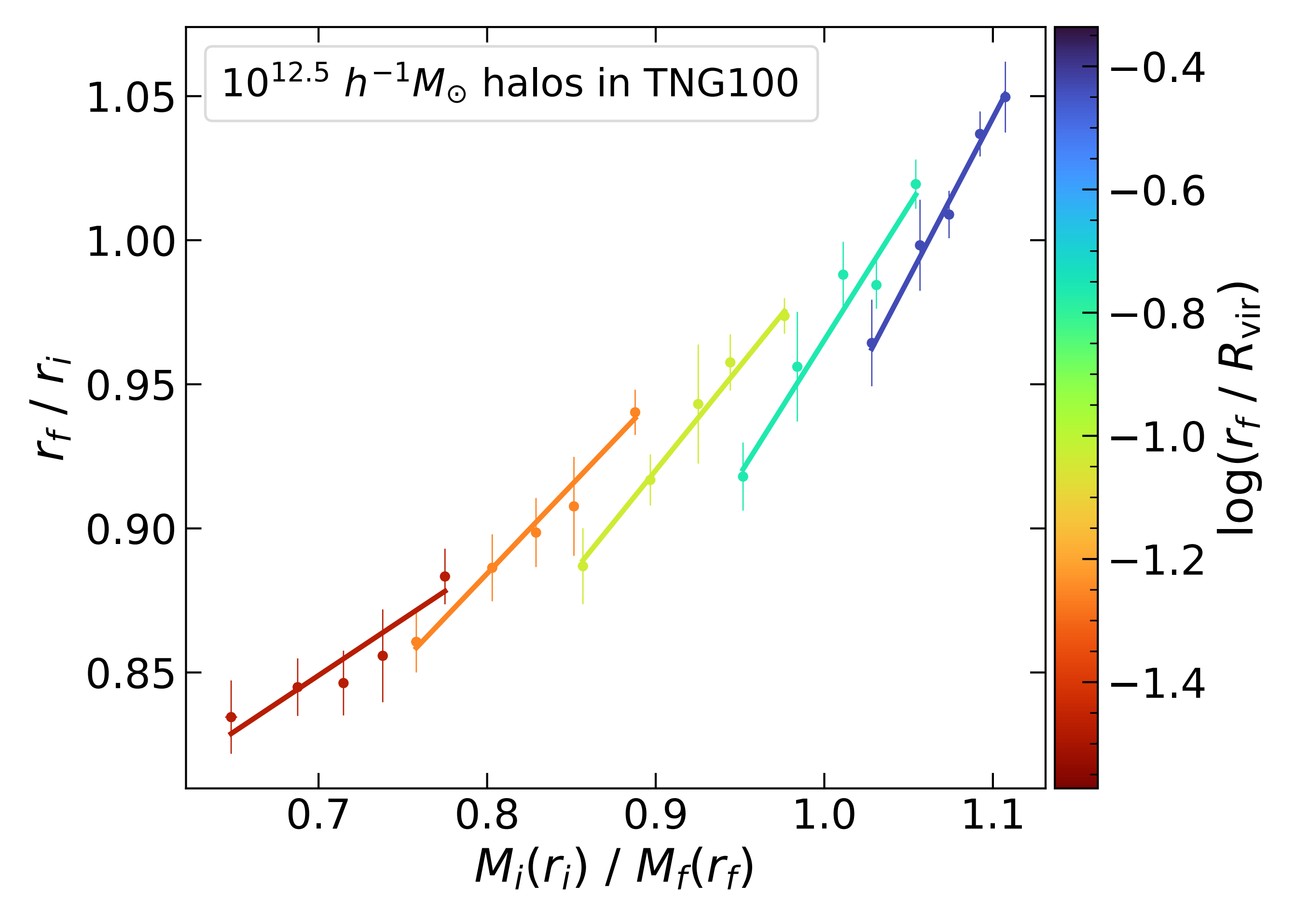

RESULTS

Radially dependent relaxation

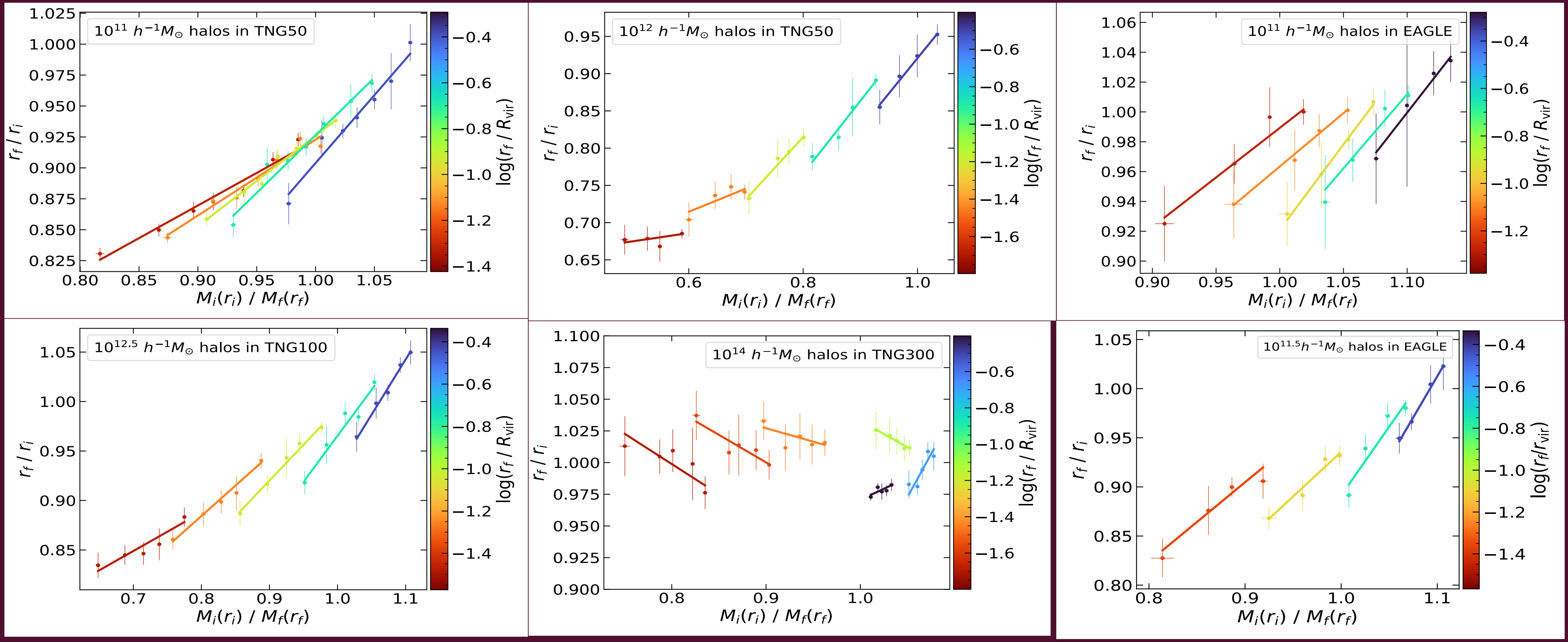

Figure: Relaxation relation at fixed radii across haloes selected by mass from IllustrisTNG and EAGLE simulations. A linear polynomial fit to this relation is shown for different relaxed radii for each of the six halo samples.

RESULTS

Radially dependent relaxation

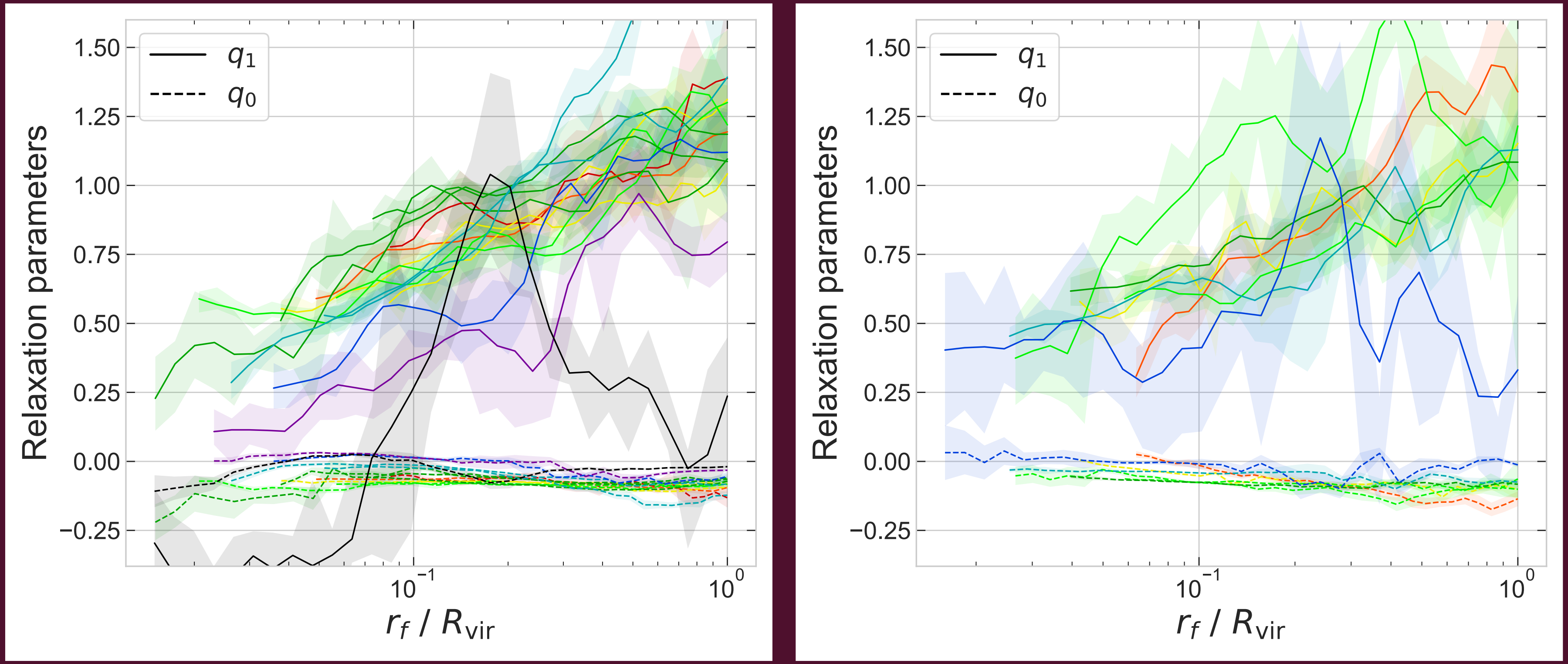

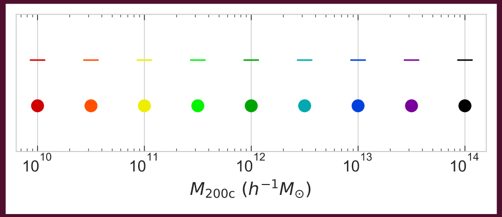

Figure: Linear quasi-adiabatic relaxation model parameters as a function of the radius of relaxed halo at different halo masses in IllustrisTNG (left panel) and EAGLE (right panel).

- The relaxation relation now appears to be more universal across all mass scales.
- With the exception of cluster scale, at all other scales, the radial dependence of the halo can be described simply.
- E.g. the slope parameter is monotonically increasing with radius.

RESULTS

Modelling the radial dependence

- Consider q_0 to be constant.
- Linear relation between q_1 parameter and log-radius.

$$q_1(r_f) = q_{10} + q_{11} \log\left(r_f / R_{\rm vir}\right)$$

$$\frac{r_f}{r_i} - 1 = \left[q_{10} + q_{11} \log\left(\frac{r_f}{R_{\rm vir}}\right)\right]\left(\frac{M_i(r_i)}{M_f(r_f)} - 1\right) + q_0$$

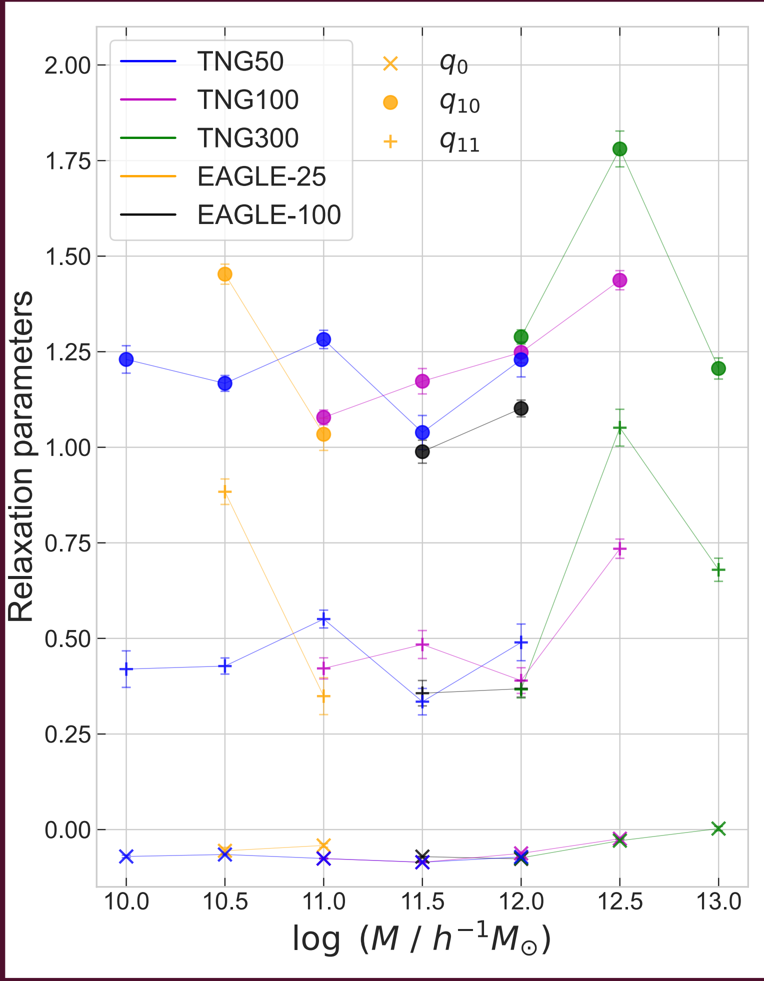

RESULTS

Offset at null relaxation

- The relaxation ratio is less than 1, even when the mass ratio is equal to unity.
- Equivalently, when the relaxation ratio is equal to 1, the mass ratio is greater than 1.

$$\frac{r_f}{r_i} - 1 = q_1 \left(\frac{M_i(r_i)}{M_f(r_f)} - 1 \right) + q_0 \,.$$

- Possible explanations: Recent feedback pushing gas away?

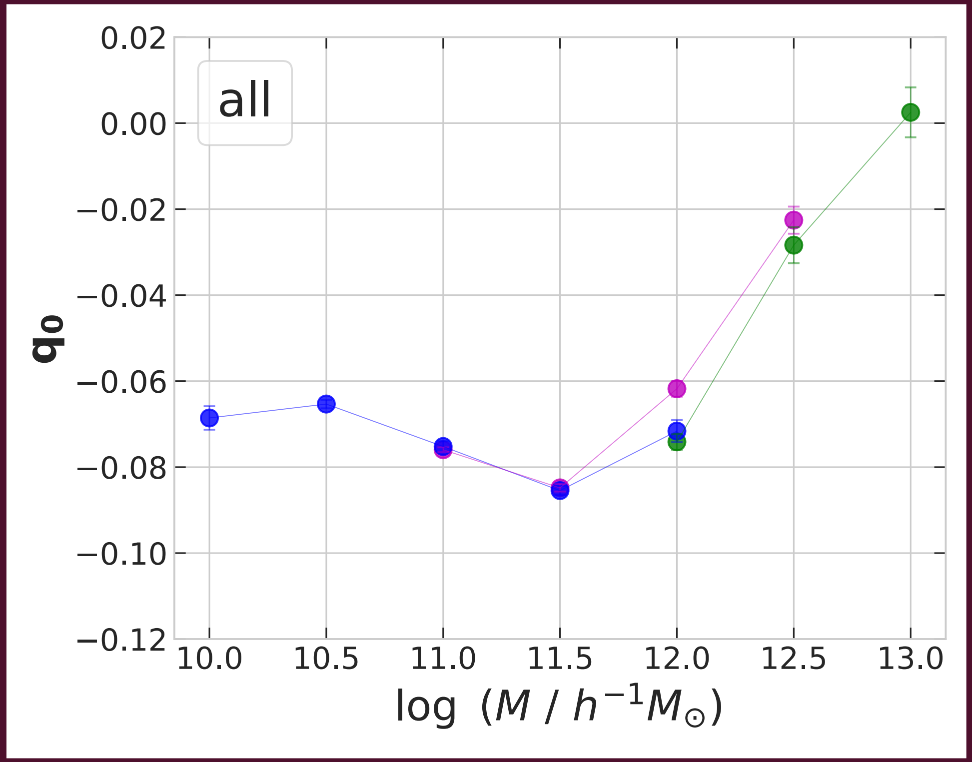

RESULTS

Dependence of the relaxation on halo concentration

- Halo concentration defined using the ratio between the virial radius and the rotation-curve peak radius.

- Concentration is correlated with mass, define concentration significance (c_s) in terms of the scatter from the mean.

- Split the halo samples selected by mass in percentiles of this c_s.

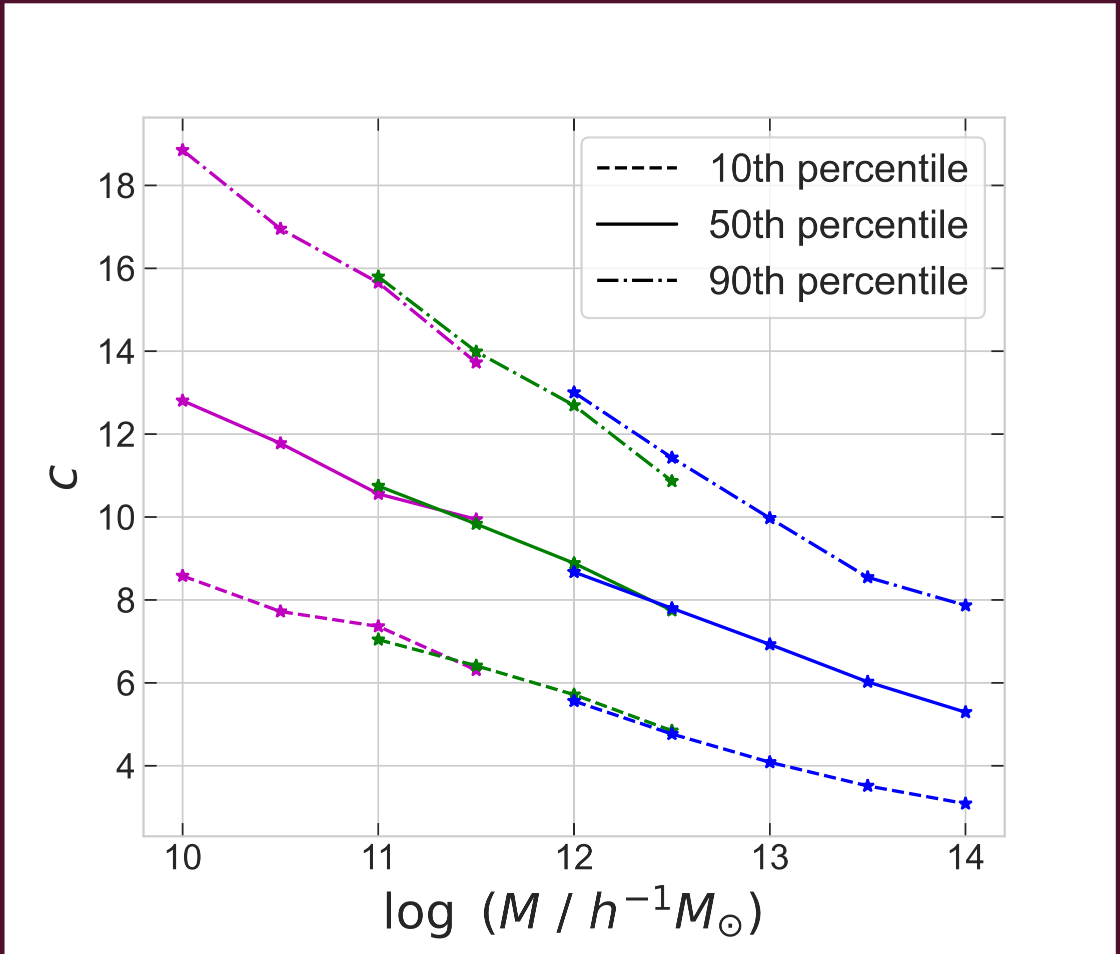

RESULTS

Dependence of the relaxation on halo concentration

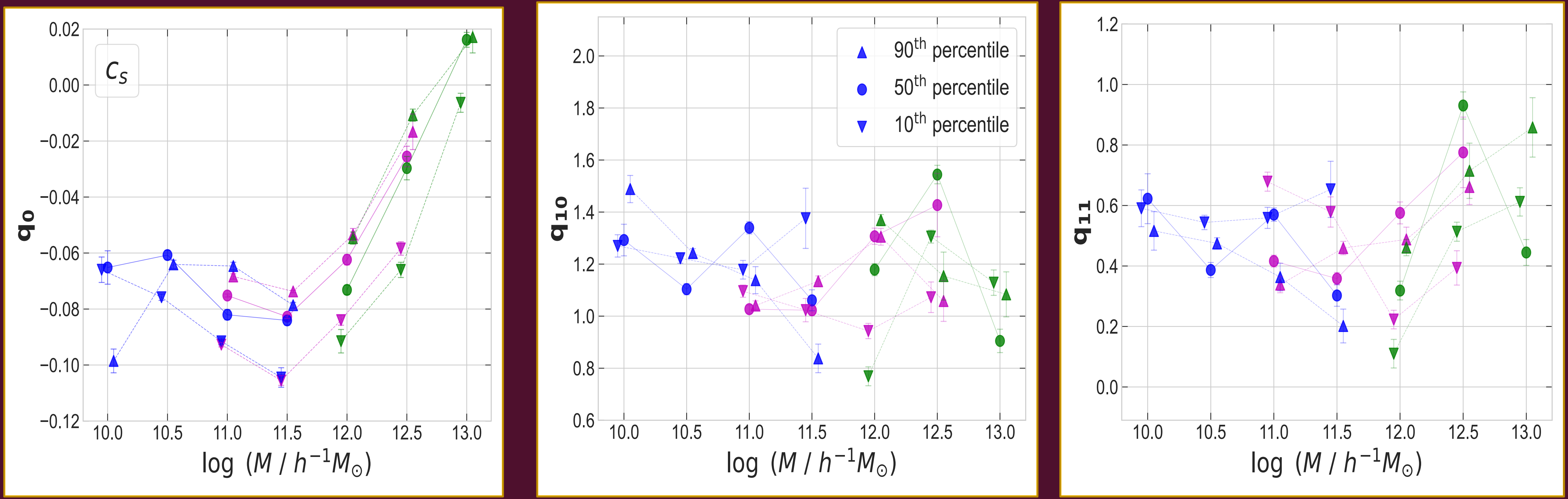

Figure: Relaxation parameters as a function of mass split by the concentration significance.

RESULTS

Dependence of the relaxation on galaxy properties

Halo-galaxy properties considered include stellar fraction, specific star formation rate and the gas fraction.

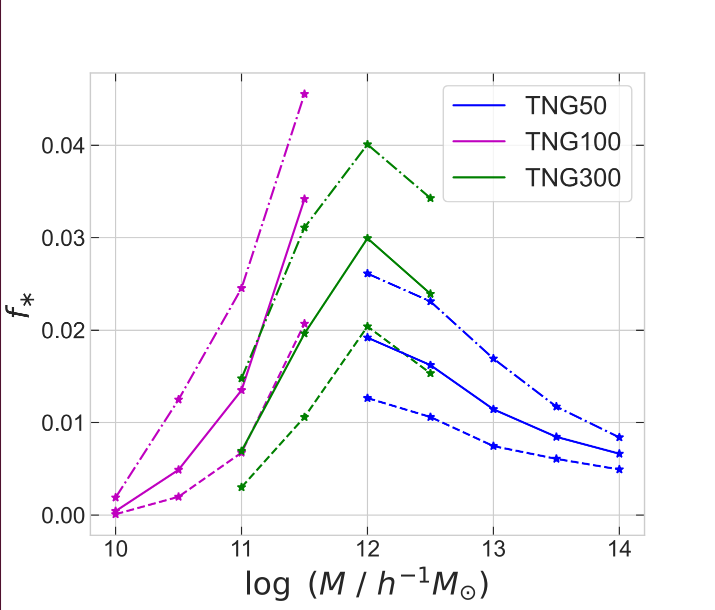

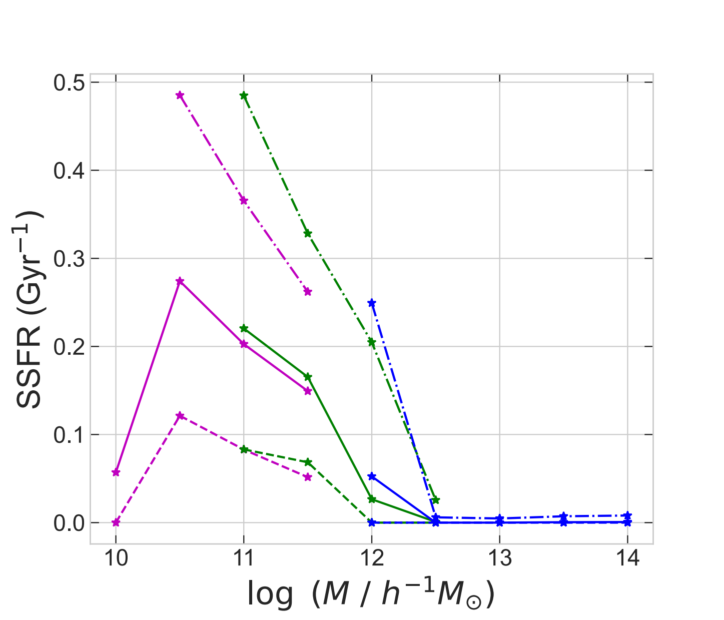

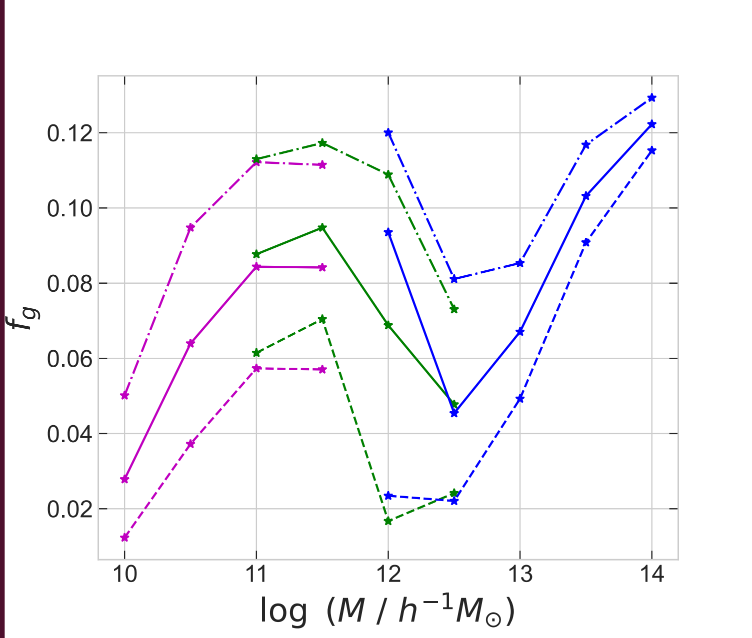

RESULTS

Dependence of the relaxation on galaxy properties

- As expected, q_0 shows strong dependence with SSFR and gas fraction that are related to the current star formation and feedback.

- It seems that the stellar fraction is not directly relevant in understanding the halo response.

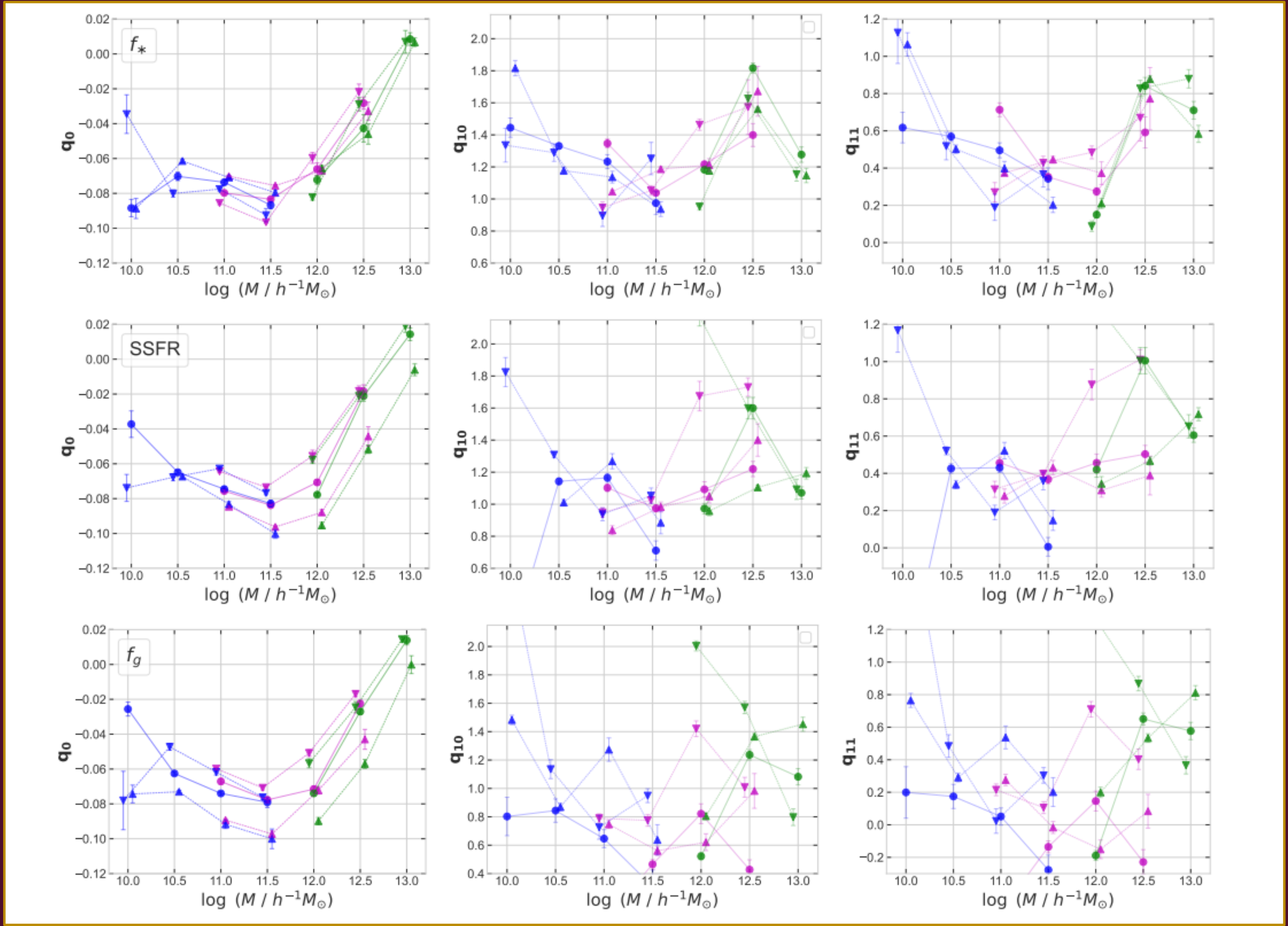

APPLICATIONS

Mass profiles

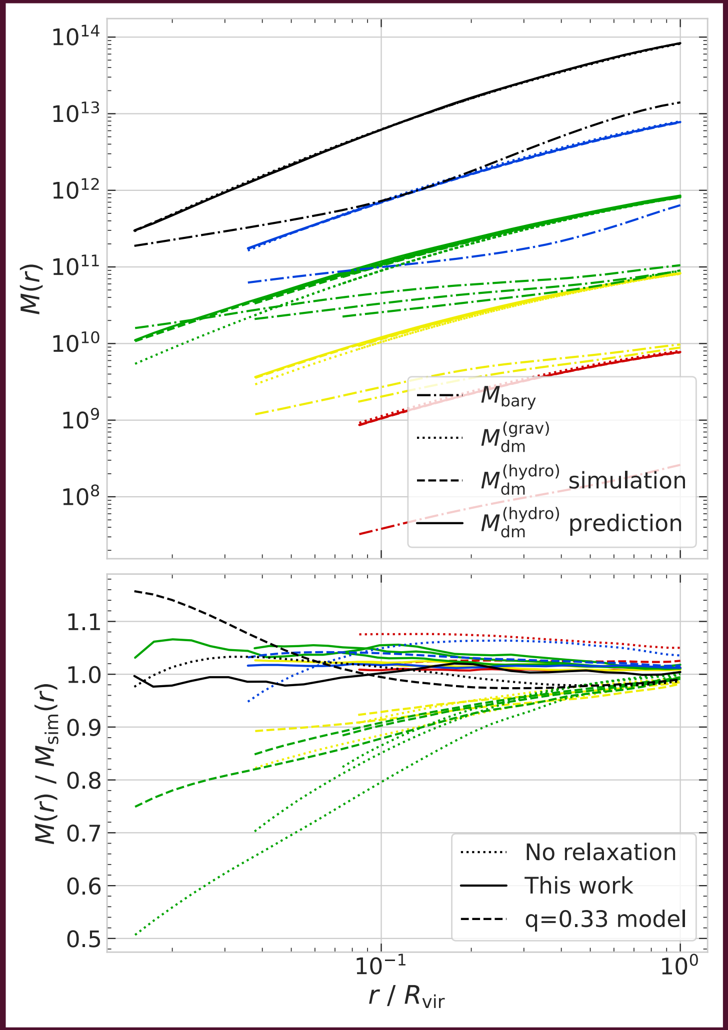

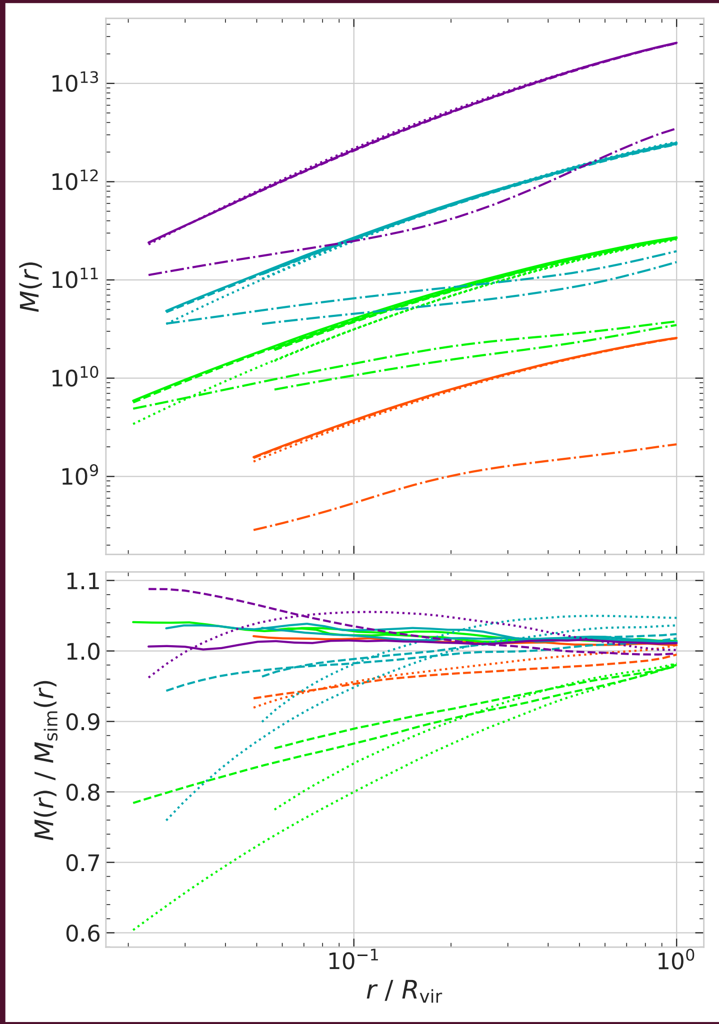

(Top row:) For the haloes in IllustrisTNG simulations, the mean radial mass profiles is shown in bins of halo mass for the baryonic component (dash-dotted curves) and dark matter component in hydrodynamic (dashed curves) and gravity-only (dotted curves) runs. The relaxed dark matter mass profile predicted is shown by solid curves; for clarity we use two panels to show the averaged mass profiles for the nine mass bins.
(Bottom row:) The ratio of the relaxed dark matter mass profile predicted by our model to that from the hydrodynamic simulation is shown by solid curves. For comparison, the corresponding ratio for quasi-adiabatic relaxation model with constant q = 0.33 is shown by dashed curves and the ratio of dark matter mass profile between gravity-only simulation to the full hydrodynamic simulation is shown by dotted curves, representing the case of no relaxation.

CONCLUSION and FUTURE WORK

- Using simulations we find that simple modifications to the standard adiabatic relaxation model can explain the relaxation in modern hydrodynamic simulations.

- In particular, adding a null offset parameter and explicit radial dependence works reasonably with EAGLE and IllustrisTNG hydrodynamical simulations.

- To make further understanding of the physics of this relaxation,
  - we compare the relaxation of haloes between simulations with different baryonic prescriptions,
  - we include baryon in the self-similar formalism to build an analytical model of relaxation.

Thank you

“Analytical growth functions for cosmic structures in a ΛCDM Universe”

Cornelius Rampf, Sonja Ornella Schobesberger and Oliver Hahn 2022

[arXiv:2205.11347 [astro-ph.CO]], submitted to MNRAS

Sonja Ornella Schobesberger
07 July 2022

Non-linear large scale dynamics of cosmic matter

universität wien

a fluid in the weak-field, non-relativistic, and collision-less limit

initially described via a phase-space distribution function $f(\mathbf{x}, \mathbf{v}, t) : \mathbb{R} \times \mathbb{R}^{3+3} \rightarrow \mathbb{R}_0^+$

given comoving space variable $\mathbf{x}$, $\mathbf{v} = d\mathbf{x}/dt$ and cosmic time t

Non-linear large scale dynamics of cosmic matter

universität wien

a fluid in the weak-field, non-relativistic, and collision-less limit

initially described via a phase-space distribution function $f(\mathbf{x}, \mathbf{v}, t) : \mathbb{R} \times \mathbb{R}^{3+3} \to \mathbb{R}_0^+$

given comoving space variable $\mathbf{x}$, $\mathbf{v} = d\mathbf{x}/dt$ and cosmic time t

Analytical methods for initially cold scalar fluids

$$f_0(\mathbf{x}, \mathbf{v}) = a^3 \rho_0(\mathbf{x}) \delta_D(\mathbf{v} - \nabla_x S_0(\mathbf{x}))$$

Euler-Poisson system of equations

for cold cosmic matter

$$\frac{\partial \delta}{\partial t} + \nabla_x \cdot \left[(1+\delta)\cdot \mathbf{v}\right] = 0$$

$$\frac{\partial \mathbf{v}}{\partial t} + (\mathbf{v}\cdot\nabla_x)\mathbf{v} + 2H\mathbf{v} = -\frac{1}{a^2}\nabla_x\phi$$

$$\Delta\phi = \frac{3}{2a}\delta$$

- single-stream regime: single velocity $\mathbf{v}$ attached to any given $(\mathbf{x}, t)$, vanishing velocity dispersion and vorticity
- exact reformulation into **hydrodynamical system of equations for $\mathbf{v}$ and $\delta(\mathbf{x}, t) := [\rho - \bar{\rho}]/\bar{\rho}$**

Euler-Poisson system of equations

for cold cosmic matter

$$\frac{\partial \delta}{\partial t} + \nabla_x \cdot \left[(1+\delta) \cdot \mathbf{v}\right] = 0$$

$$\frac{\partial \mathbf{v}}{\partial t} + (\mathbf{v} \cdot \nabla_x)\mathbf{v} + 2H\mathbf{v} = -\frac{1}{a^2}\nabla_x \phi$$

$$\Delta \phi = \frac{3}{2a}\delta$$

- single-stream regime: single velocity $\mathbf{v}$ attached to any given $(\mathbf{x}, t)$, vanishing velocity dispersion and vorticity
- exact reformulation into **hydrodynamical system of equations for $\mathbf{v}$ and $\delta(\mathbf{x}, t) := [\rho - \bar{\rho}]/\bar{\rho}$**

Linearisation for small overdensities $|\delta| \ll 1$

solution for $\delta_{lin}(\mathbf{x}, t)$ factorises into temporal and spatial part

Euler-Poisson system of equations

universität wien

for cold cosmic matter

$$\frac{\partial \delta}{\partial t} + \nabla_x \cdot \left[(1+\delta)\cdot \mathbf{v}\right] = 0$$

$$\frac{\partial \mathbf{v}}{\partial t} + (\mathbf{v}\cdot\nabla_x)\mathbf{v} + 2H\mathbf{v} = -\frac{1}{a^2}\nabla_x \phi$$

$$\Delta\phi = \frac{3}{2a}\delta$$

- single-stream regime: single velocity $\mathbf{v}$ attached to any given $(\mathbf{x}, t)$, vanishing velocity dispersion and vorticity
- exact reformulation into **hydrodynamical system of equations for $\mathbf{v}$ and $\delta(\mathbf{x}, t) := [\rho - \bar{\rho}]/\bar{\rho}$**

Linearisation for small overdensities $|\delta| \ll 1$

solution for $\delta_{lin}(\mathbf{x}, t)$ factorises into temporal and spatial part

$$\delta_{lin}(\mathbf{x}, t) \propto \delta_+(\mathbf{x})D(t)$$

given by hypergeometric function ${}_2F_1$ in ΛCDM model Chernin et al. 2003

function of the initial gravitational field

Euler-Poisson system of equations

for cold cosmic matter

$$\frac{\partial \delta}{\partial t} + \nabla_x \cdot \left[(1+\delta)\cdot \mathbf{v}\right] = 0$$

$$\frac{\partial \mathbf{v}}{\partial t} + (\mathbf{v}\cdot\nabla_x)\mathbf{v} + \boxed{2H\mathbf{v}} = -\frac{1}{a^2}\nabla_x \phi$$

$$\Delta\phi = \frac{3}{2a}\delta$$

- single-stream regime: single velocity $\mathbf{v}$ attached to any given $(\mathbf{x}, t)$, vanishing velocity dispersion and vorticity
- exact reformulation into **hydrodynamical system of equations for $\mathbf{v}$ and $\delta(\mathbf{x}, t) := [\rho - \bar{\rho}]/\bar{\rho}$**

Linearisation for small overdensities $|\delta| \ll 1$

solution for $\delta_{lin}(\mathbf{x}, t)$ factorises into temporal and spatial part

$$\delta_{lin}(\mathbf{x}, t) \propto \delta_+(\mathbf{x}) D(t)$$

given by hypergeometric function ${}_2F_1$

in ΛCDM model

Chernin et al. 2003

function of the initial gravitational field

Lagrangian perturbation theory (LPT)

solving the pressureless Euler-Poisson system of equations

Lagrangian map $\mathscr{L}_t : \mathbb{R} \times \mathbb{R}^3 \to \mathbb{R}^3 : (t, \mathbf{q}) \mapsto \mathbf{x}(\mathbf{q}, t) = \mathbf{q} + \boldsymbol{\Psi}(\mathbf{q}, t)$

with characteristic equation $\dfrac{d}{dt}\mathbf{x}(\mathbf{q}, t) = \mathbf{v}(\mathbf{x}(\mathbf{q}, t), t)$

From particle trajectories to the density via mass conservation

determinant of the Jacobian matrix $J = det(\mathbf{1} + \nabla_q \otimes \boldsymbol{\Psi})$ $\longrightarrow$ $\delta(\mathbf{x}(\mathbf{q}, t)) = \dfrac{1}{J} - 1$

Buchert 1989; Moutarde et al. 1991; Bouchet et al. 1992; Buchert 1992; Bouchet et al. 1995; Ehlers & Buchert 1997; Rampf & Buchert 2012; Zheligovsky & Frisch 2014

Lagrangian perturbation theory (LPT)

solving the pressureless Euler-Poisson system of equations

Lagrangian map $\mathscr{L}_t : \mathbb{R} \times \mathbb{R}^3 \to \mathbb{R}^3 : (t, \mathbf{q}) \mapsto \mathbf{x}(\mathbf{q}, t) = \mathbf{q} + \mathbf{\Psi}(\mathbf{q}, t)$

with characteristic equation $\frac{d}{dt}\mathbf{x}(\mathbf{q}, t) = \mathbf{v}(\mathbf{x}(\mathbf{q}, t), t)$

From particle trajectories to the density via mass conservation

determinant of the Jacobian matrix $J = det(\mathbf{1} + \nabla_q \otimes \mathbf{\Psi})$ $\longrightarrow$ $\delta(\mathbf{x}(\mathbf{q}, t)) = \frac{1}{J} - 1$

The **idea behind LPT**: solving for the displacement field perturbatively using a time-Taylor expansion

$$\mathbf{\Psi}(\mathbf{q}, t) = \sum_{n=1}^{\infty} \psi^{(n)}(\mathbf{q}) t^n$$

Buchert 1989; Moutarde et al. 1991; Bouchet et al. 1992; Buchert 1992; Bouchet et al. 1995; Ehlers & Buchert 1997; Rampf & Buchert 2012; Zheligovsky & Frisch 2014

Lagrangian perturbation theory (LPT)

solving the pressureless Euler-Poisson system of equations

Lagrangian map $\mathscr{L}_t : \mathbb{R} \times \mathbb{R}^3 \to \mathbb{R}^3 : (t, \mathbf{q}) \mapsto \mathbf{x}(\mathbf{q}, t) = \mathbf{q} + \mathbf{\Psi}(\mathbf{q}, t)$

with characteristic equation $\frac{d}{dt}\mathbf{x}(\mathbf{q}, t) = \mathbf{v}(\mathbf{x}(\mathbf{q}, t), t)$

From particle trajectories to the density via mass conservation

determinant of the Jacobian matrix $J = det(\mathbf{1} + \nabla_q \otimes \mathbf{\Psi})$ $\longrightarrow$ $\delta(\mathbf{x}(\mathbf{q}, t)) = \frac{1}{J} - 1$

The **idea behind LPT**: solving for the displacement field perturbatively using a time-Taylor expansion

local breakdown of the single-stream assumption at shell-crossing
=> LPT no longer physically meaningful

Buchert 1989; Moutarde et al. 1991; Bouchet et al. 1992; Buchert 1992; Bouchet et al. 1995; Ehlers & Buchert 1997; Rampf & Buchert 2012; Zheligovsky & Frisch 2014

Analytical avenues beyond matter domination

- accurate forward modelling at the field level Leclercq 2015
- effective fluid descriptions Schmidt et al. 2019, Barreira et al. 2021, Schmidt 2021
- growth functions within massive neutrino cosmologies Bird et al. 2012, Partmann et al. 2020, Yoshikawa et al. 2020, Zhiyu Chen et al. 2021

Analytical avenues beyond matter domination

- accurate forward modelling at the field level Leclercq 2015
- effective fluid descriptions Schmidt et al. 2019, Barreira et al. 2021, Schmidt 2021
- growth functions within massive neutrino cosmologies Bird et al. 2012, Partmann et al. 2020, Yoshikawa et al. 2020, Zhiyu Chen et al. 2021

1) "Beyond EdS"

$$\mathbf{\Psi}_{EdS}(\mathbf{q}, a) = \sum_{n=1}^{\infty} \psi_{EdS}^{(n)}(\mathbf{q}) a^n$$

$$H_{EdS}$$

$$\mathbf{\Psi}_{EdS}(\mathbf{q}, a) \longrightarrow \mathbf{\Psi}_{\Lambda CDM}(\mathbf{q}, D)$$

replace a with $D(a)$

2) Leading-order asymptotic considerations for growth functions $G(t)$ corresponding to spatial kernels $\psi^{(G)}$
Bouchet et al. 1995

$$\mathbf{\Psi}(\mathbf{q}, t) = \sum \psi^{(G)} G(t)$$

Structure growth via D-time formalism

- refined time variable D $\quad \boldsymbol{\Psi}_{\Lambda CDM}(\mathbf{q}, D) = \sum_{n=1}^{\infty} \psi^{(n)}_{\Lambda CDM}(\mathbf{q}) D^n$

- all-order D-time **recursion relations for** $\psi^{(n)}_{\Lambda CDM}(\mathbf{q})$

Structure growth via D-time formalism

- refined time variable D $\quad \mathbf{\Psi}_{\Lambda CDM}(\mathbf{q}, D) = \sum_{n=1}^{\infty} \psi_{\Lambda CDM}^{(n)}(\mathbf{q}) D^n$

- all-order D-time **recursion relations for** $\psi_{\Lambda CDM}^{(n)}(\mathbf{q})$

- resummation technique to yield

$$\mathbf{\Psi}(\mathbf{q}, D) = \sum \psi^{(G)} G(D) = D\mathbf{\Psi}^{(1)}(\mathbf{q}) + E(D)\mathbf{\Psi}^{(2)}(\mathbf{q}) + F^{(3a)}(D)\mathbf{\Psi}^{(3a)}(\mathbf{q}) \ldots$$

- **true ΛCDM temporal growth functions**

Rampf, Schobesberger & Hahn 2022

$$\boxed{E(D) = -\frac{3}{7}D^2 - \frac{3\Lambda}{1001}D^5 - \frac{960\Lambda^2}{3\,556\,553}D^8 + O(D^{11})}$$

=> velocity coefficients $\partial \mathbf{v}/\partial D$ and matter power- and bispectra

universität wien

Results

growth functions

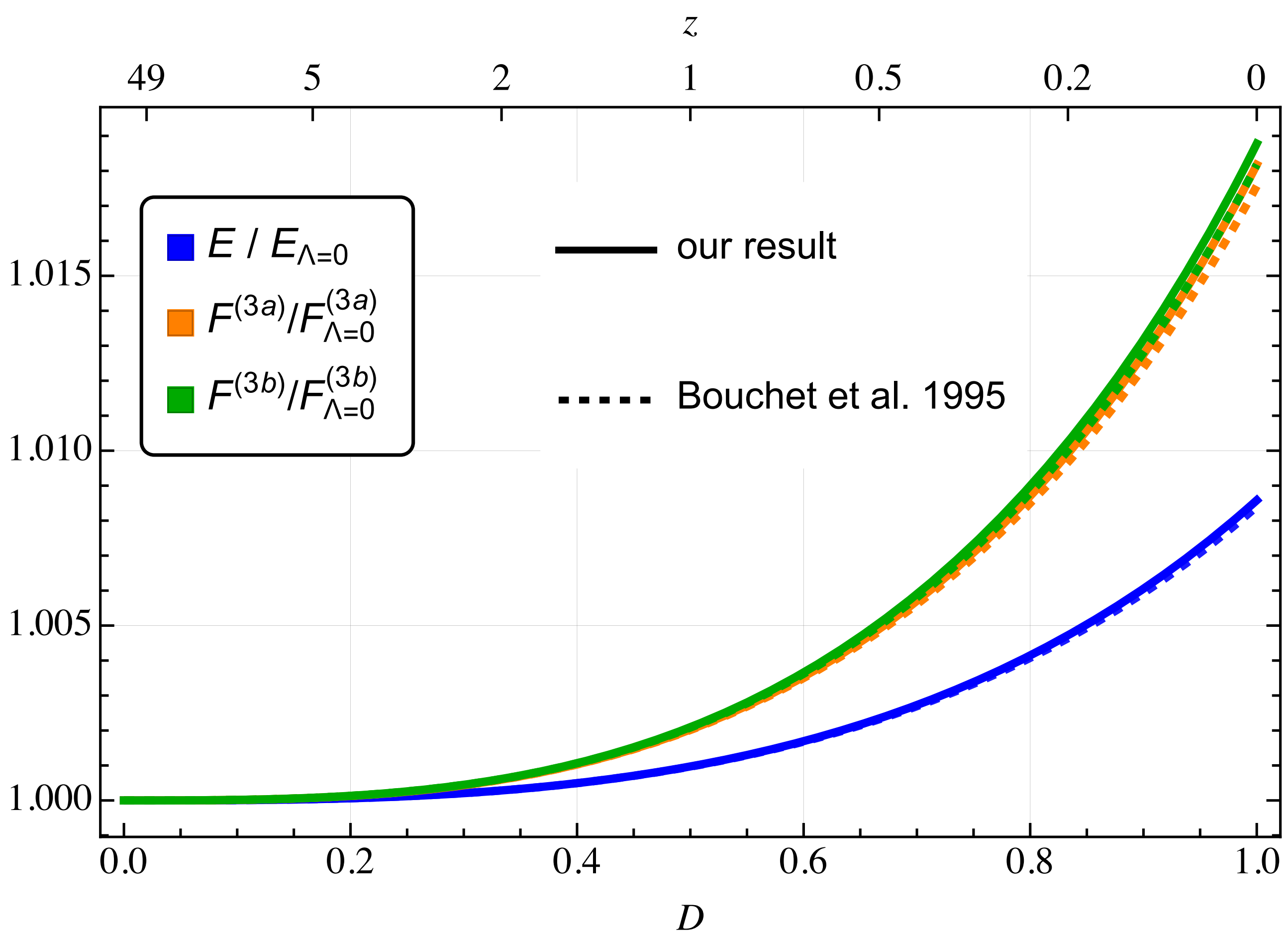

velocity coefficients

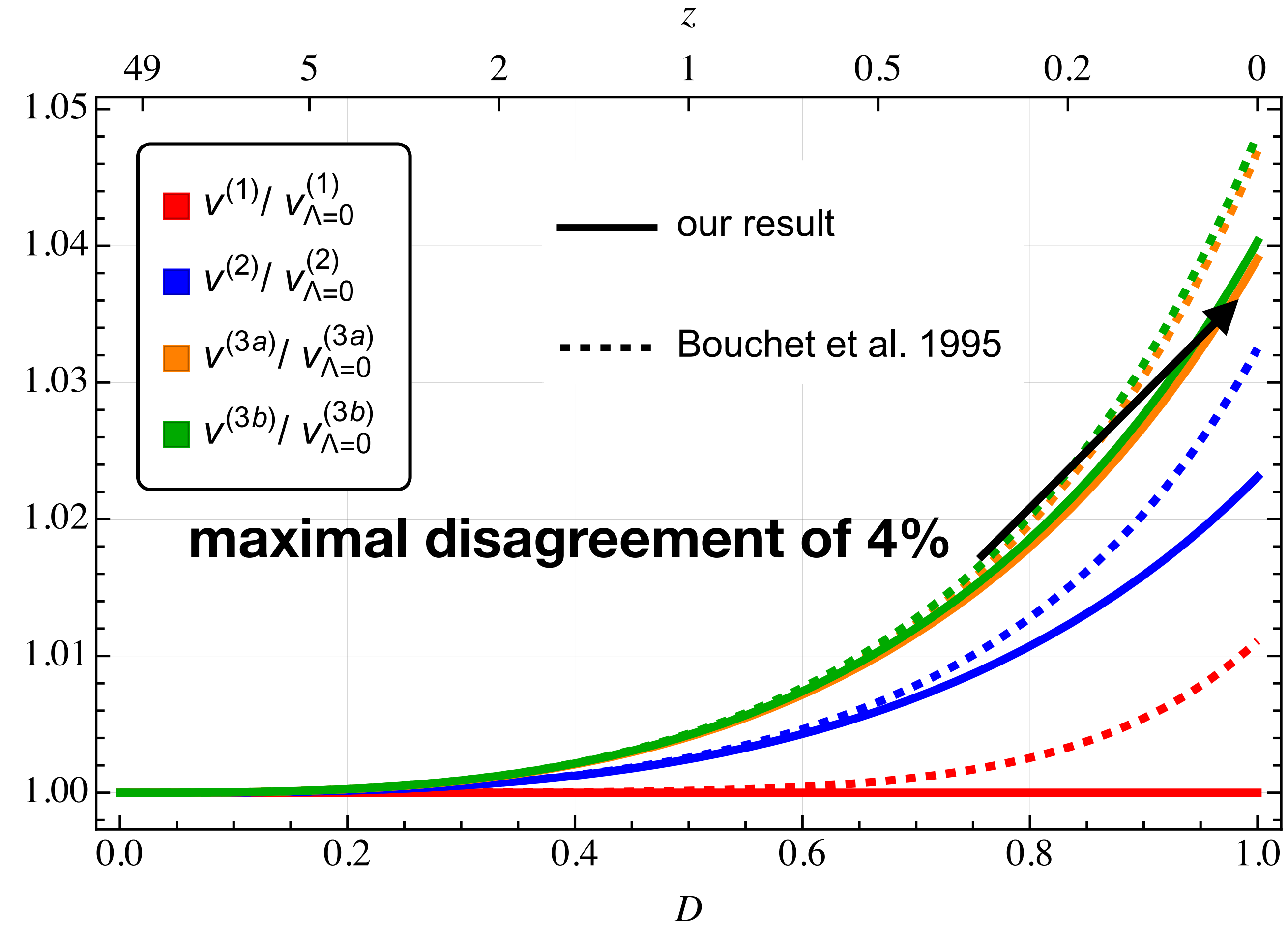

power- and bispectra

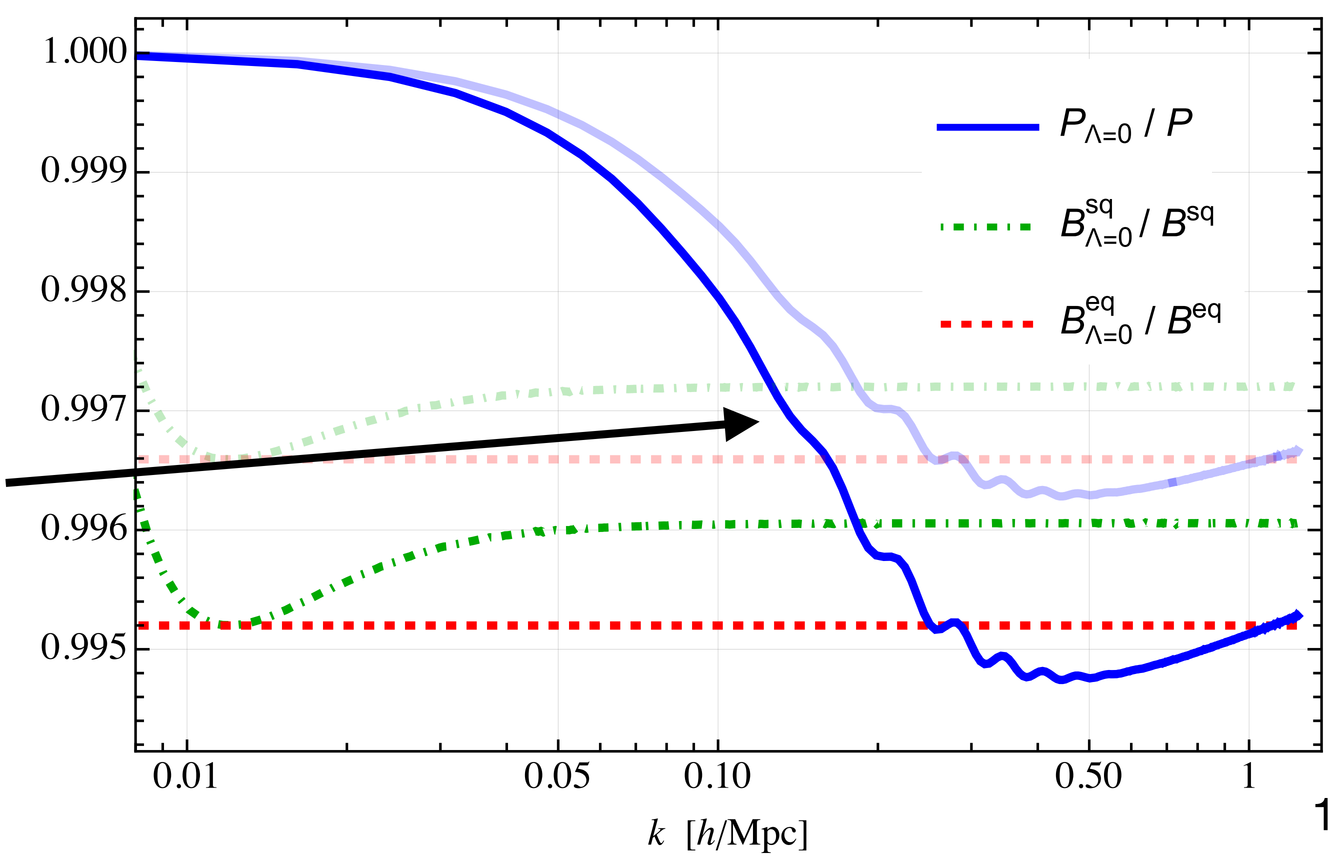

scale-dependent power suppression similar to massive neutrino signature

Rampf, Schobesberger & Hahn 2022

Take-home messages

- there exist now **true analytical solutions for structure growth** in the cold limit of a ΛCDM Universe up to arbitrary precision which are implemented in the monofonIC 3LPT initial condition generator
  Hahn et al. 2020; Michaux et al. 2021
- possibility of extension to **more generic cosmologies**
- usage of true analytical solutions is advised for forward modelling, **effective field theories and massive neutrino cosmologies**

BAO scale inference from biased tracers using the EFT likelihood

arXiv: 2203.06177, accepted for publication in JCAP

Ivana Babić, Fabian Schmidt, Beatriz Tucci

Max-Planck-Institut für Astrophysik

Baryon Acoustic Oscillations

Baryon acoustic oscillations method

- Measuring the apparent size of the BAO scale in the late-time matter distribution allows us to estimate the angular-diameter distance and the Hubble parameter as a function of redshift.
- Before we can apply this method, we have to face two problems:
    1. Matter evolved nonlinearly
    2. We do not directly observe the evolved matter density field, but rather biased tracers of this field (halos, galaxies, galaxy clusters…)

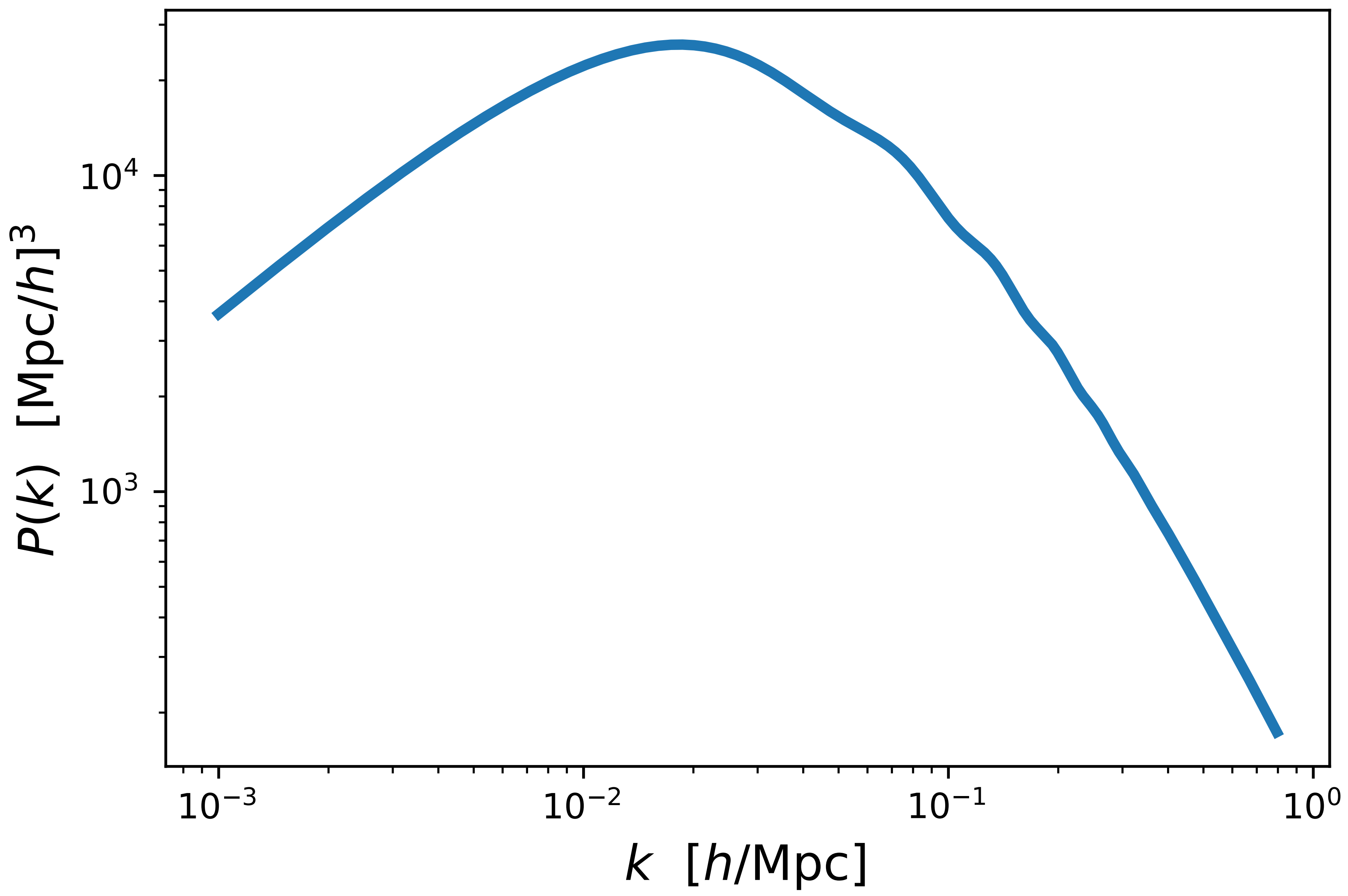

Baryon acoustic oscillations method

- Measuring the apparent size of the BAO scale in the late-time matter distribution allows us to estimate the angular-diameter distance and the Hubble parameter as a function of redshift.

- Before we can apply this method, we have to face two problems:

    1. Matter evolved nonlinearly

    2. We do not directly observe the evolved matter density field, but rather biased tracers of this field (halos, galaxies, galaxy clusters…)

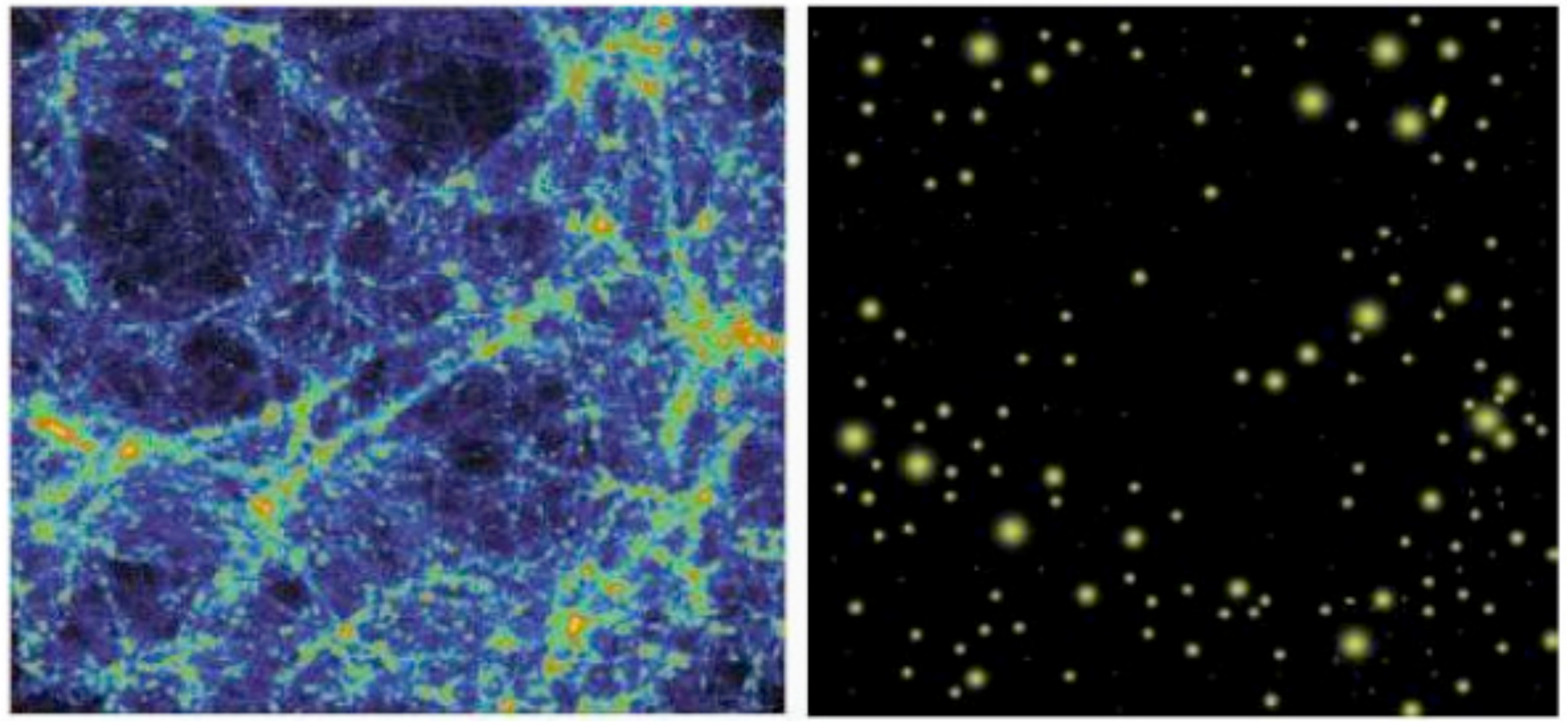

Cooray & Sheth (2002)

Baryon acoustic oscillations method

Nonlinear structure formation shifts and broadens the BAO peak in the correlation function, and equivalently dampens the oscillations in the power spectrum → Precision with which the BAO can be measured from galaxy clustering is reduced

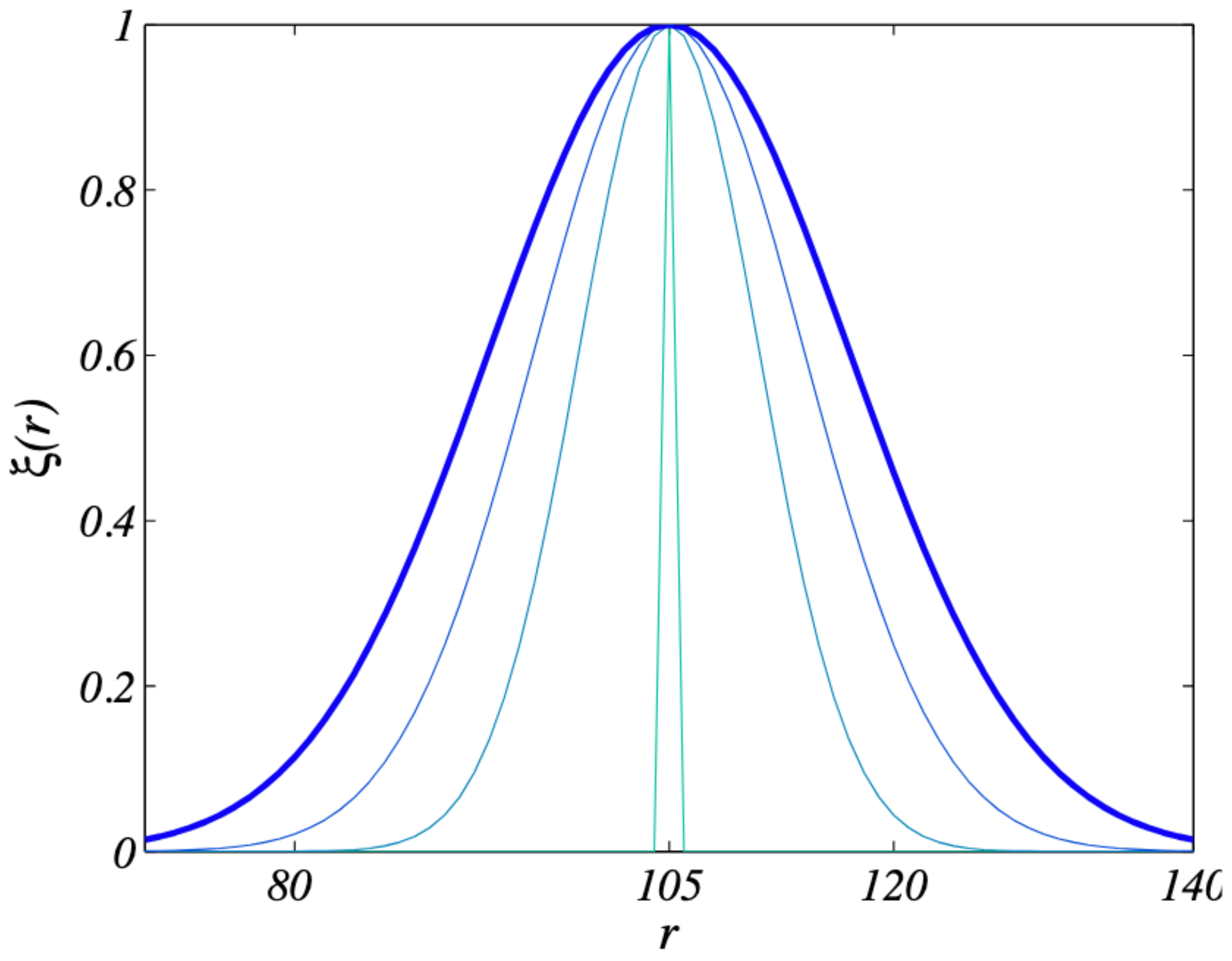

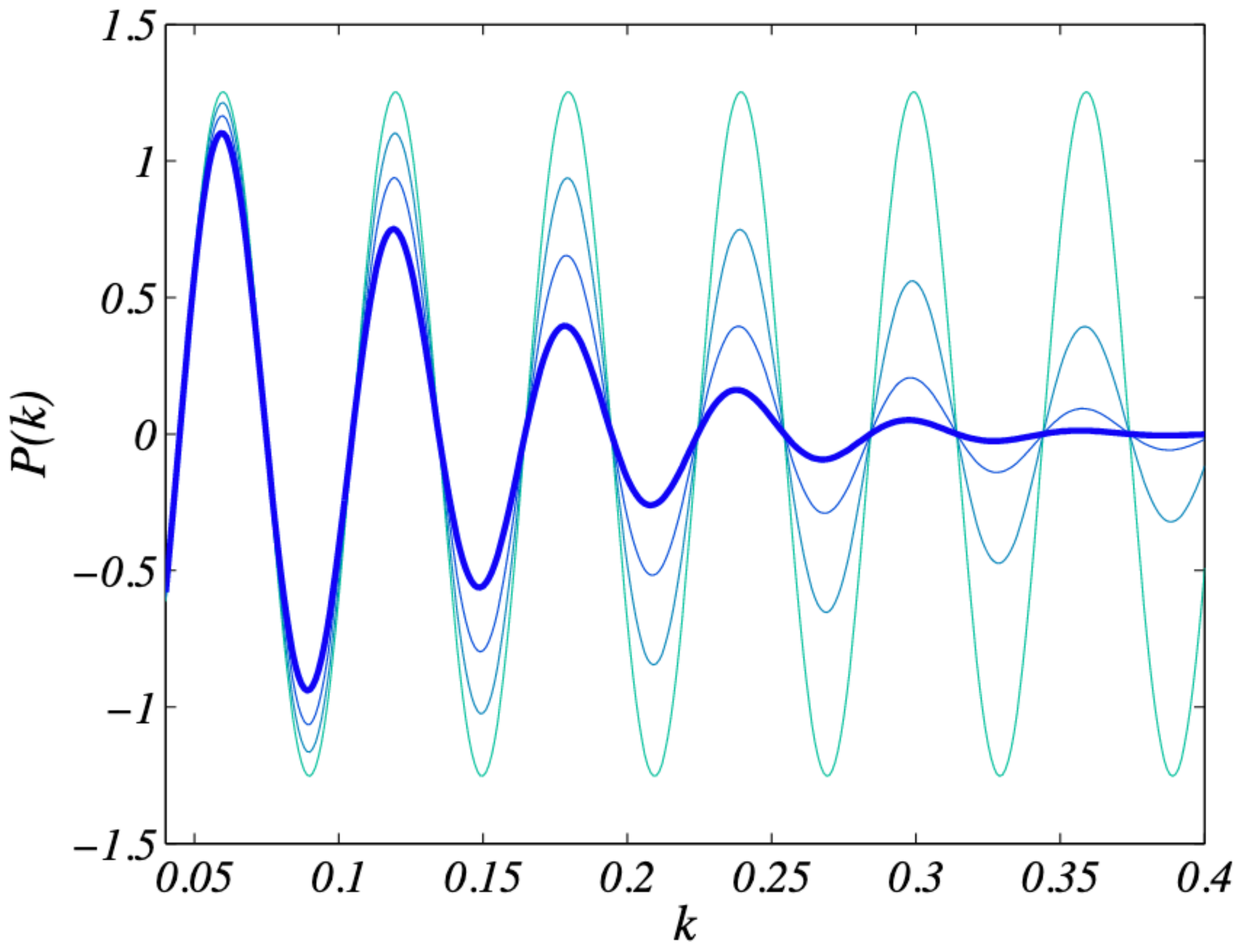

How well can we infer BAO using forward modeling approach?

Forward Model

Cosmology inference using Forward modeling

- Forward model starts from the initial phases $\delta_{\rm in}$ corresponding to primordial fluctuations and evolves them into observable structures today
- The goal of forward modeling is to find a joint posterior for the initial density field, cosmological parameters, bias parameters and stochastic amplitudes

Theory: $\delta_{\rm in}(k) \rightarrow$ **Forward model for matter + bias expansion** $\rightarrow \delta_{h,\rm det}(k)$

Data: **N-body simulation** $\rightarrow \delta_{\rm h}(k)$

$\rightarrow$ **Likelihood**

Changing BAO scale in the initial field

- To constrain the BAO scale from the information available in the oscillatory part of the power spectrum, without referring to its broad band part, we use the approximation

$$P_L(k) = \underbrace{P_{\mathrm{L,sm}}(k)}_{\text{Broad band}}[1 + A\,\underbrace{\sin(k\beta r_{fid})}_{\text{BAO feature}}\underbrace{\exp(-k/k_D)}_{\text{Silk damping}}]$$

- Changing β will result in changes in the oscillatory part of the power spectrum while keeping its overall shape intact

$$\beta = \frac{r_s}{r_{fid}}$$

$$\boxed{\text{Changing } \beta} \longleftrightarrow \boxed{\text{Changing BAO scale}}$$

- Factor $f(k, \beta)$ relates the fiducial power spectrum to the one with a different BAO scale

$$f^2(k,\beta) = \frac{P_{\mathrm{L}}(k,\beta)}{P_{\mathrm{fid}}(k)} = \frac{1 + A\sin(k\beta r_{\mathrm{fid}})\exp(-k/k_{\mathrm{D}})}{1 + Asin(kr_{\mathrm{fid}})\exp(-k/k_{\mathrm{D}})} \longrightarrow \delta_{\mathrm{in}}(k,\beta) = f(k,\beta)\delta_{\mathrm{fid}}(k)$$

Theory: $\delta_{\rm in}(k, \beta) \longrightarrow$ **Forward model for matter + bias expansion** $\longrightarrow \delta_{h,\rm det}(k)$

Data: **N-body simulation** $\longrightarrow \delta_{\rm h}(k)$

$\longrightarrow$ **Likelihood**

EFT 'field-level' likelihood

Schmidt et al 2018
arXiv:1808.02002

Cabass & Schmidt 2019
arXiv:1909.04022

Cabass & Schmidt 2020
arXiv:2004.00617

Schmidt et al 2020
arXiv:2004.06707

- Conditional probability for finding a measured halo density field δ_h given the predicted deterministic halo density field $\delta_{h,\mathrm{det}}$
- EFT likelihood is given as

$$\ln P(\delta_h | \delta_{\mathrm{in}}, \{b_O\}) = -\frac{1}{2} \sum_{|\mathbf{k}|<\Lambda} \left[\ln[2\pi\sigma_\varepsilon^2(k)] + \frac{1}{\sigma_\varepsilon^2(k)} |\delta_h(\mathbf{k}) - \delta_{h,\mathrm{det}}[\delta_{\mathrm{in}}, \{b_O\}](\mathbf{k})|^2 \right]$$

- Λ - cut-off
- σ_ε^2 - power spectrum of halo stochasticity in the large scale limit

EFT likelihood captures all information at once
(power spectrum, bispectrum…)

How EFT likelihood constraints BAO compares to standard likelihood?

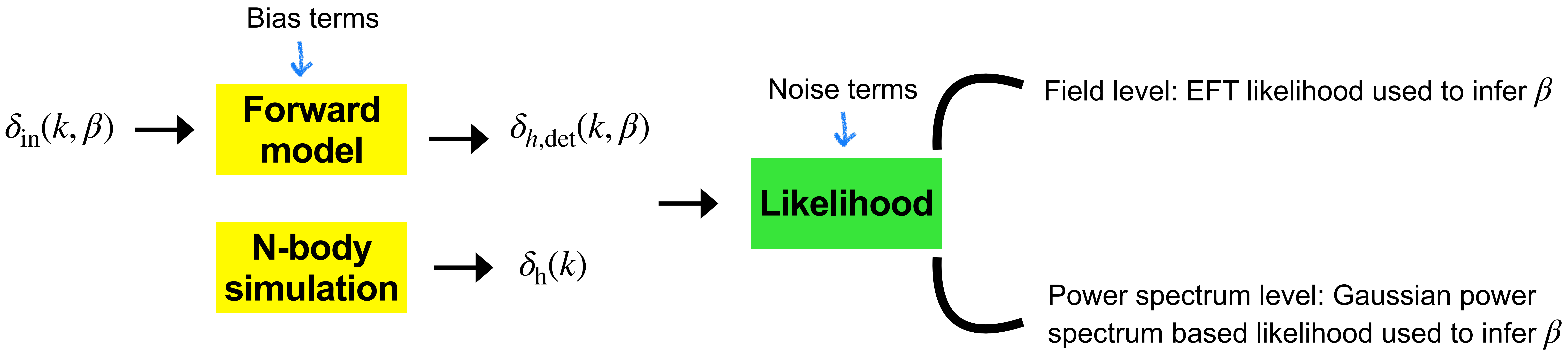

Results

Field level: BAO inference at different z

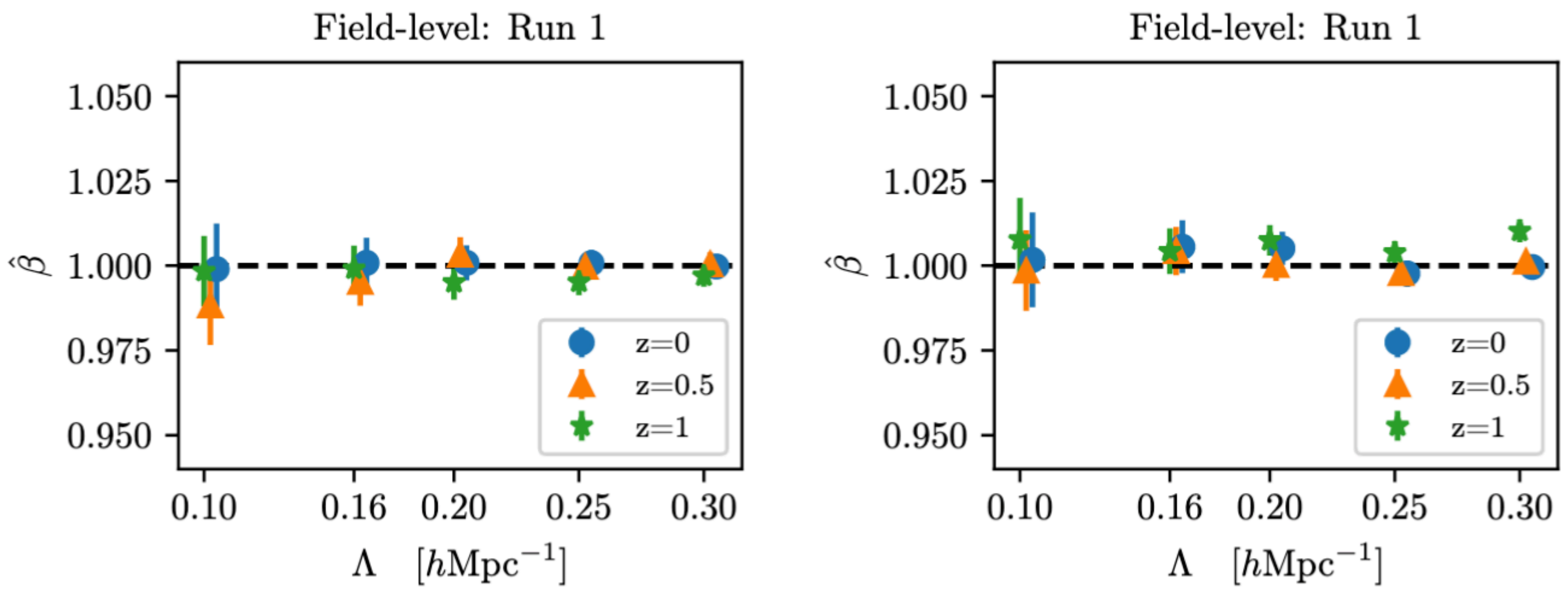

(a) $\log_{10}(M/h^{-1}M_{\odot}) = 12.5 - 13.0$

(b) $\log_{10}(M/h^{-1}M_{\odot}) = 13.0 - 13.5$

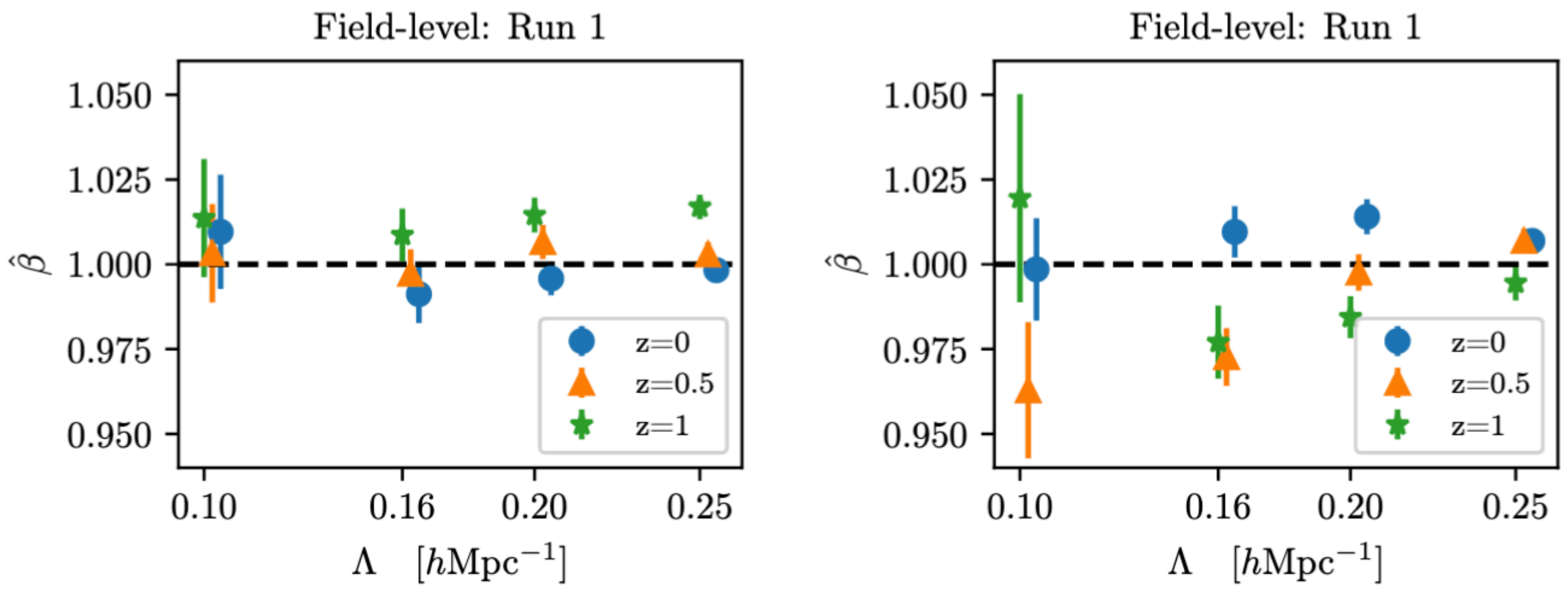

(c) $\log_{10}(M/h^{-1}M_{\odot}) = 13.5 - 14.0$

(d) $\log_{10}(M/h^{-1}M_{\odot}) = 14.0 - 14.5$

- The remaining systematic bias is very low across all the redshifts and mass ranges
- Bias below 2% across all redshifts

Comparing Field-level to Power spectrum likelihood

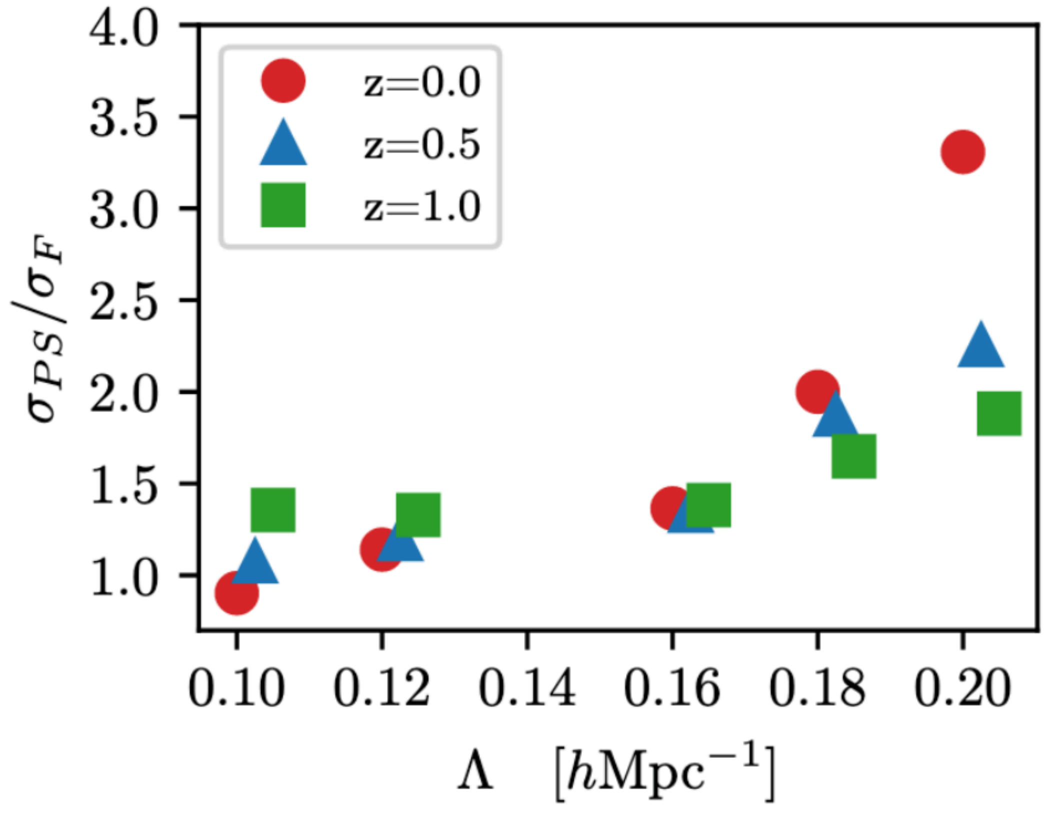

(a) $\log_{10}(M/h^{-1}M_\odot) = 12.5 - 13.0$

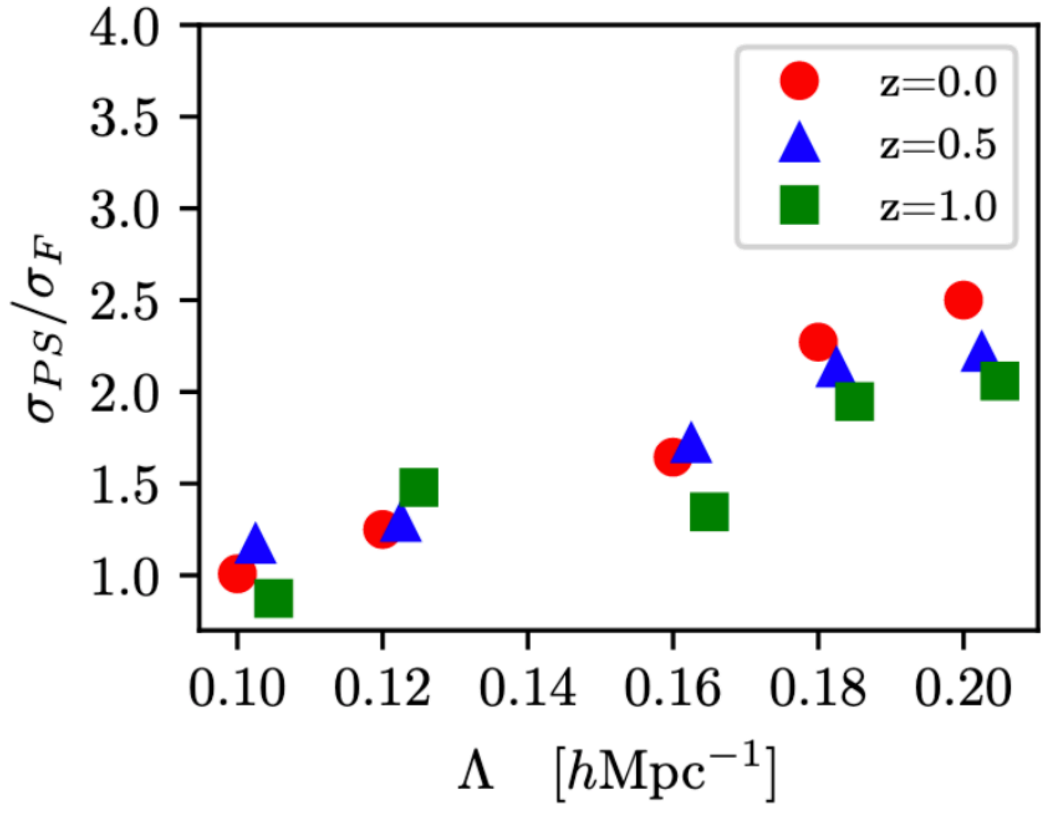

(b) $\log_{10}(M/h^{-1}M_\odot) = 13.0 - 13.5$

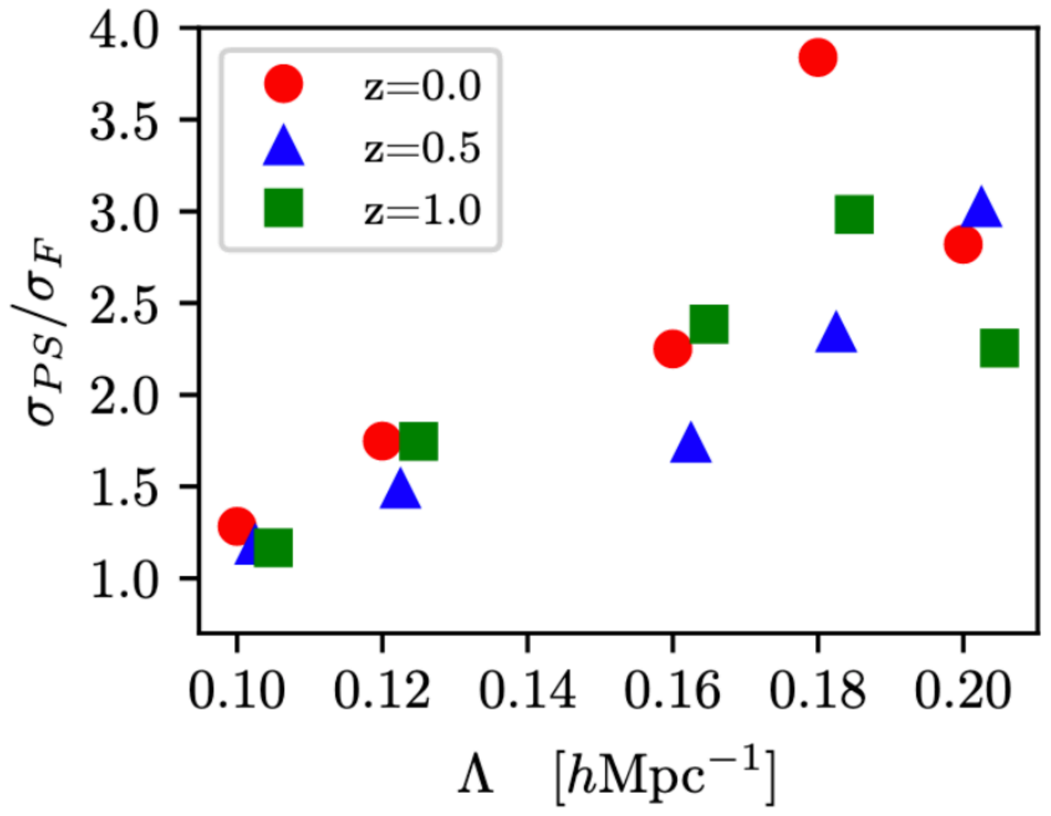

(c) $\log_{10}(M/h^{-1}M_\odot) = 13.5 - 14.0$

- For smaller cutoffs, both likelihoods give similar results, which is the expected result if the data δ_h are well approximated as a Gaussian random field
- The field-level likelihood knows about the velocity field, and can compare the expected BAO scale at a given location with the data.
- The power spectrum is averaged over all locations, and suffers from the damping of the BAO peak

Takeaway

- BAO inference with EFT likelihood in the case of fixed phases:
  - **Remaining systematic bias for EFT likelihood is below 1%** and consistent with zero for all but the most highly biased samples
  - **EFT 'field level' likelihood outperforms Power Spectrum likelihood** (σ_{PS}/σ_F is between 1.1 and 3.3 depending on Λ)
- In future work we plan to investigate how well we can constrain the BAO scale from the EFT likelihood in the case when the initial conditions are not fixed, but sampled

Augmenting redshift information in large cosmological surveys

Università degli Studi di Milano - Dipartimento di Fisica

Marina S. Cagliari
Collaborators: B.R. Granett, F. Tosone, L. Guzzo

Summer School on Cosmology 2022 - ICTP
Contributed talk

Introduction

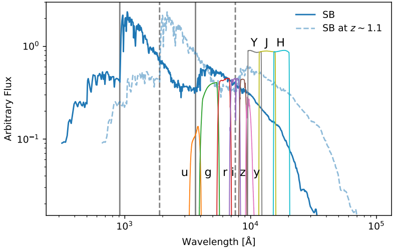

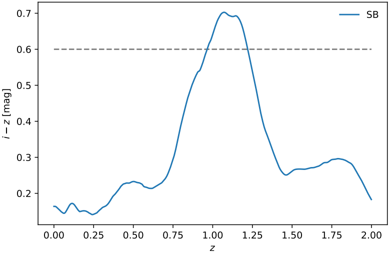

- Redshifts can be measured either with spectroscopy or photometry.
- Photometric measurements are deeper and faster than spectroscopic ones.

Introduction

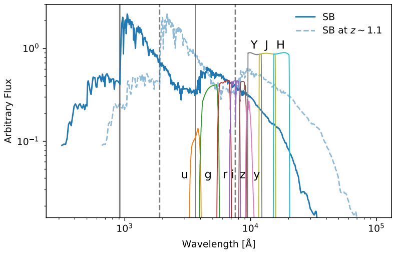

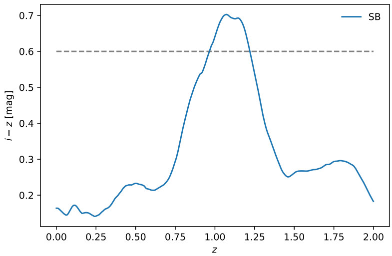

- Our idea is to augment photometric data with ancillary spectroscopic information.
- We worked on two methods with this aim.

Euclid

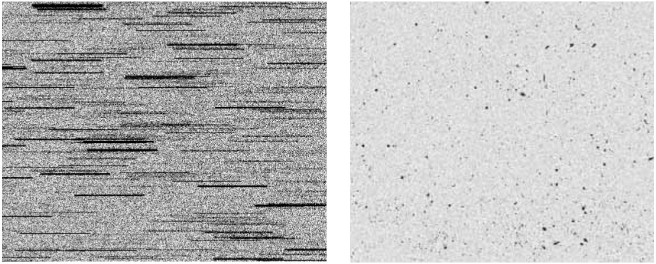

Figure from Laureijs et al. (2011)

- Euclid will obtain NIR photometry and a shallow spectrum for every galaxy.
- Euclid will not be able to measure the spectroscopic redshift of every galaxy.

Ensemble photometric redshifts

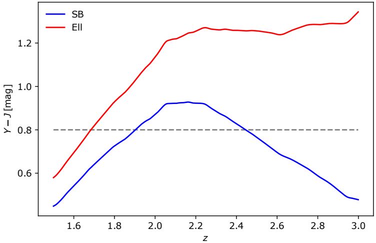

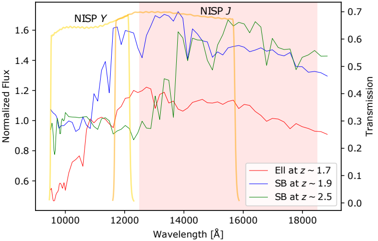

Cagliari et al. (2022)

- The ensemble photometric redshifts method (Padmanabhan et al., 2019) aims at constraining the redshift distribution of a *photometrically-selected galaxy sample* by using the *stacked spectrum* built from the average of many low signal-to-noise spectra.

Results

Non-attenuated catalogue

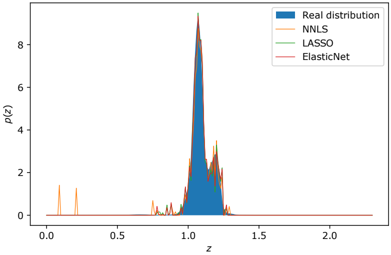

Real attenuation catalogue

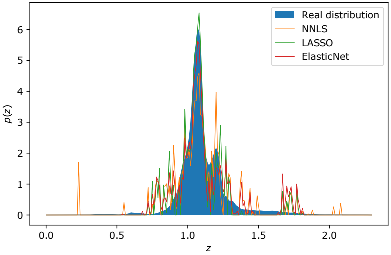

Figures from Cagliari et al. (2022)

VIPERS

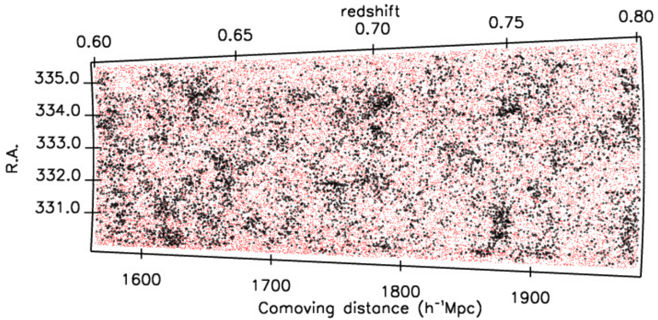

Figure from Cucciati et al. (2014)

- In VIPERS only about the 35% of the galaxies in the parent sample have a measured spectroscopic redshift.

NezNet

- Not all angular neighbours are real spatial neighbours.
- The ratio between real and false angular neighbours depends on the depth of the survey.
- We built a Graph Neural Network (GNN), which given a galaxy pair classifies it as *true* or *false* neighbours.

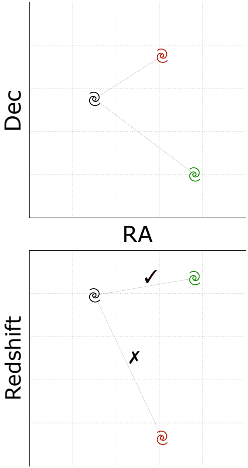

Preliminary Results

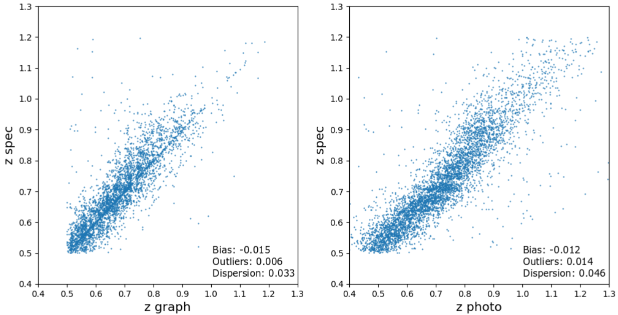

z graph: spectroscopic redshift of the most probable neighbours,
z photo: photometric redshift measured with spectral SED fitting.

Thanks for your Attention!

Euclid mock stacked spectra

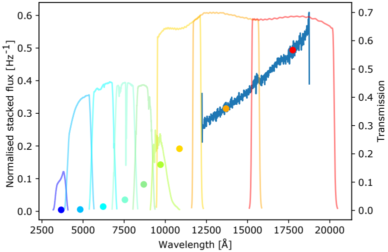

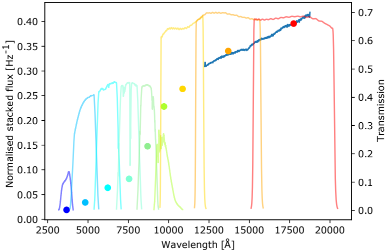

Figures from Cagliari et al. (2022)

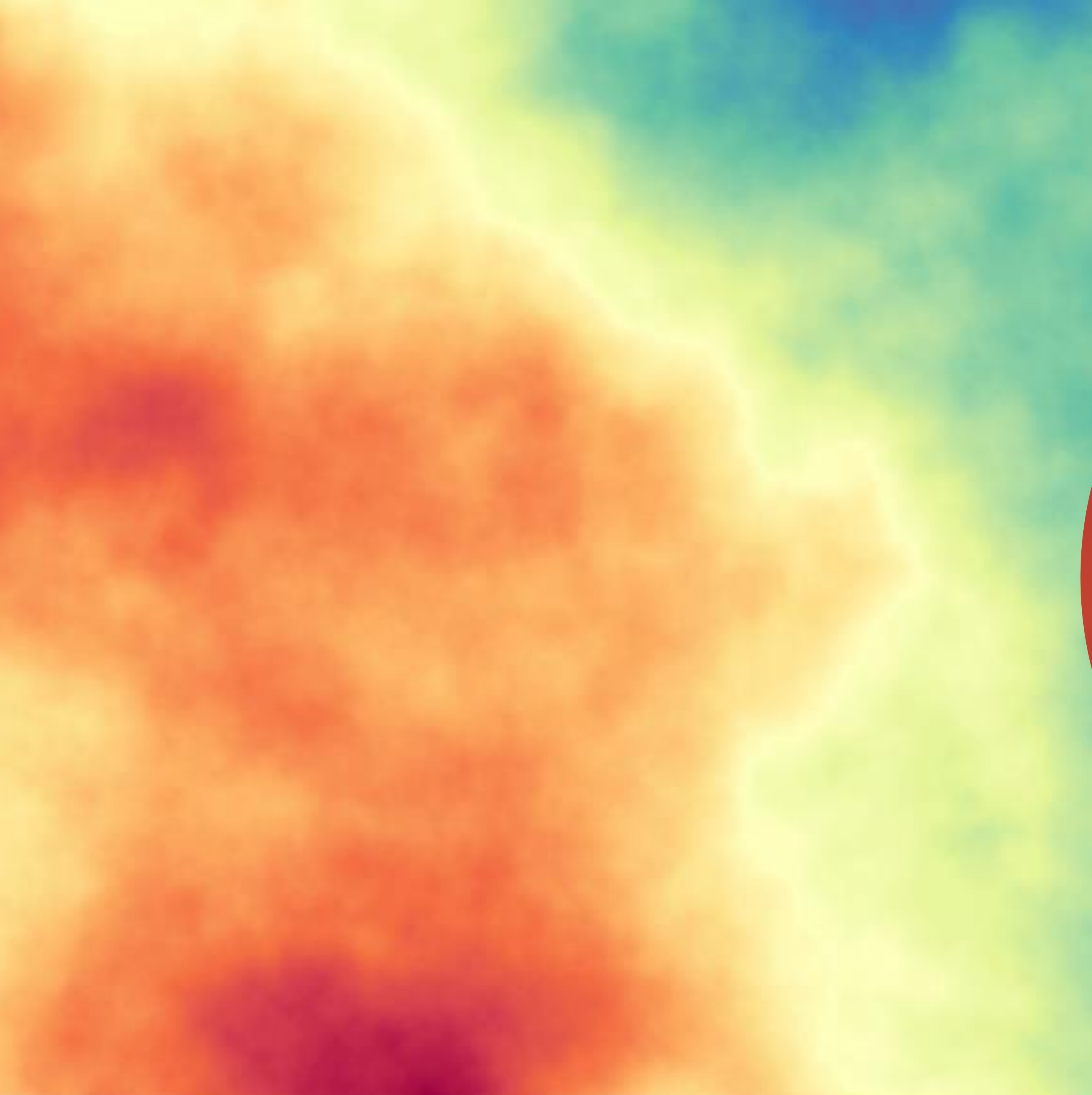

Baseline-Dependent Ionospheric Effects on Interferometer Calibration of LOFAR EoR Observations

Stefanie Brackenhoff
Kapteyn Astronomical Institute

Advisors:
Prof. dr. Léon Koopmans (Kapteyn)
Prof. dr. ir. Alle-Jan van der Veen (TU Delft)
Dr. André Offringa (ASTRON/Kapteyn)
Dr. Maaijke Mevius (ASTRON)

Mertens et al. 2020 (MNRAS)

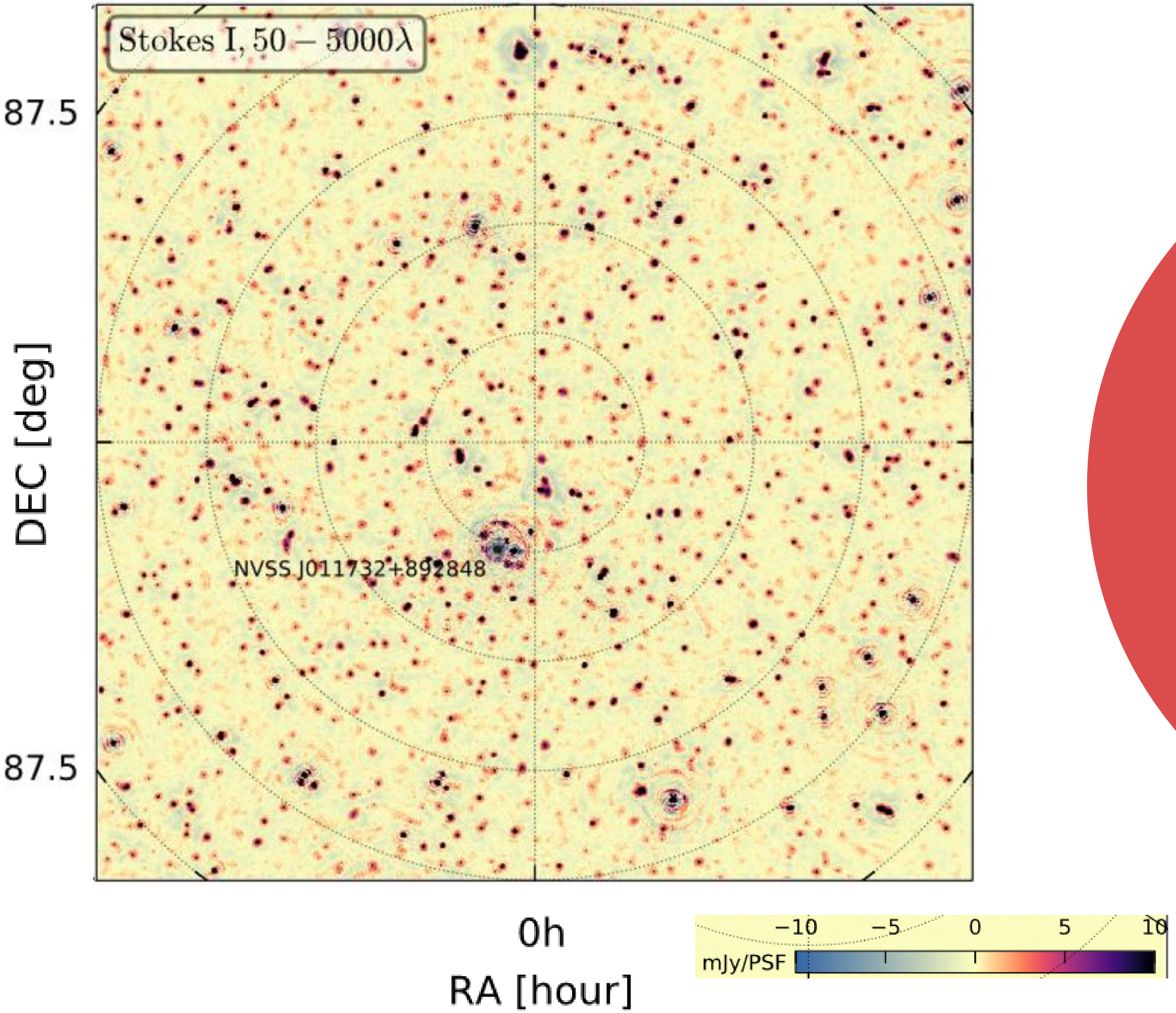

Baseline-Dependent Ionospheric Effects on Interferometer Calibration of LOFAR EoR Observations

Stefanie Brackenhoff
Kapteyn Astronomical Institute

Advisors:
Prof. dr. Léon Koopmans (Kapteyn)
Prof. dr. ir. Alle-Jan van der Veen (TU Delft)
Dr. André Offringa (ASTRON/Kapteyn)
Dr. Maaijke Mevius (ASTRON)

Mertens et al. 2020 (MNRAS)

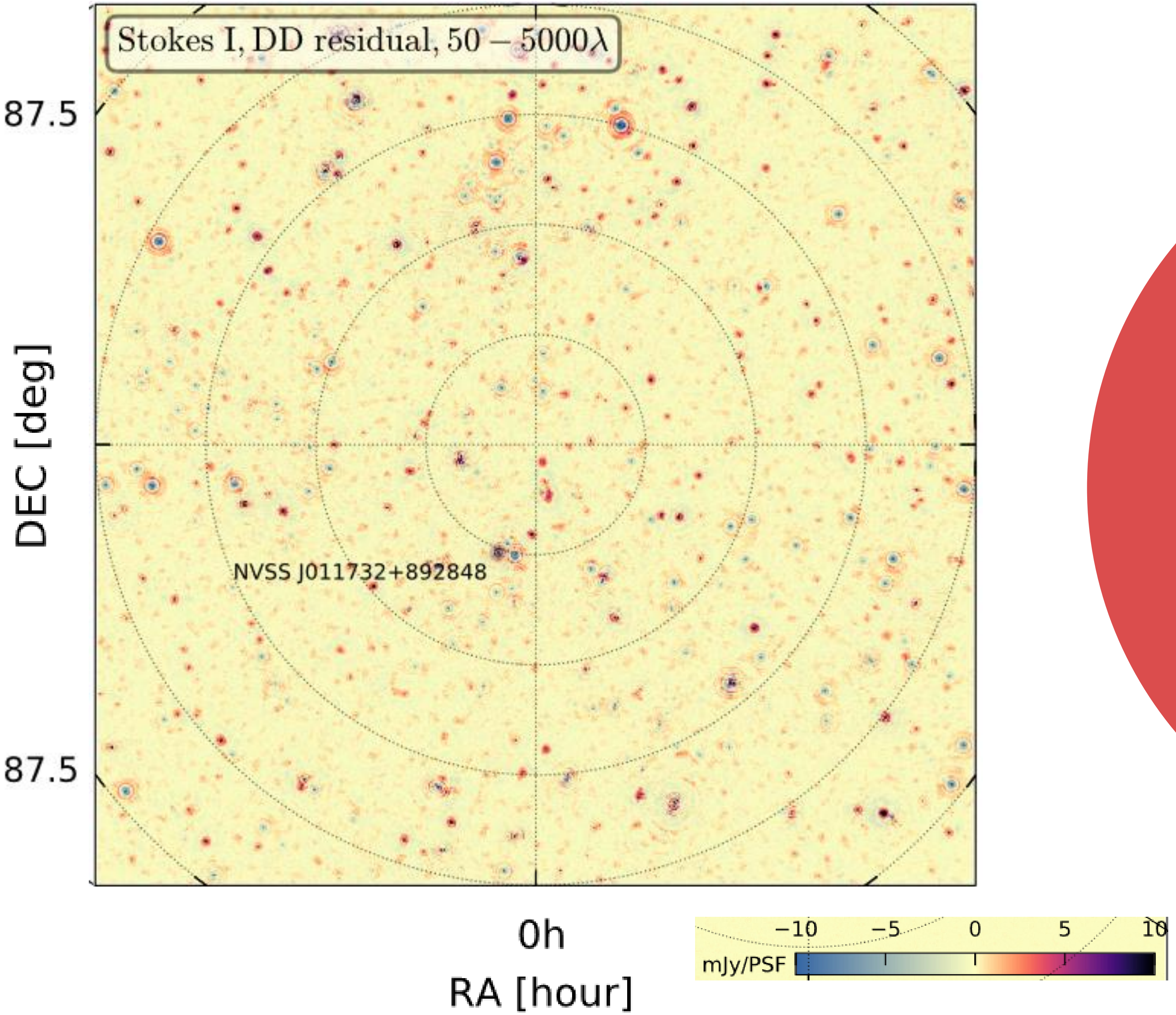

Baseline-Dependent Ionospheric Effects on Interferometer Calibration of LOFAR EoR Observations

Stefanie Brackenhoff
Kapteyn Astronomical Institute

Advisors:
Prof. dr. Léon Koopmans (Kapteyn)
Prof. dr. ir. Alle-Jan van der Veen (TU Delft)
Dr. André Offringa (ASTRON/Kapteyn)
Dr. Maaijke Mevius (ASTRON)

Mertens et al. 2020 (MNRAS)

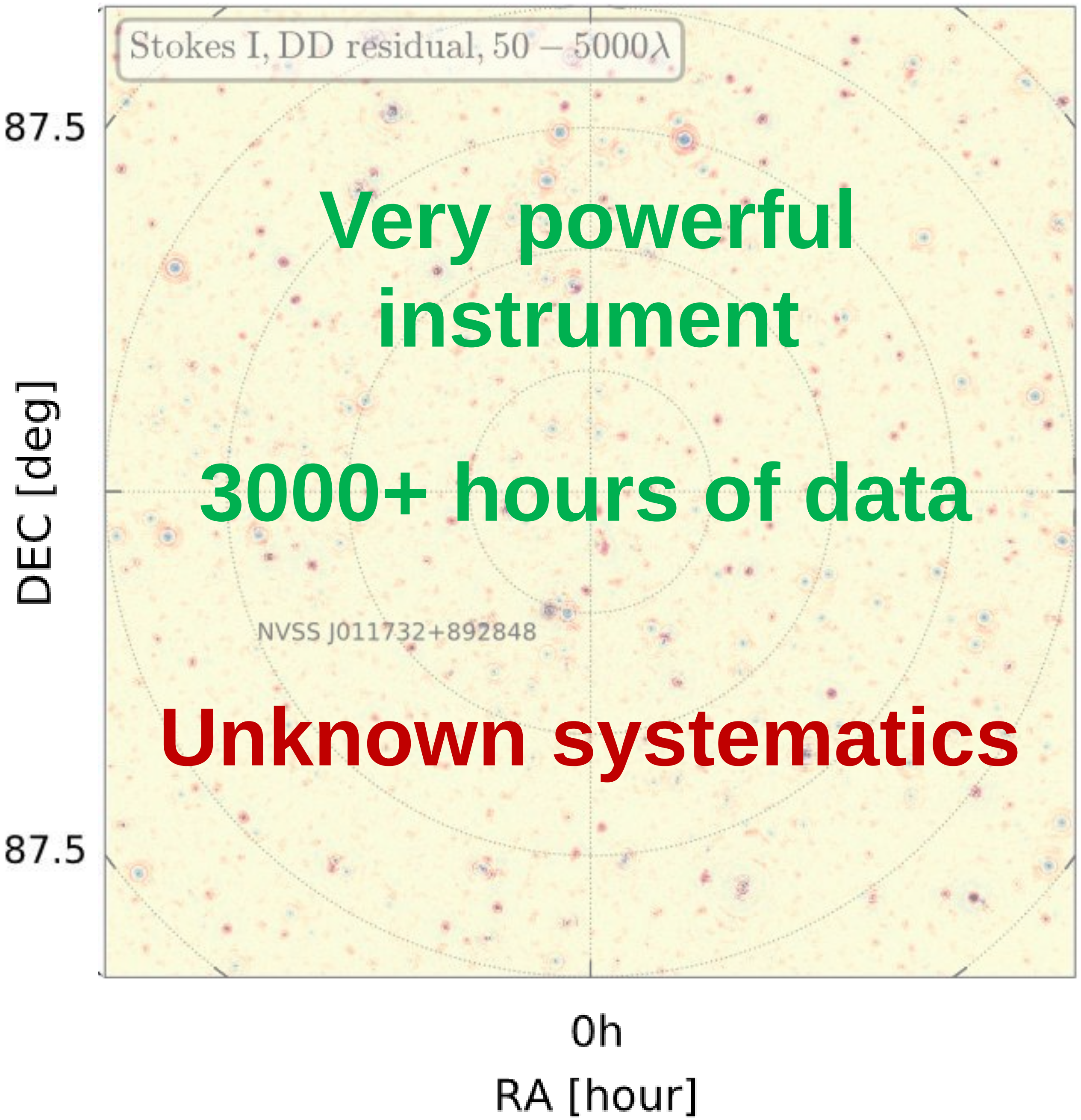

Very powerful instrument

3000+ hours of data

Unknown systematics

Baseline-Dependent Ionospheric Effects on Interferometer Calibration of LOFAR EoR Observations

Stefanie Brackenhoff
Kapteyn Astronomical Institute

Advisors:
Prof. dr. Léon Koopmans (Kapteyn)
Prof. dr. ir. Alle-Jan van der Veen (TU Delft)
Dr. André Offringa (ASTRON/Kapteyn)
Dr. Maaijke Mevius (ASTRON)

The redshifted 21-cm signal

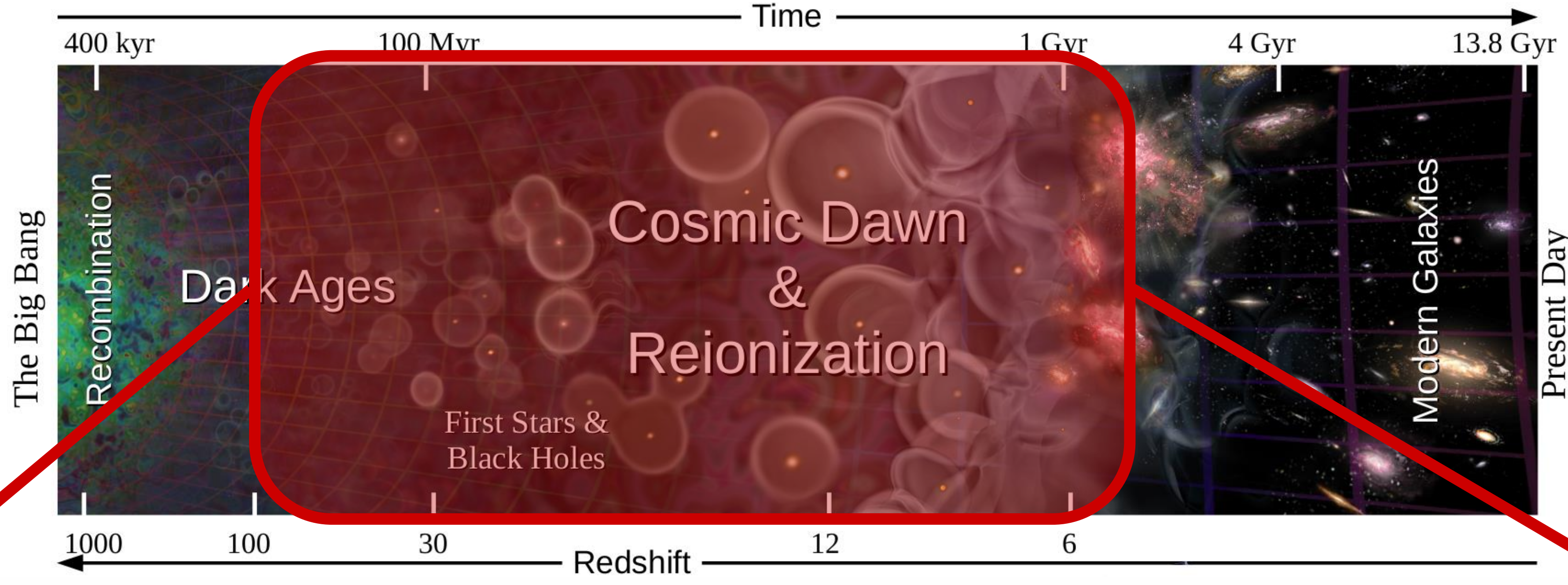

Loeb, 2006 (Sci. Am)

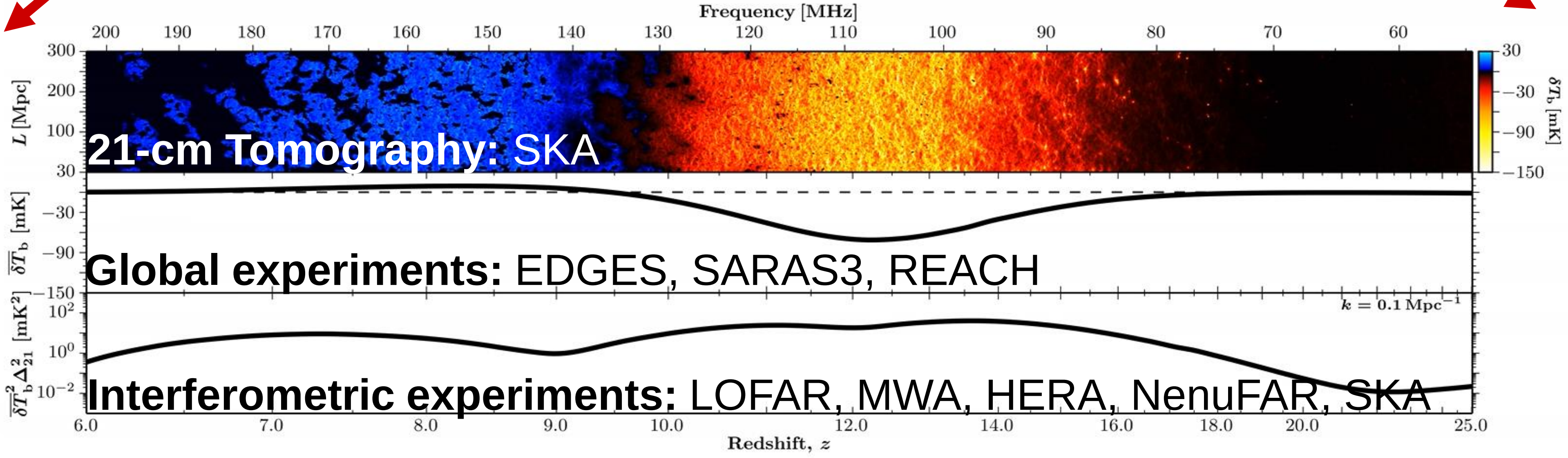

Mesinger, Greig & Park
http://homepage.sns.it/mesinger/21CMMC.html

university of groningen
faculty of science and engineering
Kapteyn Astronomical Institute

The redshifted 21-cm signal

Mesinger, Greig & Park
http://homepage.sns.it/mesinger/21CMMC.html

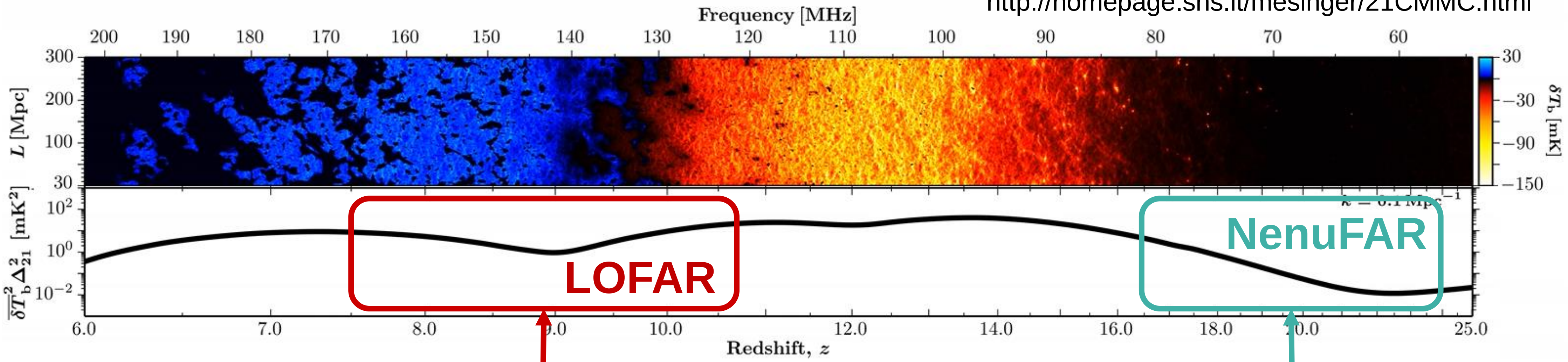

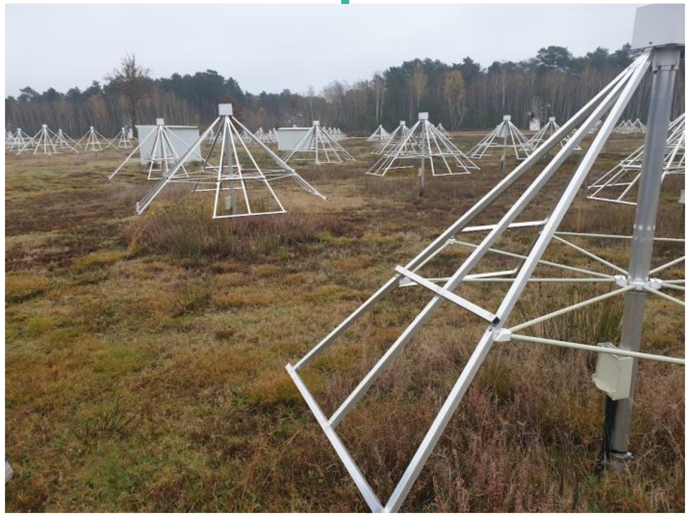

university of groningen

faculty of science and engineering

Kapteyn Astronomical Institute

Technical Challenge

Finding a needle in a haystack!

Contaminations:

- Astrophysical foregrounds
- **Earth's Ionosphere**
- Radio Frequency Interference
- Instrumental imperfections
- Data processing artifacts

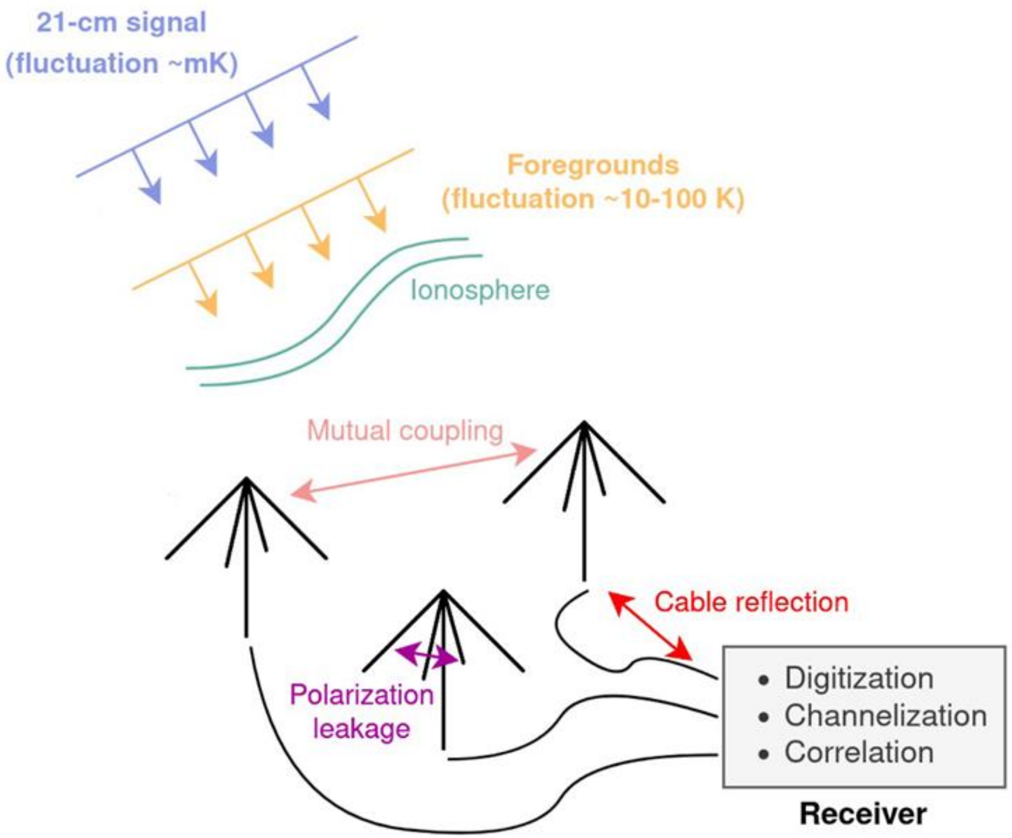

Courtesy of Dr. B.K. Gehlot

Ionosphere

Turbulent ionized layer → phase shifts

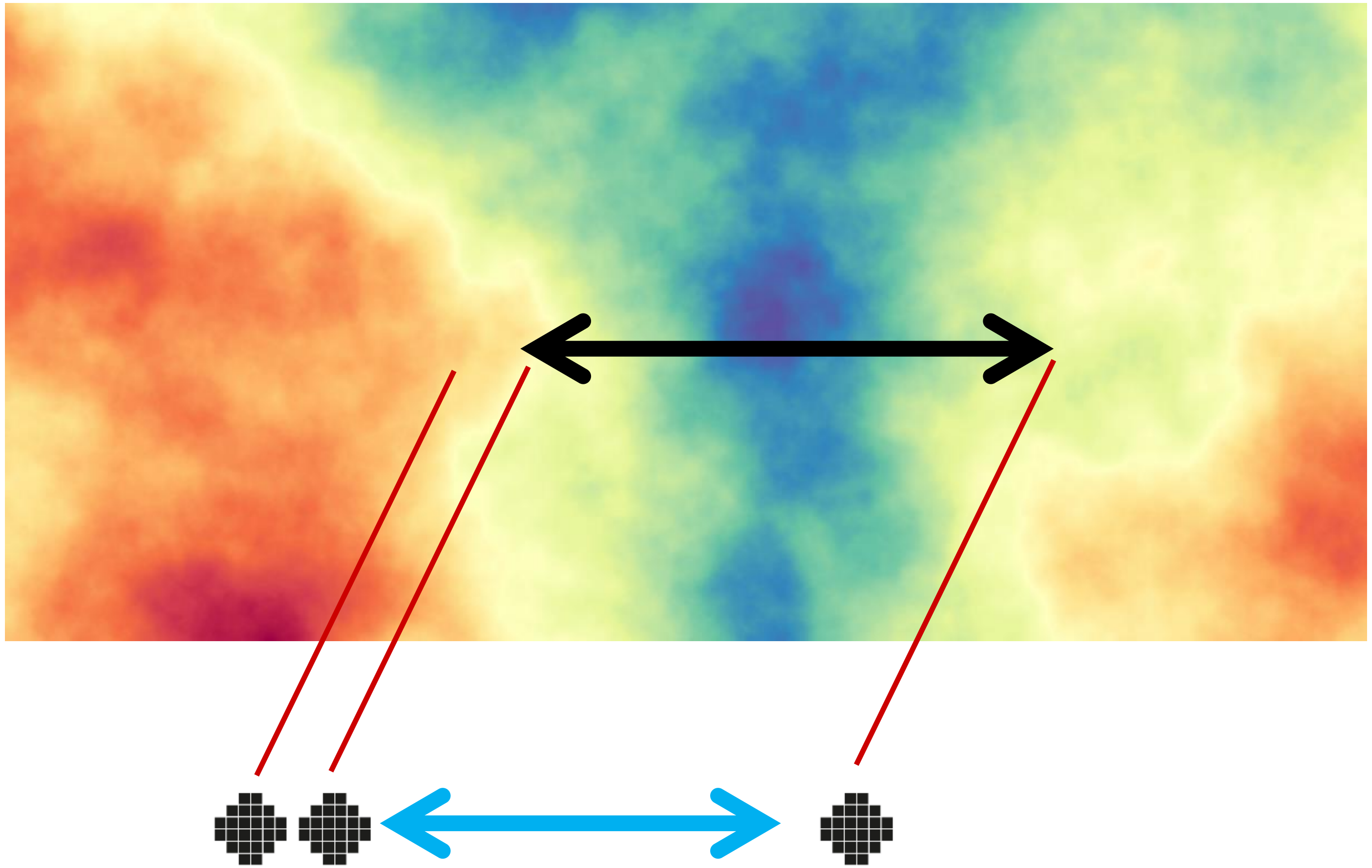

Longer baseline

Larger scale

Larger phase variation

Longer time correlation

Easier to calibrate on bright point sources

Power Spectra

Without ionosphere

Ratio spectrum / thermal noise realization

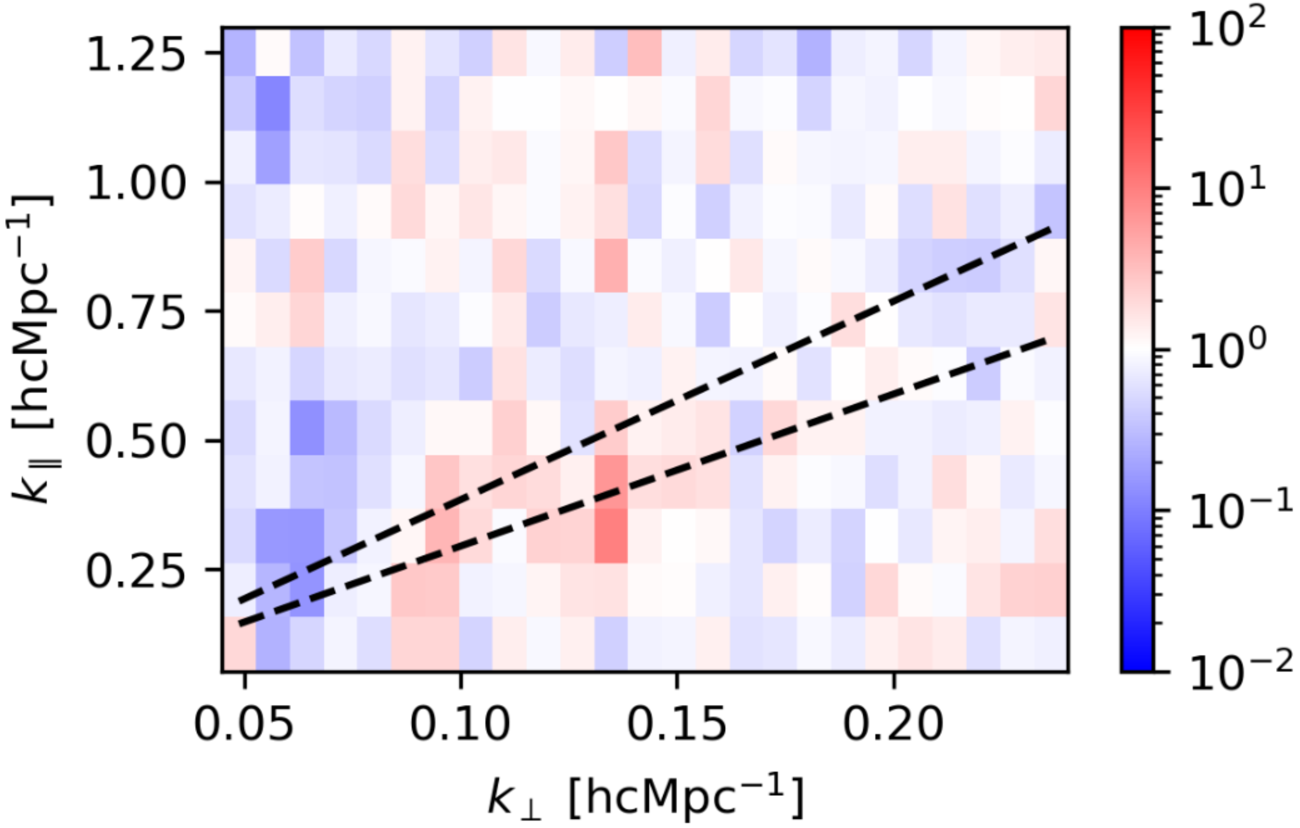

With ionosphere

Ratio spectrum / thermal noise realization

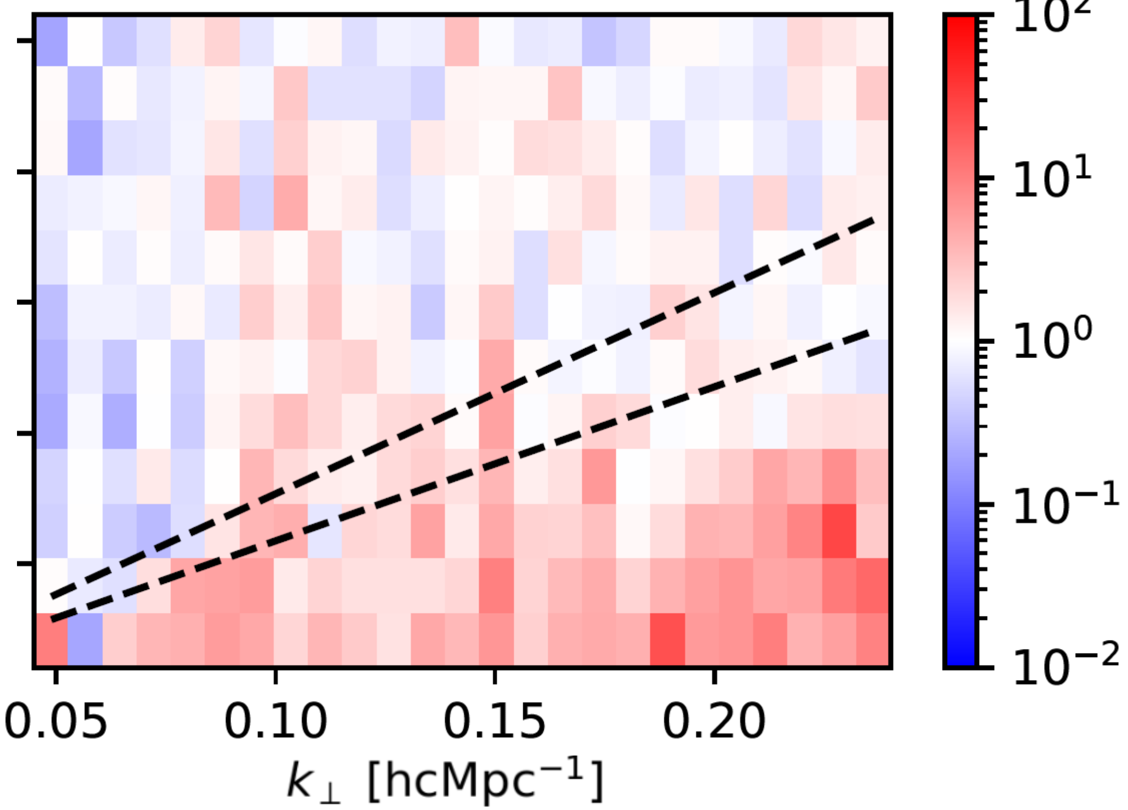

Simulation and reality

Real LOFAR data

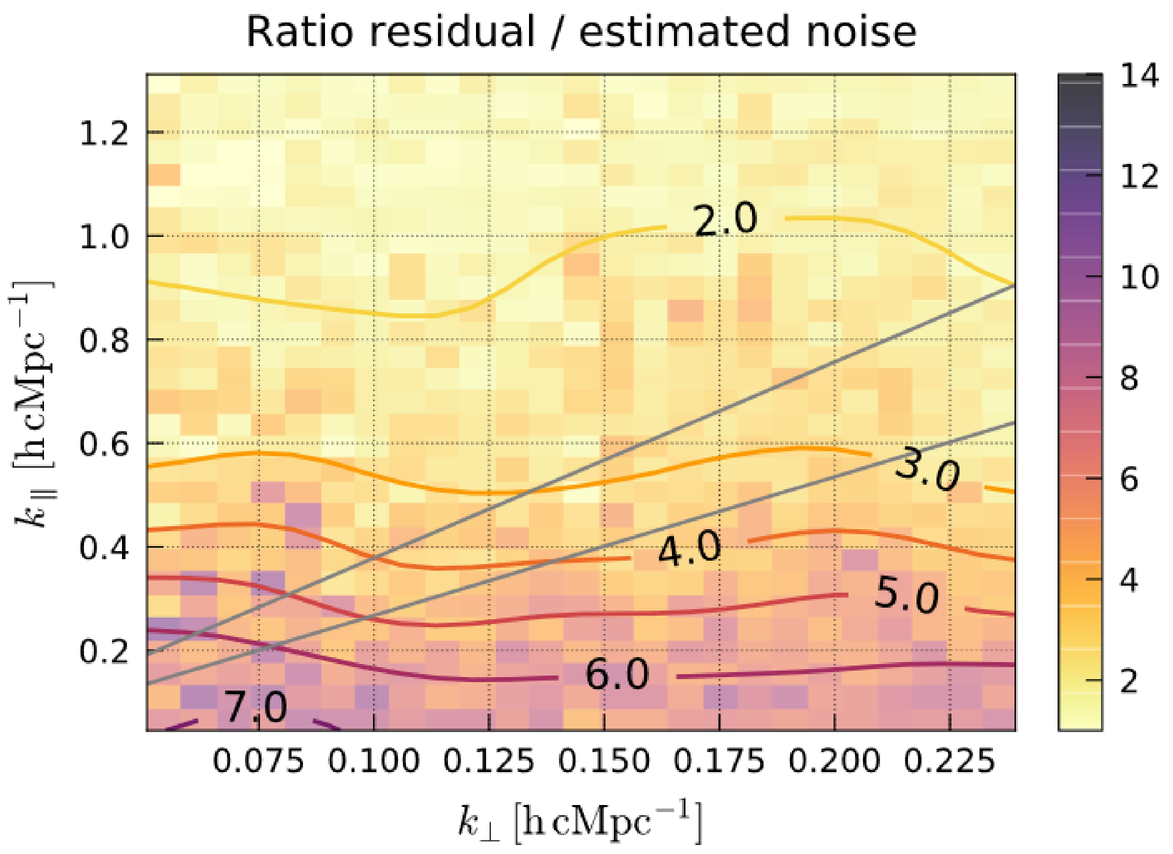

Mertens et al. 2020 (MNRAS)

Simulation with ionosphere

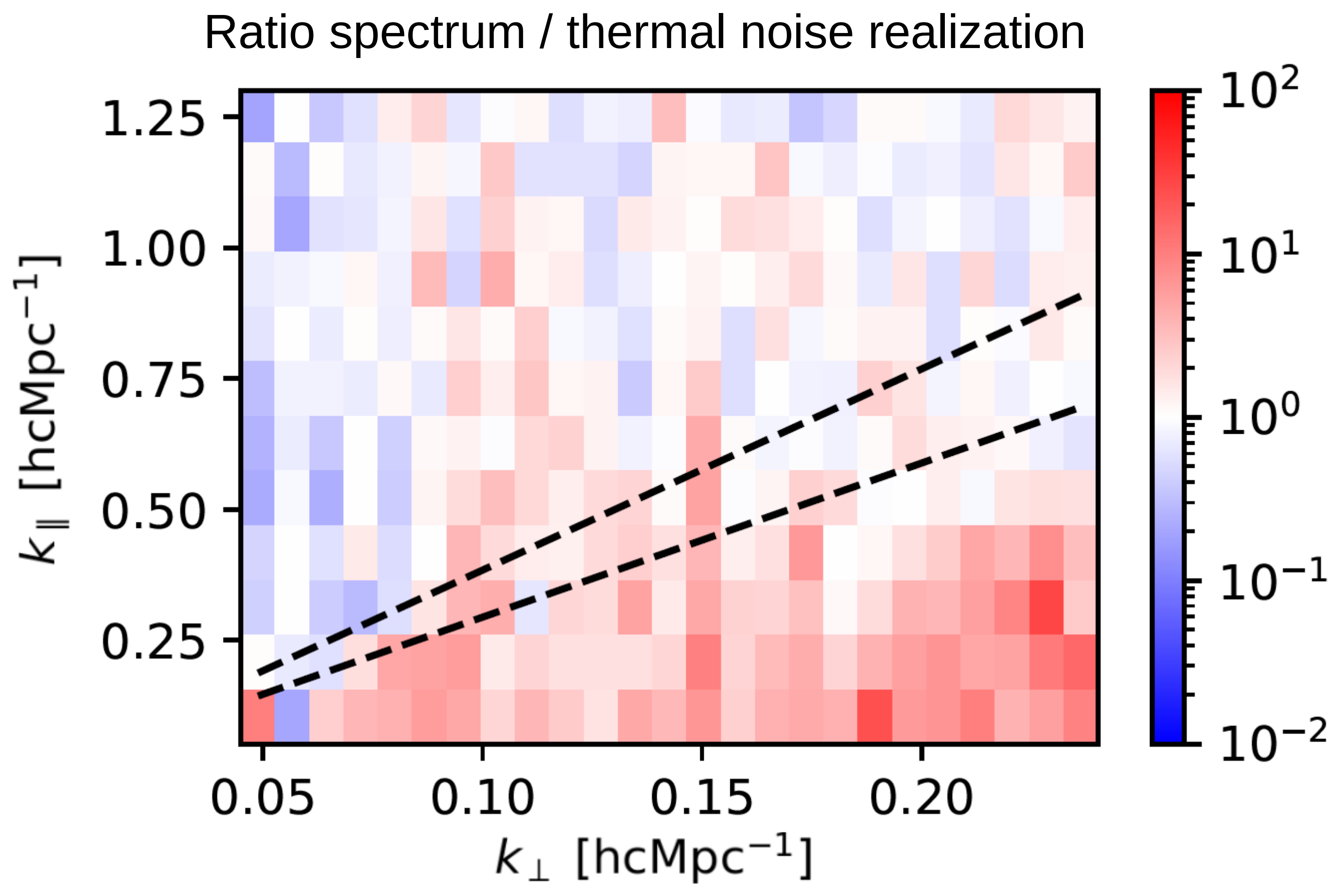

Take home message

- Estimating the 21-cm power spectrum from the EoR/CD is **very difficult**
- Exact effects of contaminants **not fully analyzed**
  - We need **forward simulations**
  - **Ionosphere** is one piece of this puzzle

university of groningen
faculty of science and engineering
Kapteyn Astronomical Institute

The Effective Field Theory of Large-Scale Structure and Multi-Tracer

Thiago Mergulhão, Henrique Rubira, Rodrigo Voivodic, Raul Abramo

ICTP - Summer School on Cosmology
July 2022

thiago.mergulhao@ed.ac.uk

Thiago Mergulhão *et al* JCAP04(2022)021

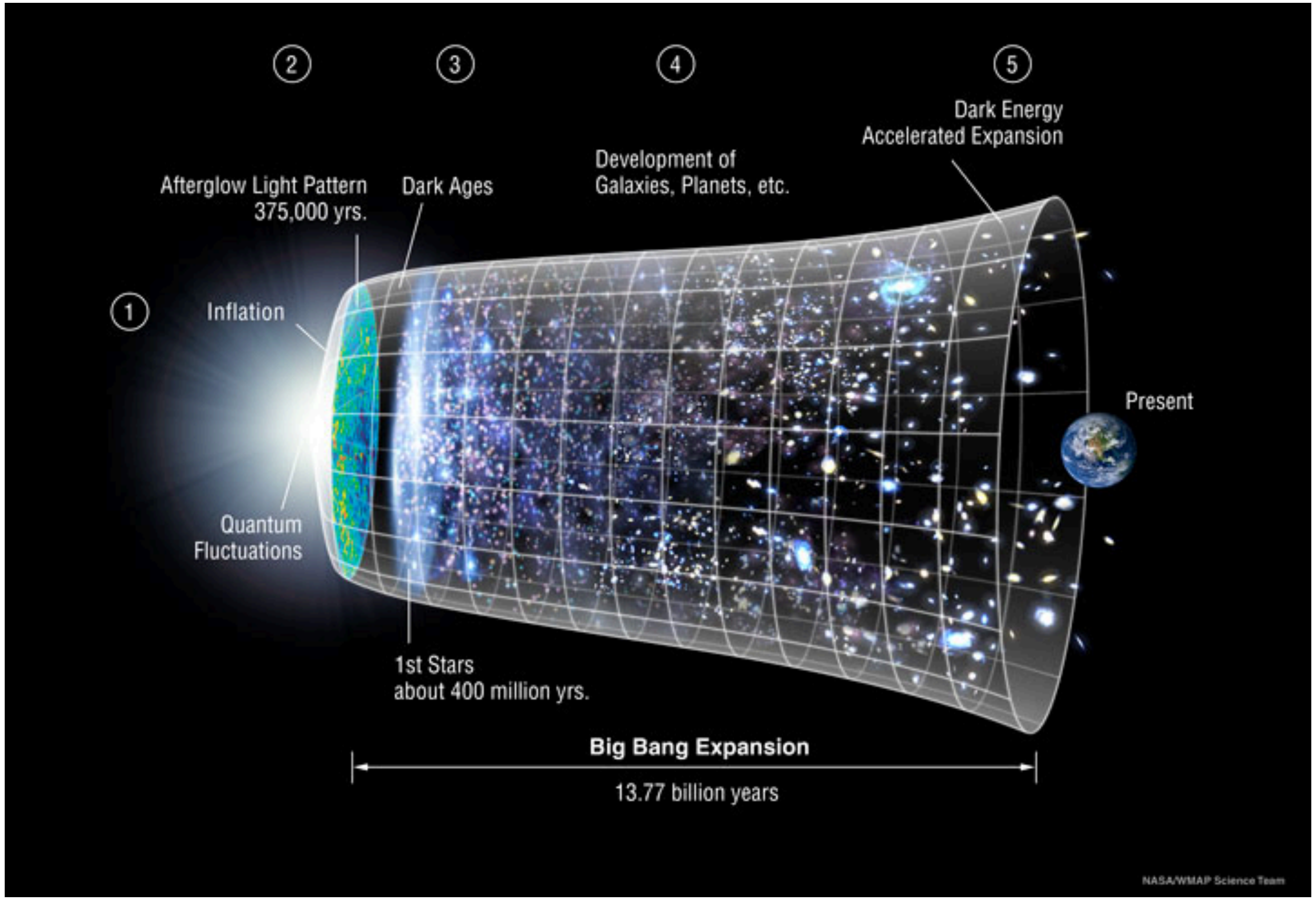

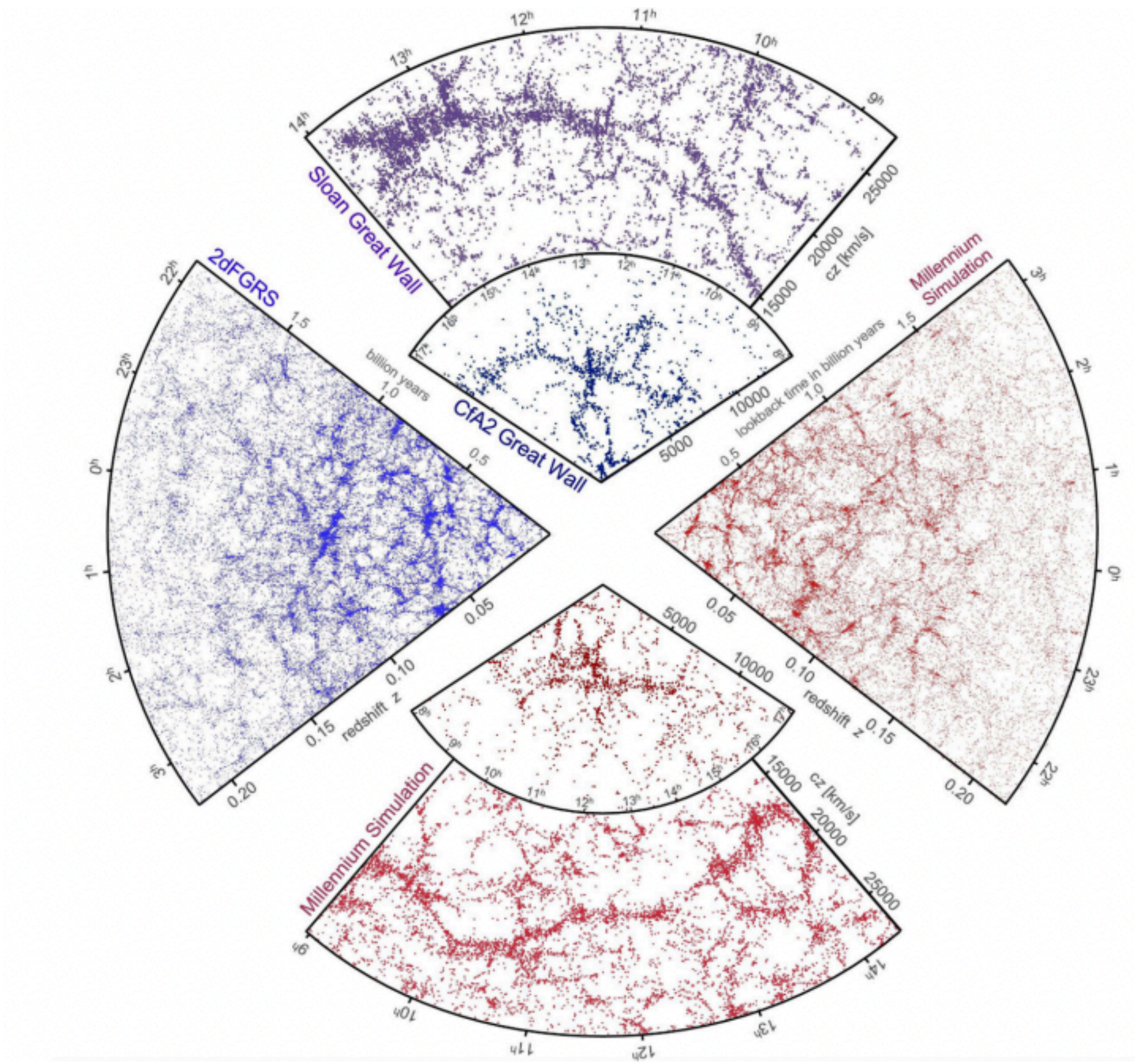

Credit: NASA/WMAP Science Team

V. Desjacques, D. Jeong and F. Schmidt (2016)

How can we optimise the information we extract from Large-Scale Structures?

One idea to answer the question:

Multi-tracer

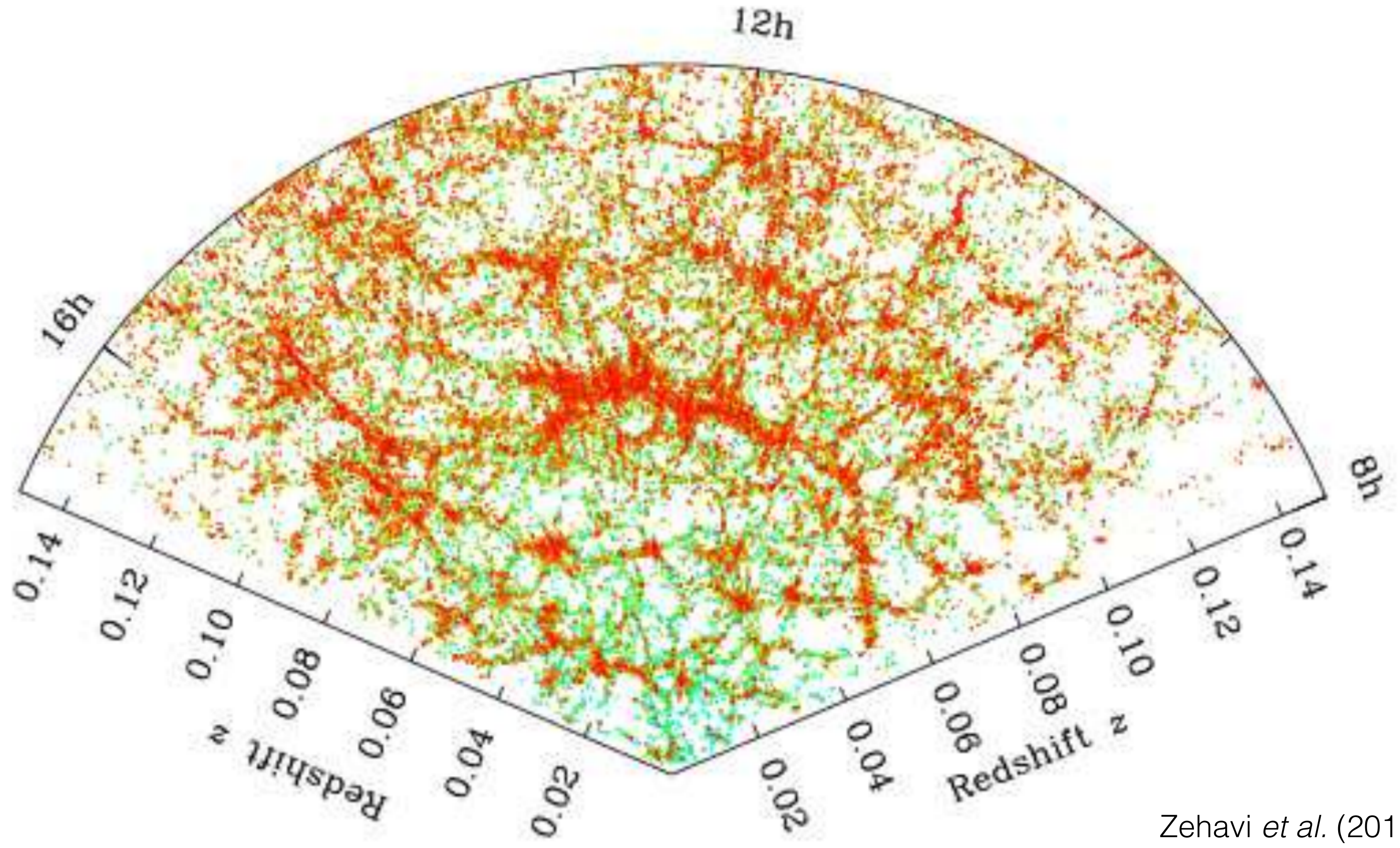

Zehavi *et al.* (2011)

+

Perturbation theory

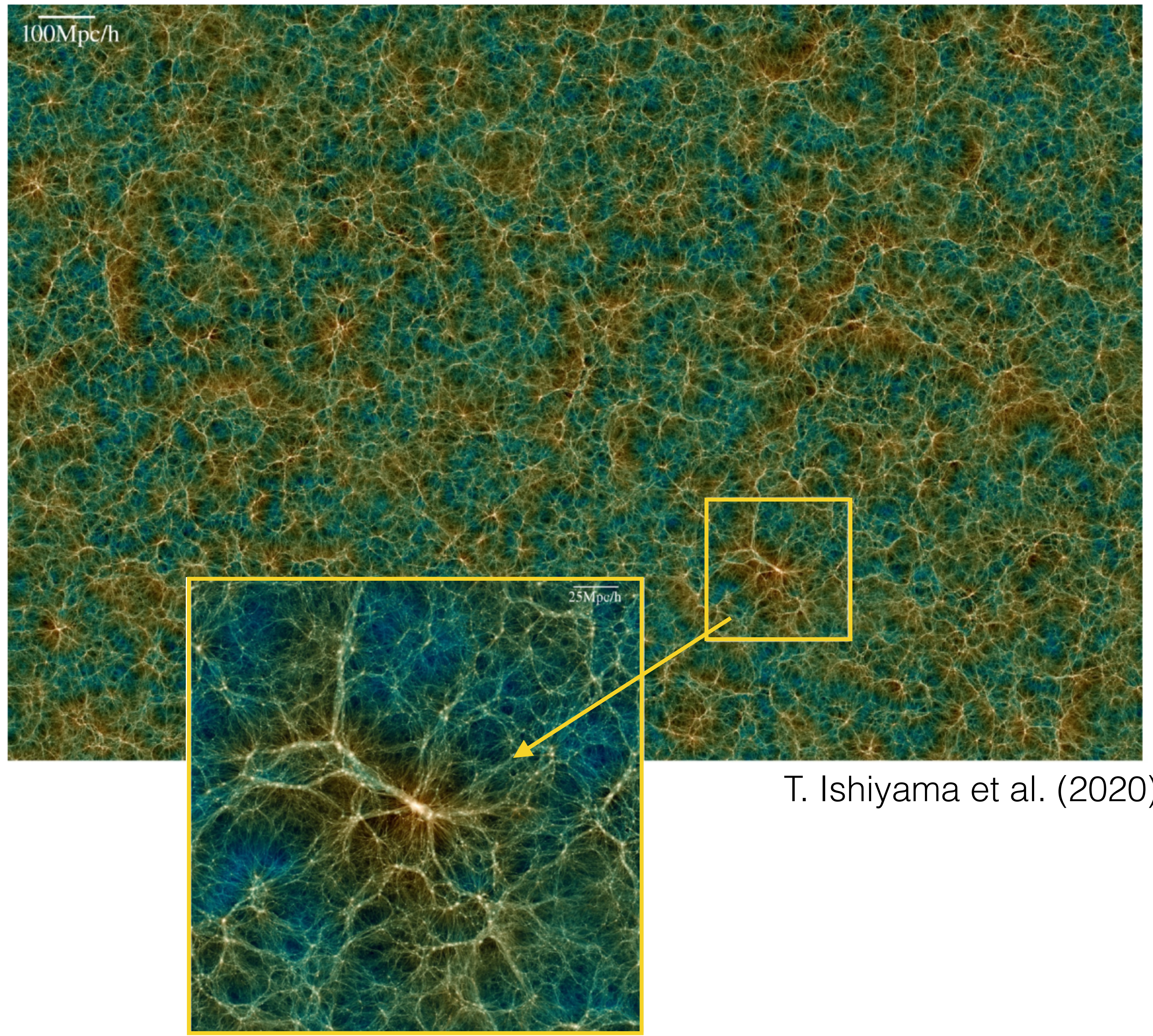

T. Ishiyama et al. (2020)

- Extract more information from the large scales

U. Seljak (2009)

- Extract more information from the small scales

D. Baumann *et. al* (2010)

In that way, we expected to have the best of the two worlds!

How did we do it?

First Step: Link the Large-Scale Structure tracers with the matter field

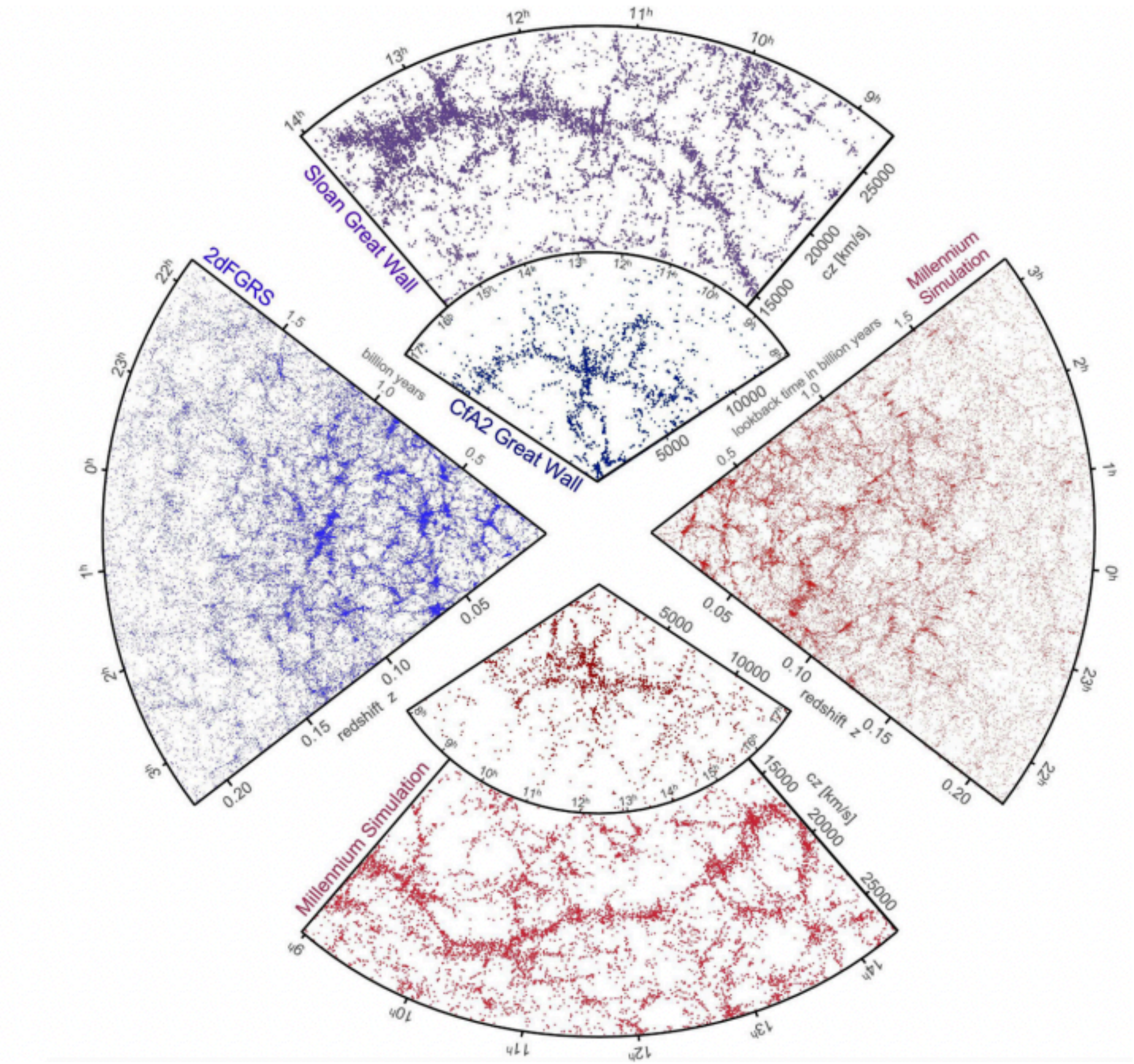

How it is done:

$$\delta_g = \mathcal{F}\left(\Phi, \Phi_v\right) = \sum_{\mathcal{O}} b_{\mathcal{O}} \mathcal{O}\left(\boldsymbol{x}, \tau\right)$$

How to identify the relevant operators?

$$\mathcal{O} \in \left\{\delta, \delta^2, \mathcal{G}_2\left[\Phi_v\right], \Gamma_3\left[\Phi_g, \Phi_v\right]\right\}$$

Invariant under Galilean transformations

Assassi *et. al* (2014)

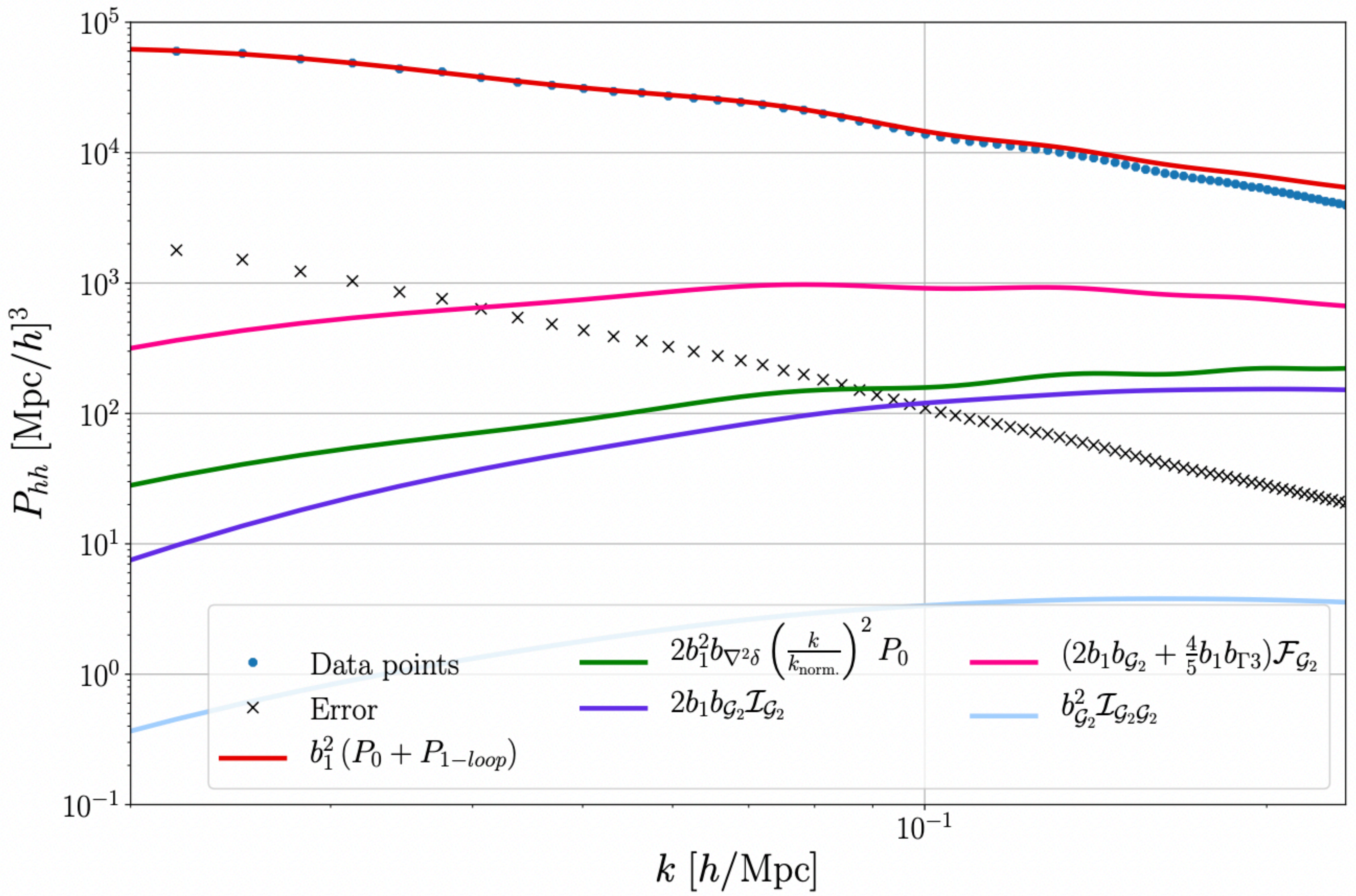

For the multi-tracer approach:

$$\delta_A = b_1^A \delta + \frac{b_2^A}{2!}\delta^2 + b_{\mathcal{G}_2}^A \mathcal{G}_2 + b_{\Gamma_3}^A \Gamma_3 + \dots$$

$$\delta_B = b_1^B \delta + \frac{b_2^B}{2!}\delta^2 + b_{\mathcal{G}_2}^B \mathcal{G}_2 + b_{\Gamma_3}^B \Gamma_3 + \dots$$

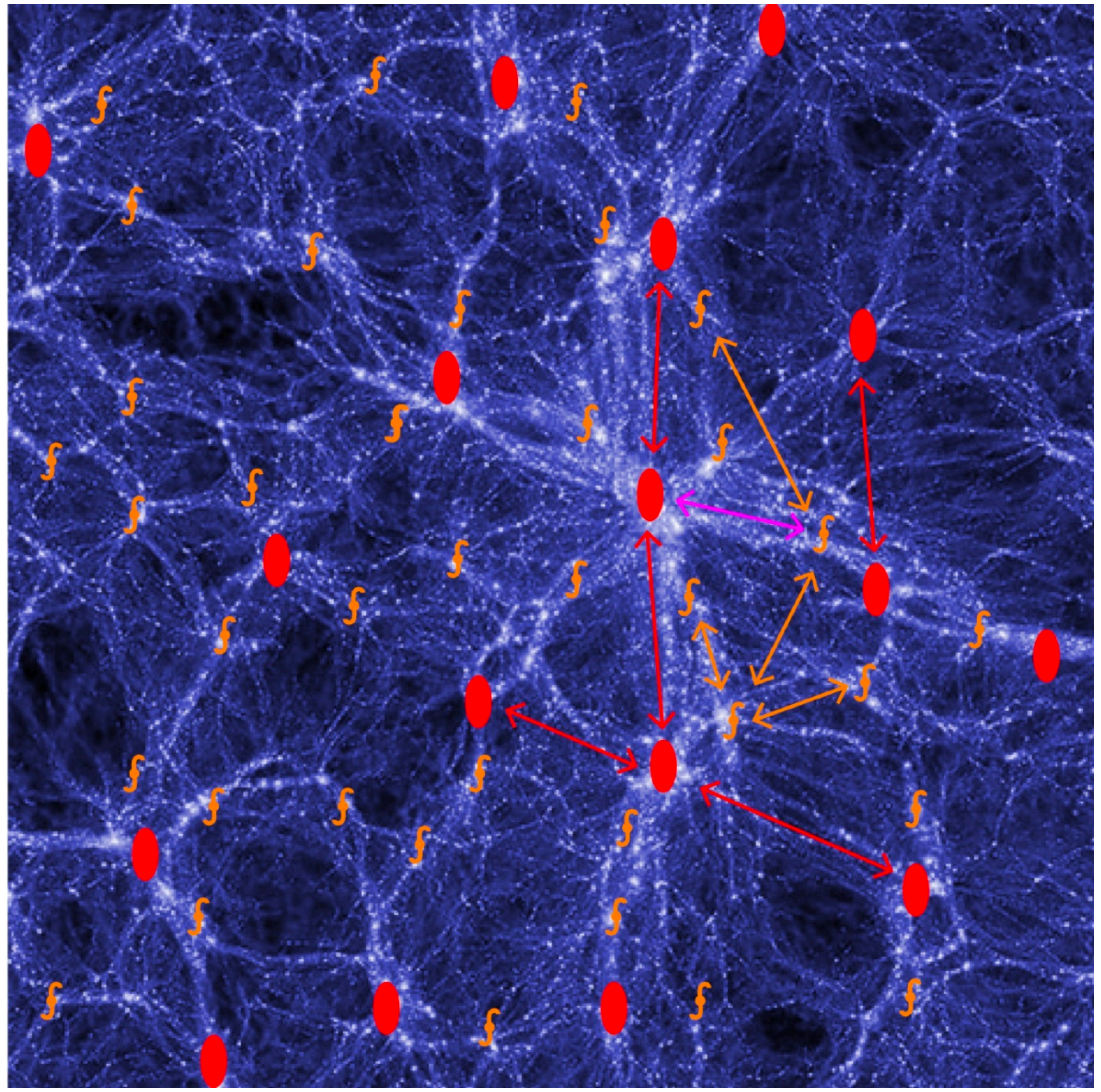

Case 1: Single-Tracer

$$b_1, b_2, b_{\mathcal{G}_2}, b_{\Gamma_3}$$

vs.

Case 2: Multi-Tracer

$$b_1^A, b_2^A, b_{\mathcal{G}_2}^A, b_{\Gamma_3}^A$$
$$b_1^B, b_2^B, b_{\mathcal{G}_2}^B, b_{\Gamma_3}^B$$

Results

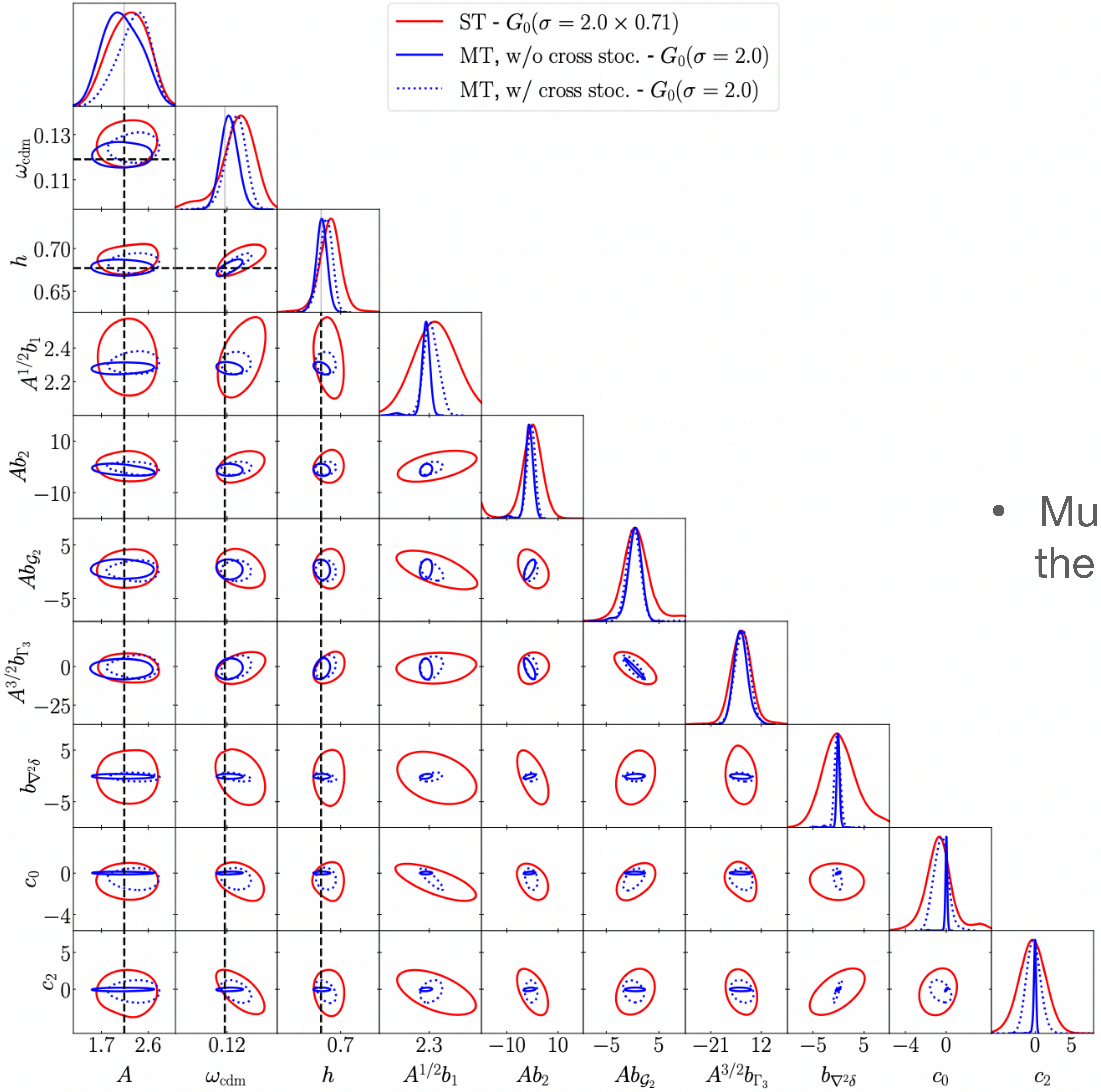

- Multi-tracer lead to smaller error bars not only on the bias but also on the cosmological parameters

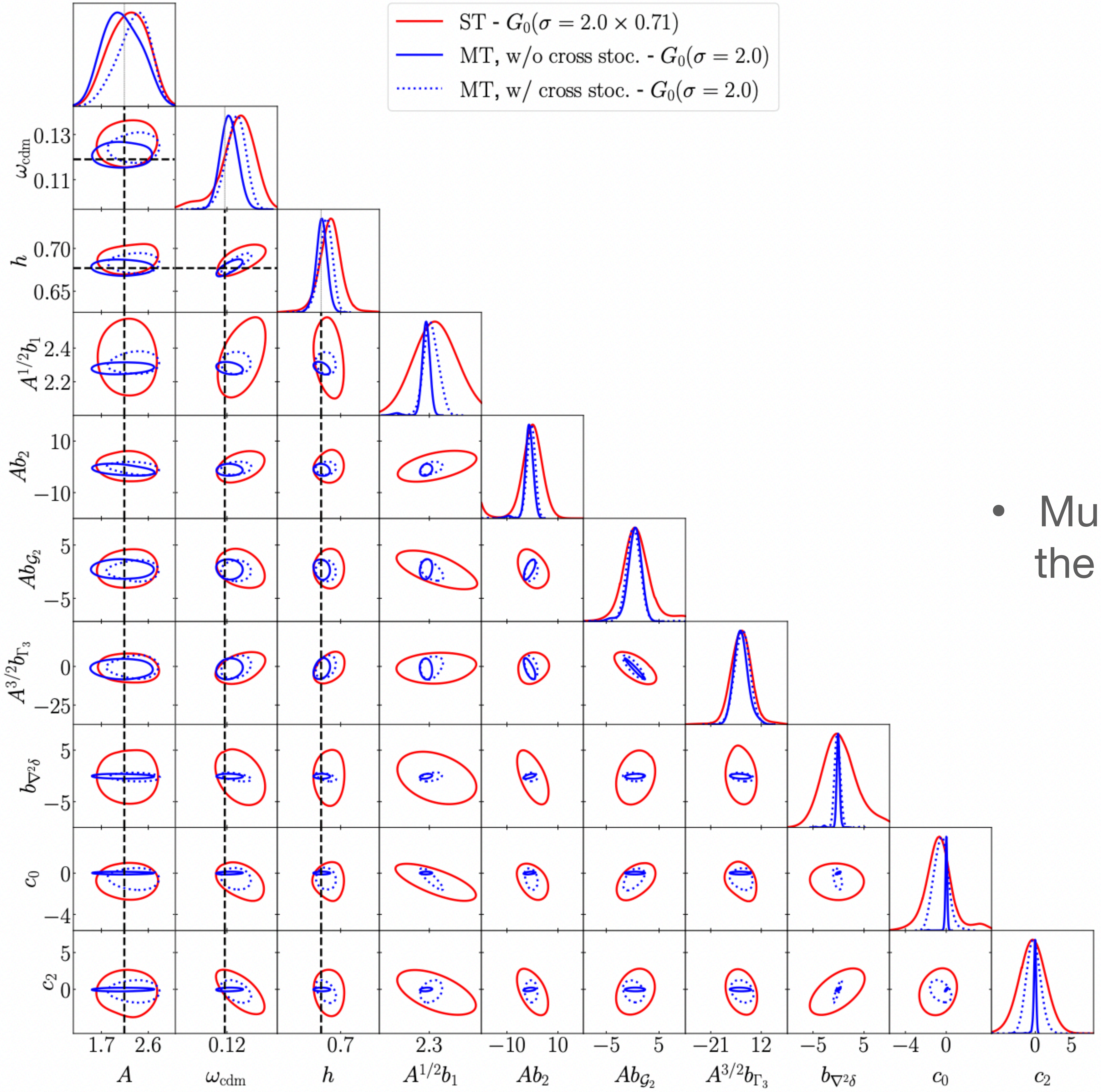

- Multi-tracer lead to smaller error bars not only on the bias but also on the cosmological parameters

Why?

Different tracers populate different large-scale structure environments → Different non-linear responses!

It can also be seen by looking at the bias co-evolution relations:

$$b_{K^2} = -\frac{2}{7}(b_1 - 1)$$

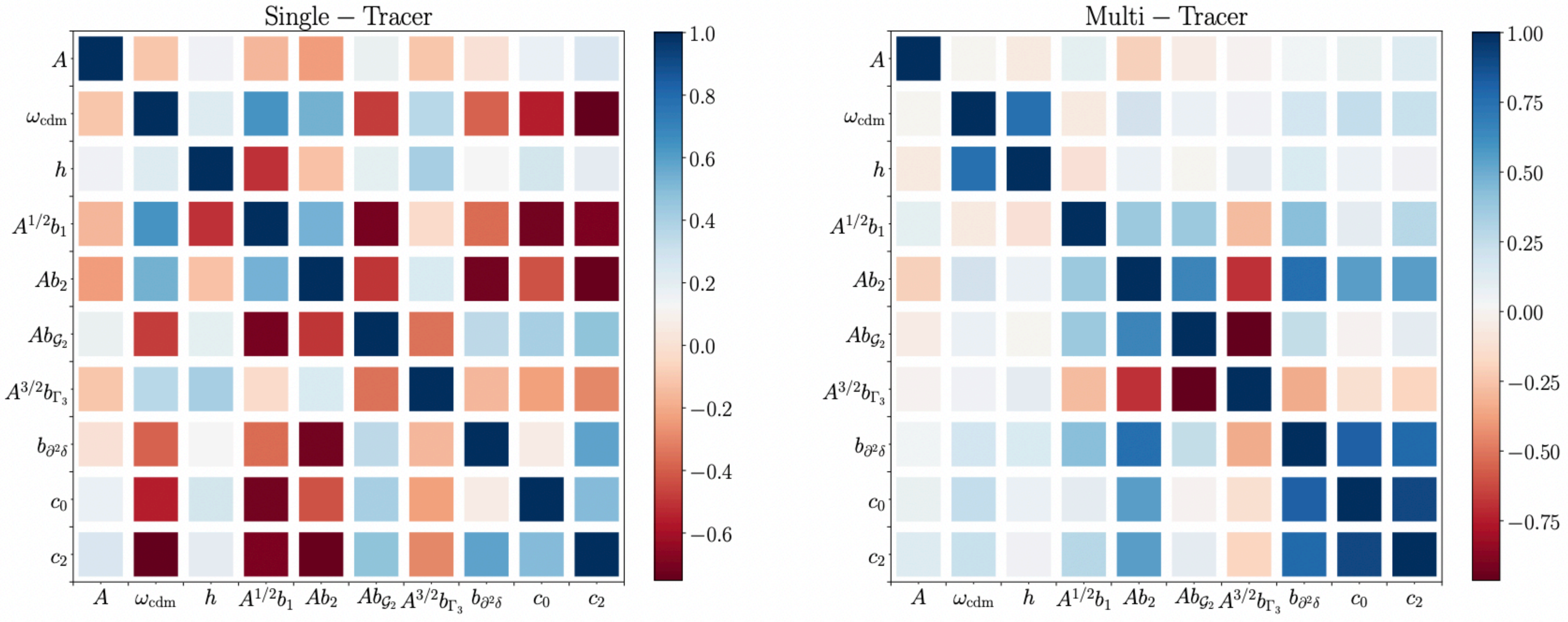

Conclusion:

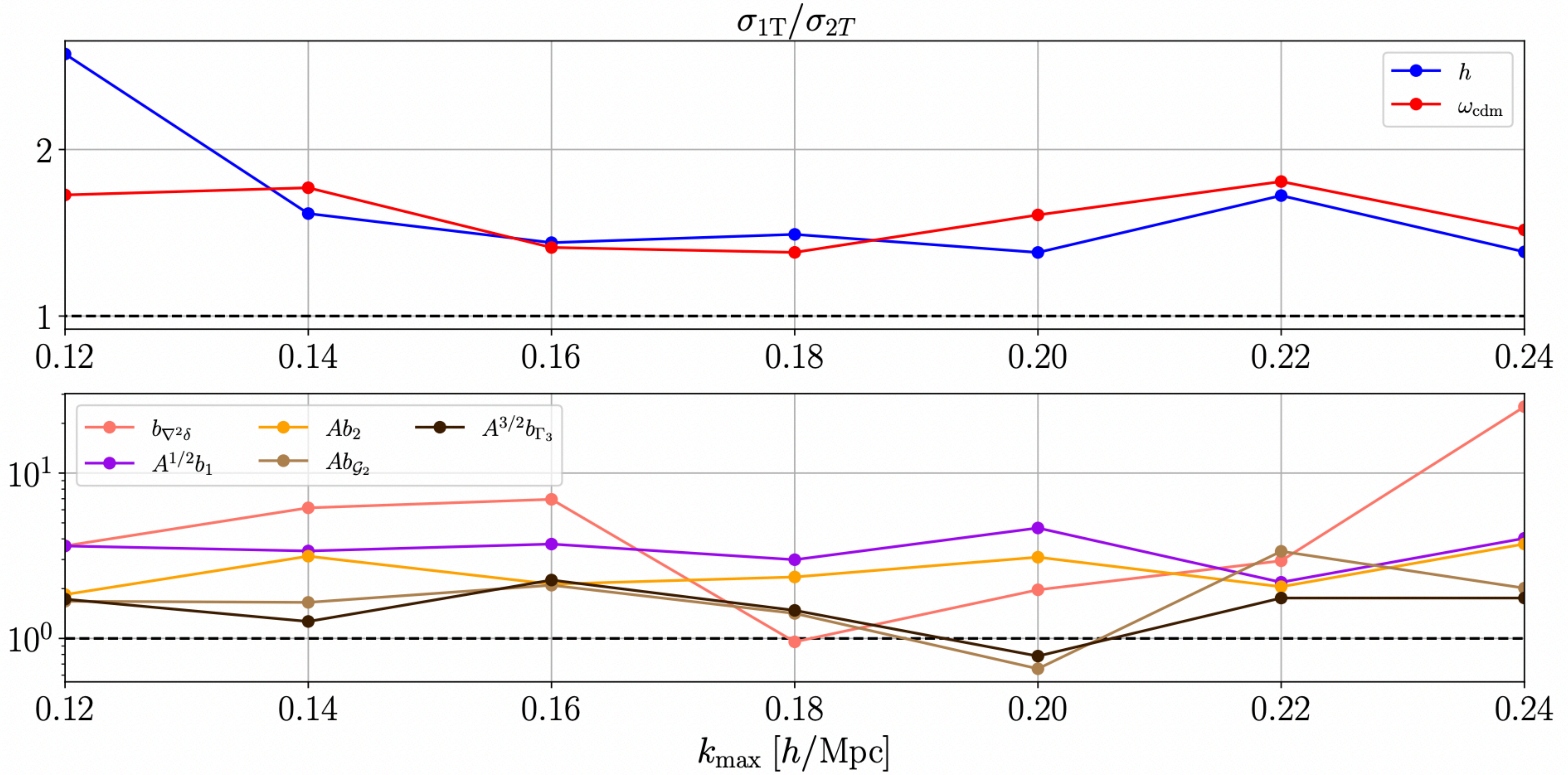

- MT is better than ST when it comes to performing full-shape analysis of the power spectrum
- MT is useful to break degeneracies between bias parameters
- Information from small scales is better translated into separated tracers bias

The next step is to include redshift-space distortions (work in progress!)

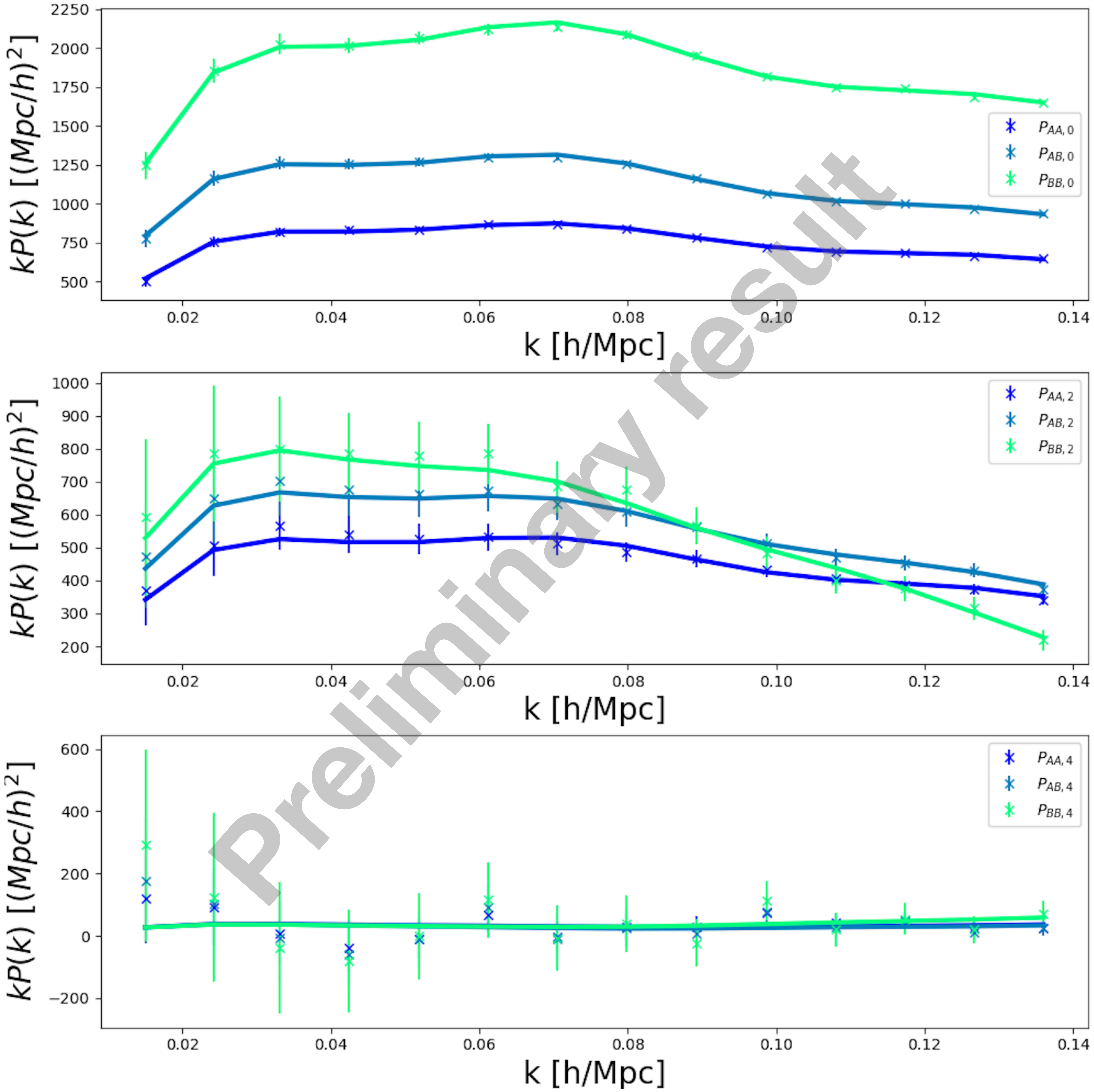

In Collaboration with H. Rubira, R. Voivodic, F. Beutler and J. Peacock

Thank you!

thiago.mergulhao@ed.ac.uk

EXTRA:

Variation of the analysis cut-off

- Multi-tracer outperforms the Single-Tracer in all cases